RCA REVIEW

a technical journal

RADIO AND ELECTRONICS
RESEARCH • ENGINEERING

VOLUME IX DECEMBER 1948 NO. 4

RCA REVIEW

GEORGE M. K. BAKER
Manager

CHAS. C. FOSTER, JR.
Business Manager

SUBSCRIPTIONS:

anada, and Postal Union: One Year $2.00, Two Years $3.50, Three Years $4.50
ountries: One Year $2.40, Two Years $4.30, Three Years $5.70

SINGLE COPIES:

ates: $.75 each. Other Countries: $.85 each

orporation of America, RCA Laboratories Division

ember, and December by Radio Corporation of
Rockefeller Plaza, New York 20, N. Y.

ew, Radio Corporation of America,
inceton, New Jersey

1946, at the Post
of March 3, 1879

LE *Treasurer*

RCA REVIEW

a technical journal

RADIO AND ELECTRONICS
RESEARCH · ENGINEERING

Published quarterly by

RADIO CORPORATION OF AMERICA
RCA LABORATORIES DIVISION

in cooperation with

RCA VICTOR DIVISION
RADIOMARINE CORPORATION OF AMERICA
RCA INTERNATIONAL DIVISION
RCA COMMUNICATIONS, INC.
NATIONAL BROADCASTING COMPANY, INC.
RCA INSTITUTES, INC.

VOLUME IX DECEMBER 1948 NUMBER 4

CONTENTS

RCA Review is regularly abstracted and indexed by *Industrial Arts Index, Science Abstracts* (I.E.E.-Brit.), *Engineering Index, Electronic Engineering Master Index, Abstracts and References* (*Wireless Engineer*-Brit. and *Proc. I.R.E.*) and *Digest-Index Bulletin.*

RCA REVIEW

FIELD TEST OF ULTRA-HIGH-FREQUENCY TELEVISION IN THE WASHINGTON AREA*

By

George H. Brown

Research Department, RCA Laboratories Division,
Princeton, N. J.

Summary—A field test of ultra-high-frequency television was conducted by RCA and NBC in the Washington area during the fall of 1948. A picture transmitter and a sound transmitter, together with a high-gain transmitting antenna, were installed at the Wardman Park Hotel.

Two types of converters were designed and constructed for these field tests. More than fifty converters and appropriate receiving antennas were installed in homes having conventional receivers.

A field intensity survey was conducted and the results are analyzed in terms of coverage.

At each of the home locations, voltages corresponding to the ultra-high-frequency transmission and to the transmission of WNBW on Channel 4 were measured. An analysis of this data is included, with respect to power requirements for satisfactory picture reception and with respect to comparative coverage at the low and high frequencies. The results of the field intensity survey are compared to the results obtained at home locations.

Observations concerning the effectiveness of directional receiving antennas as well as conclusions concerning multipath effects are included.

Introduction

MEASUREMENTS and observations have already been published[1] which afford a direct comparison of the propagation characteristics of radio waves at the frequencies 67.25, 288, 510 and 910 megacycles. The major portion of this work consisted of field intensity measurements taken with mobile equipment, so it seemed logical to follow this project with a program which would look toward reception in home locations under typical operating conditions. In the spring of 1948, the work of RCA Laboratories on color television was aimed in the direction of a field test involving transmissions on frequencies in the region of 500 megacycles; four transmitters were being built. Three of these transmitters were needed for the simultaneous color system of transmission, while the fourth was the accompanying sound transmitter. It was planned to install the sound transmitter and one of the picture transmitters at the Empire State Building in

* Decimal Classification: R583.16.

[1] George H. Brown, Jess Epstein, and Donald W. Peterson, "Comparative Propagation Measurements; Television Transmitters at 67.25, 288, 510 and 910 Megacycles", *RCA Review*, Vol. IX, No. 2, pp. 177-201; June, 1948.

New York prior to the completion of the entire system. This was to hasten the gathering of data typical to a broadcast operation and to gain experience with the installation of converters in home receiving locations.

With the announcement by the Federal Communications Commission of a public hearing in the matter of utilization of frequencies in the band 475 to 890 megacycles for television broadcasting, plans were altered and a decision was made to carry out the initial phase of the experiment in Washington. Hence, one picture transmitter and the sound transmitter were moved to Washington and installed in the transmitter room of Television Station WNBW at the Wardman Park Hotel.

The Washington experiment was intended to provide typical broadcast coverage with receivers installed in home conditions. The results of the transmissions could then be observed by many interested parties while field intensity measurements and other pertinent data were being accumulated.

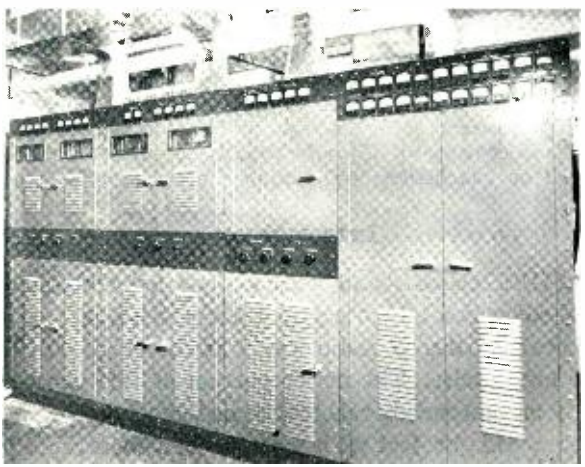

Fig. 1—The ultra-high-frequency transmitter installed in the transmitter room of WNBW.

Description of the Washington Installation

The Transmitters

The transmitters installed at the Wardman Park Hotel operated in the band of frequencies between 504 and 510 megacycles. The picture carrier frequency was 505.25 megacycles, while the sound carrier frequency was 509.75 megacycles. Figure 1 shows these two transmitters in their location at the Wardman Park Hotel.

A monochrome transmission was provided using the same standards

that apply in the 12 channels now used for commercial television broadcasting. The power amplifier tube in each transmitter was a modified Type 8D21. The 8D21 is a production type tube used in commercial five-kilowatt television transmitters. However, for the high-frequency experiments, it has been necessary to modify the construction slightly to reduce high-frequency power losses. This tube is capable of operation at only the low-frequency end of the 475 to 890 megacycle band and then at considerably reduced power.

The picture transmitter operated with a peak power of 1000 watts, while the sound transmitter delivered 1000 watts of average power.

The Transmitting Antenna and Transmission Line

In anticipation of field tests of color television in the vicinity of 500 megacycles, a broadcast antenna with a power gain of 10 was developed. This antenna uses the Turnstile principle, which provides a well-matched antenna over a broad band of frequencies and permits the use of a simple diplexer for feeding the sound and picture signals into a single antenna. The antenna structure consists of a seamless steel tube six inches in diameter and over twenty feet in length. When the Washington experiment was proposed, it seemed logical to place the high-frequency antenna on top of the Channel 4 antenna used by WNBW. A study of the mechanical problem revealed that it would be desirable to design and construct an antenna of smaller dimensions in order that the supporting pole not be stressed unduly. Hence an antenna ten feet in length and six inches in diameter was constructed especially for the Washington installation. Sixteen slots were cut in the tube and each slot was energized from a transmission line inside the tube.

The power gain of this antenna used in the Washington field tests was 5, with a single half-wave dipole used as the unit of reference.

Figure 2 shows the high-band antenna mounted above the WNBW Superturnstile, with the center of the high-band antenna 357 feet above ground and 563 feet above sea level.

As in the case of the larger antenna with a power gain of 10, a simple diplexer may be used to feed the picture signal and the sound signal into the same antenna. It was intended to use the diplexer in this manner, with the diplexer mounted in the base of the antenna and with two separate transmission lines, one running from the picture transmitter to the diplexer and the other running from the sound transmitter to the diplexer. However, because of the short time available to construct a very special transmission line as well as the installation problem on the tower, it was decided to use only one line from

the transmitter room to the antenna and to couple the two transmitters to this transmission line through an isolating filter.

A diplexer was nevertheless mounted in the base of the antenna, but not for the usual purpose. At the point where the sound line is connected in conventional operation, a resistance of fifty ohms was inserted. The inclusion of this resistor was brought about through a theoretical study carried out at these laboratories which revealed that a resistance of the proper value placed at this point on the diplexer, when the diplexer is used in conjunction with a Turnstile antenna, will provide a perfect termination for the other end of the diplexer and will insure a circular radiation pattern in the horizontal plane. The term chosen for this approach is "resistance stabilization."

Fig. 2 — The high-band antenna mounted above the WNBW Super-turnstile.

While the antenna used in Washington had a power gain of 5, it should be recalled that the power gain was limited to this figure by the mechanical strength of the supporting pole and that an antenna with a power gain of 10 has already been constructed and tested. In an installation where one had complete control of the design of the supporting structure, it would be quite feasible to realize this higher power gain.

It was originally intended to use commercially available transmission lines to carry power from the transmitters to the antenna. A critical examination soon revealed that none of the familiar commercial lines would be suitable for use in the range of frequencies between 475 and 890 megacycles. The unsuitability was caused by electrical discontinuities on the line due to the insulator effect. A transmission line which is electrically smooth throughout this range of frequencies was developed and it was this new type of construction which was used in the Washington field tests. The outer conductor of the line was over three inches in diameter. Even with this large line, the attenuation was 0.31 decibels per 100 feet, so that with a line 450 feet in length, only 72.5 per cent of the transmitter power arrived at the antenna.

While the power gain of the antenna itself was 5, one must consider the transmission line, with a "power gain" factor of 0.725, to be part of the antenna system. Hence, the power gain of the antenna system was 3.625. Then the effective radiated peak power for the picture transmission was 3625 watts, with 3625 watts average power for the sound transmission.

The Vestigial Sideband Filter

New circuit developments were applied to the problem of designing a vestigial sideband filter for use in the ultra-high-frequency range which resulted in a compact filter that had the same electrical characteristics as those used with present commercial television transmitters. This filter was installed with the ultra-high-frequency transmitter in Washington and has been used throughout the tests. This successful operation means that as far as the transmission standards are determined by the vestigial sideband characteristics they may be the same as the present commercial standards.

Converters and Receiving Antennas

Two television converters were developed at the laboratories for experimental use in the Washington field tests. The converters were intended for operation in conjunction with any standard television receiver having a push-pull input connection of 300 ohms impedance.

The Model A converter had a tuning range from 480 to 800 megacycles, while the Model B converter had a tuning range from 480 to 600 megacycles. Both models had self-contained power supplies and both models converted ultra-high-frequency television signals down to Channel 3 on a standard television receiver.

The noise factor for the Model A converter, using a crystal mixer, was 10 decibels above thermal noise, and the corresponding factor for the Model B converter was 22 decibels above thermal noise.

In Table I, the results of a number of calculations concerning the noise limitations of these converters are shown. In the case of the theoretical noise voltage for the 300-ohm resistor, the band width was taken as 4 megacycles. The noise voltages for the two converters are shown in the same column. The right-hand column shows the peak radio-frequency signal required to give a signal-to-noise ratio (i.e., the ratio of peak radio-frequency signal to root-mean-square noise voltage) of 30 decibels. A radio-frequency signal-to-noise ratio of 30 decibels gives a useful peak-to-peak signal to root-mean-square noise at the kinescope of 28.6 decibels, assuming standard synchronizing pulse and black level, with white level at 15 per cent. This is a value

which is considered to be a nominal value for acceptable service, and possibly may be considered a minimum acceptable signal.

Table I

Source of Noise	Root-Mean-Square Noise Voltage (Microvolts)	Peak Radio-Frequency Signal Required to Give Signal/Noise Ratio of 30 Decibels (Microvolts)
300-ohm resistor	2.19	69.0
Model A converter (Noise factor 10 db.)	6.9	219.0
Model B converter (Noise factor 22 db.)	27.1	860.0
Commercial television receiver in average adjustment (Noise factor 14.5 db.)	11.5	365.0

By using the equation on page 194 of Reference 1, the field intensity required to produce 219 microvolts on the 300-ohm input terminals of the Model A converter can be computed. In deriving this equation, it was assumed that the signal was being received on a half-wave dipole and that this dipole in turn fed the signal to a 300-ohm transmission line through a suitable matching section. It is found that at a frequency of 505.25 megacycles, the microvolts on the receiver terminals should be multiplied by a factor of 5.3 to obtain the field intensity in microvolts per meter. Then, a field intensity of 1160 microvolts per meter would be required to produce, under these circumstances, a voltage of 219 microvolts on the terminals of the Model A converter.

Lower field intensities could be used if circumstances permit the use of a directional receiving antenna. However, in many locations, the field is so distorted that little or no benefit is derived from a directional receiving antenna.

In designing television receiving antennas, one is concerned with the problems of obtaining a desirable radiation pattern over a wide band of frequencies and of obtaining a reasonable impedance match between the antenna and transmission line. If the receiver is well matched to the transmission line, the efficiency of signal transfer from the antenna to the transmission line may be expressed in terms of the antenna impedance. However, a more convenient method makes use of the measurement of the voltage standing-wave-ratio on the transmission line when the antenna is used in the transmitting condition. If we call this ratio of minimum voltage to maximum voltage K,

$$E'/E'' = \frac{2\sqrt{R}}{1+R}$$

where E'' is the voltage received on the receiver terminals when the antenna is perfectly matched to the line and E' is the voltage received on the receiver terminals when the actual antenna which is not perfectly matched is used. Table II gives a number of values for this ratio of voltages.

Table II

Standing-Wave Ratio, R	$(E'/E'') \times 100$
1.0	100.
0.7	98.5
0.6	96.7
0.5	94.2
0.4	90.2
0.3	84.2
0.2	74.3
0.1	57.4
0.05	42.5

Thus it can be seen that if the standing-wave-ratio R is not less than 0.5, less than 6 per cent of the maximum possible voltage is lost.

In preparation for the Washington experiment, several simple antenna types were designed and constructed. Since it was planned to install converters in a large number of homes under a variety of conditions, it seemed appropriate to concentrate on relatively inexpensive constructions that would not in general be objectionable when installed on the average home.

A broad-band receiving dipole is shown in Figure 3. This antenna retains its characteristics as an effective dipole over the entire band of frequencies from 475 to 890 megacycles. The impedance match expressed in terms of transmitting standing-wave-ratio is better than 0.6, so Table II shows that less than 4 per cent of the received voltage is sacrificed by mismatching losses over the entire band. In the neighborhood of 500 megacycles, the radiation pattern is very similar to that of a conventional dipole, while at the upper end of the band the pattern is somewhat narrower with a slightly higher antenna gain factor.

A rather simple directional receiving antenna is the rhombic shown in Figure 4. This antenna is a little over six feet in length and less than four feet in width. The impedance match is excellent over the entire band.

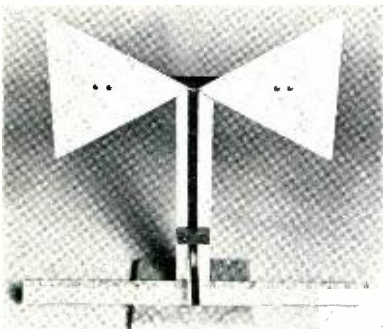

Fig. 3—A fan dipole useful in the ultra-high-frequency band.

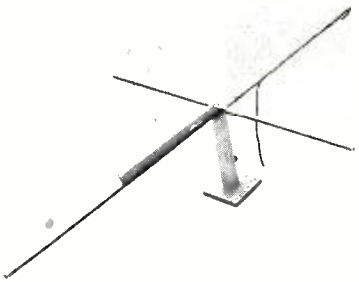

Fig. 4—A rhombic receiving antenna used in the Washington field tests.

A simple directional antenna using a dipole and a parasitic director is shown in Figure 5. This antenna is limited in use to the 504 to 510 megacycle channel by its impedance characteristic and by its changing directional pattern. Through this limited band, the standing-wave-ratio under transmitting conditions is greater than 0.5 and the antenna thus operates at good efficiency.

A compact broad-band unidirectional antenna using four dipoles connected by a transmission line network has been developed and is shown in Figure 6. The pattern does not change materially in the band between 475 to 890 megacycles, and the impedance match is also very good throughout this same band.

The simplicity of installation with the relatively unobtrusive fan dipole is illustrated by the photograph of a typical home installation shown in Figure 7.

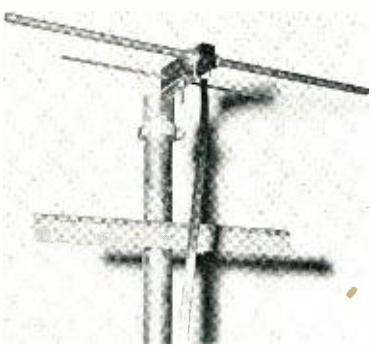

Fig. 5—A dipole-director array for the band from 504 to 510 megacycles.

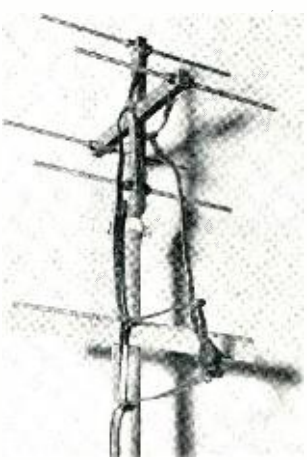

Fig. 6 — A broad-band unidirectional array developed for use in the ultra-high-frequency channels.

Installation of converters and receiving antennas started shortly after the beginning of transmissions on September 1, 1948. During that month, 35 Model A converters and 16 Model B converters were installed in the Washington area. Of these installations, 47 were accompanied by an antenna installation which appeared to be appropriate for the particular set of circumstances. These included 3 dipole-director arrangements, 5 broad-band unidirectional arrays, 15 rhombics, and 24 fan dipoles. In each case, the installation crew tried a variety of antenna positions as well as the various antenna types. The predominance of the fan dipoles was due to two factors. Where a satisfactory picture could be obtained with the fan dipole, it was selected because of its simplicity. In many other instances, particularly in the shadowed areas, it was often found that the fan dipole gave at least as strong a signal as the directional antennas. The rhombic antenna often gave results superior to any other type and was used

Fig. 7—A fan dipole installed in a typical home location.

in those instances. In some of the shadowed areas it was inferior to the fan dipole, but in at least one extremely obstructed position it was far better than the other antennas. The dipole-director was found to be of little value in any location.

Data Obtained from the Washington Experiment

The Field Intensity Survey

For measurements of field intensity in the New York area, a truck-mounted receiving antenna at an elevation of 30 feet was used, the truck was moved around a local area, where possible, and the receiving antenna was rotated at the same time. In this way, a search was made

for maximum signal with the most usable picture. Since maximum signal did not always correspond to the most usable picture, the field intensity corresponding to best picture was recorded. Receiving sites were chosen in a variety of surroundings: in open fields, in wooded areas, along highways, atop hills, and in valleys. An effort was made to stay away from electric lines and large buildings. The same procedure was followed in the Washington area.

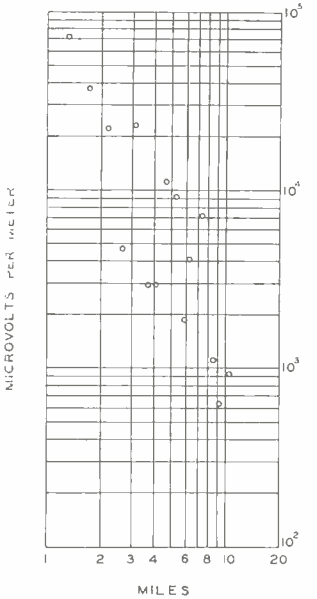

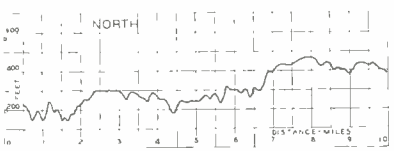

Fig. 8 — Field intensity measured along the north radial. The receiving antenna was 30 feet above ground. The effective radiated power at 505.25 megacycles was 3.6 kilowatts.

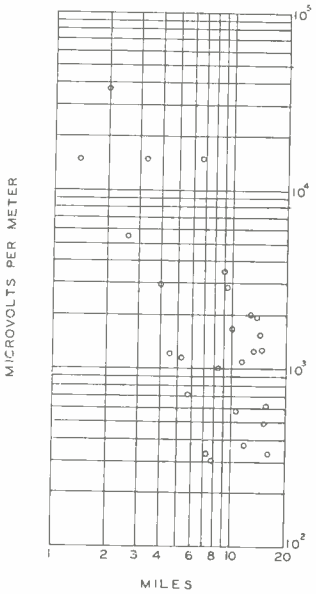

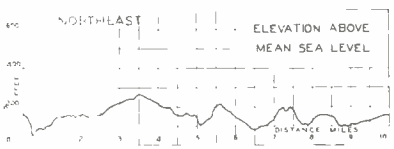

Fig. 9—Field intensity along the northeast radial.

For reference in connection with this survey and to show the type of terrain in the Washington area, profiles have been plotted for eight radial lines with the WNBW tower as the point of origin. These profiles are shown at the bottom of Figures 8 to 15, inclusive. Only part of the story is indicated by these figures, since Washington has a great number of large trees, large homes, and many apartment buildings. The profile of the southeast radial looks very flat in the first

five miles, but actually this is the region of large hotels and office buildings.

The field intensity measured along these eight radial lines is shown in Figures 8 to 15, inclusive. The exception should be noted that in Figure 15 the profile is along the northwest radial while the field intensity measurements are taken along the northnorthwest radial. This change was necessary in order to use available roads. During the course of these measurements, the effective radiated power referred to peak of synchronizing signal was 3.6 kilowatts. The field intensity recorded in these figures refers to peak of synchronizing pulse.

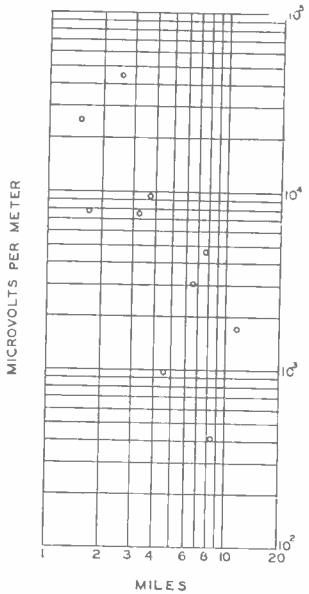

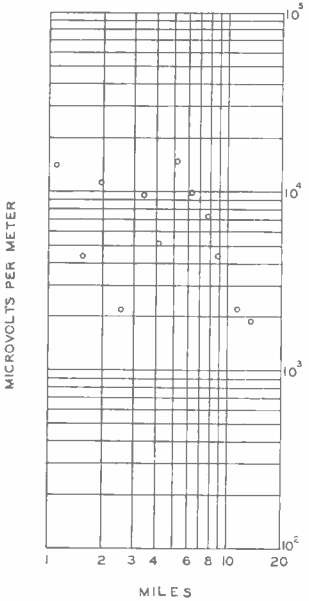

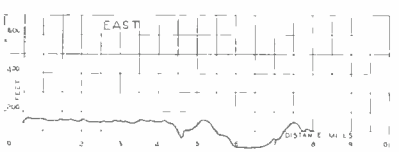

Fig. 10—Field intensity along the east radial.

Fig. 11—Field intensity along the southeast radial.

A comparison of Figures 8 to 15 with the corresponding profile reveals a distinct correlation between the profile and the measured field intensity, with some departure due to local effects such as trees and buildings.

In making a comparison of the measured field intensity with theoretical values, the profiles on each of the eight radials shown in Figures

8 to 15 were averaged. The average elevation for each profile was then used in a calculation of the theoretical field intensity curve for the particular radial. Then the measurements of Figures 8 to 15 were analyzed on a statistical basis, with the results shown in Figure 16. Curve A relates the measured values to the theoretical curve at 505.25 megacycles. Curve B was constructed by comparing the measured values at 505.25 megacycles with the theoretical field intensity curve at 67.25 megacycles, with the same effective radiated power in each case.

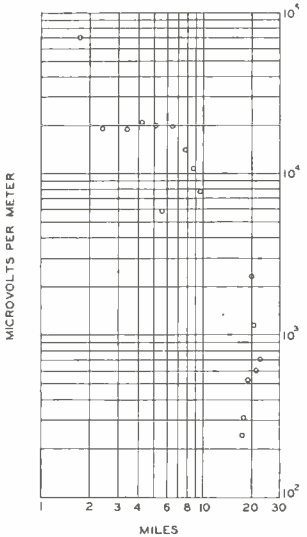

Fig. 12—Field intensity along the south radial.

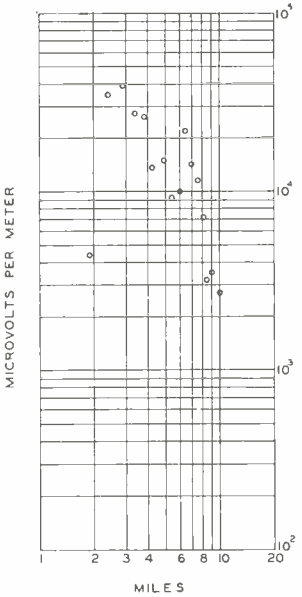

Fig. 13—Field intensity along the southwest radial.

Signal Strength on Receiver Terminals in Home Locations

The locations of 44 converter installations in the Washington area are shown in Figure 17. At these locations, the 505.25-megacycle voltage on the terminals of the converter was measured. At the same time, the voltage on the receiver terminals of the low-band antenna was measured for the WNBW Channel 4 transmission. At the time of these measurements, the effective radiated power for the 505.25-mega-

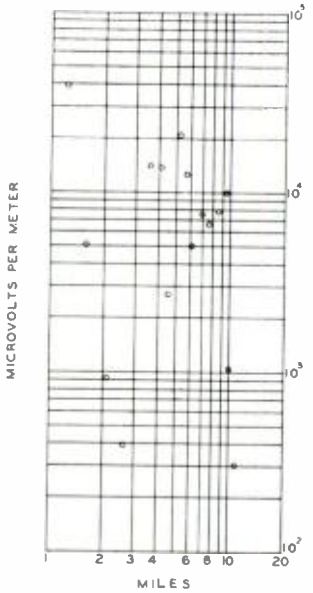

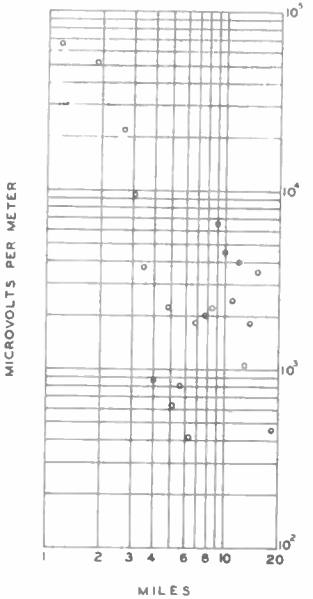

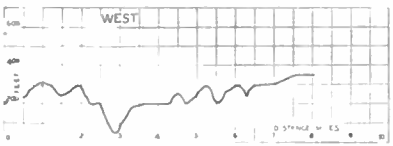

Fig. 14—Field intensity along the west radial.

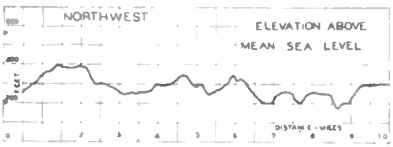

Fig. 15—Field intensity along the northnorthwest radial.

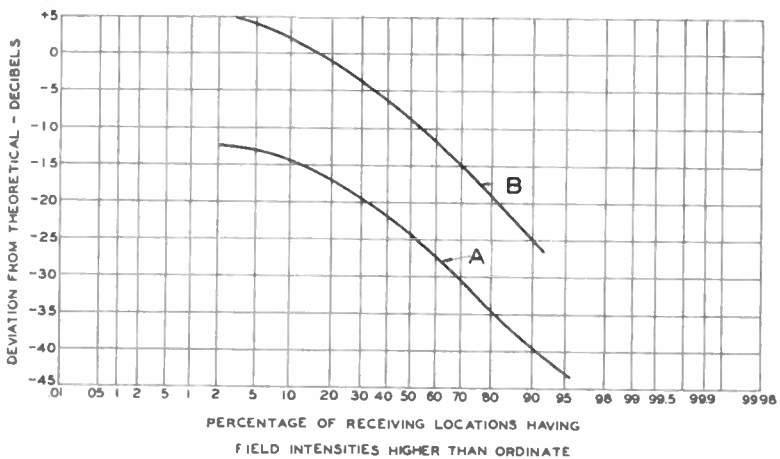

Fig. 16—An analysis of the data shown in Figures 8 to 15. Curve A relates the measured field intensities at 505.25 megacycles to the theoretical curve for the same frequency. Curve B relates the measured field intensities at 505.25 megacycles to the theoretical curve at 67.25 megacycles.

cycle transmission was 3.6 kilowatts, while the effective radiated power for WNBW was 20.5 kilowatts.

Table III lists the map location and distance from WNBW for the converter installations shown on Figure 17, as well as the 505.25 megacycle and 67.25 megacycle voltages measured on the receiver terminals.

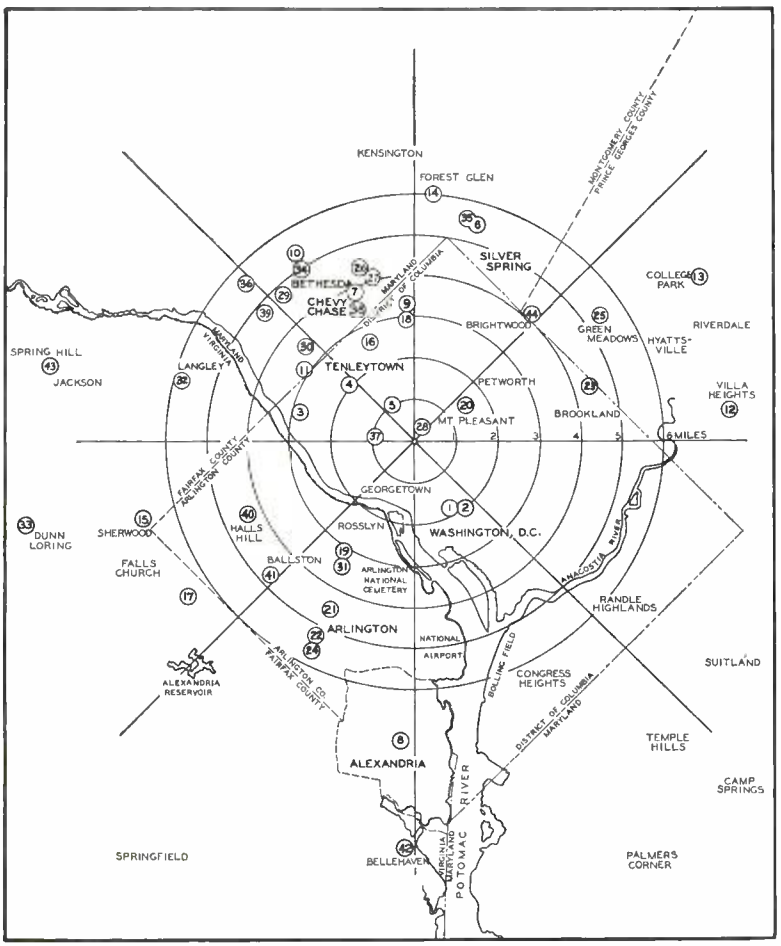

Fig. 17—A map of the Washington area showing the locations of converters and receiving antennas listed in Table III.

From a comparison of the measured voltages on the receiver terminals at 505.25 megacycles and at 67.25 megacycles, the probability curve shown in Figure 18 has been constructed. From this curve one can find the power needed at 505.25 megacycles in order that the receiver voltages at a given percentage of the receiver locations shall

TABLE III

Location Number	Distance (miles)	Receiving antenna	Receiving antenna height (ft.)	Converter	Receiver voltage (microvolts) 505.25 Mc	67.25 Mc
1	2	Dipole director	Roof of 12 story bldg.	A	2,250.	188,000.
2	2	Fan	Roof of 12 story bldg.	A	4,750.	137,000.
3	3	Rhombic	50	A	338.	950.
4	2	Fan	40	A	565.	9,250.
5	1	Broad-band array	47	A	485.	18,800.
6	5.3	Rhombic	45	A	350.	3,500.
7	4	Broad-band array	75	A	1,950.	25,000.
8	7.2	Fan	Indoor, attic of apartment bldg.	A	580.	7,000.
9	3.3	Rhombic	45	A	1,010.	10,000.
10	5.3	Rhombic	—	A	127.	11,000.
11	3.2	Fan	55	A	338.	8,250.
12	7.2	Rhombic	40	A	466.	8,000.
13	7.7	Rhombic	12	A	Below 50	325.
14	5.8	Dipole-director	42	A	1,650.	1,375.
15	7	Rhombic	35	B	1,430.	32,500.
16	2.5	Fan	10	B	8,000.	82,500.
17	6.6	Rhombic	10	A	Below 50	8,500.
18	2.9	Fan	50	A	775.	50,000.
19	3.3	Fan	42	B	503.	25,000.
20	1.4	Fan	30	A	233.	23,800.
21	4.6	Fan	33	B	2,760.	2,250.
22	5.3	Broad-band array	Attic	A	Below 50	3,750.
23	4.1	Fan	10	A	Below 50	8,250.
24	5.6	Fan	Attic	B	Below 50	3,660.
25	5	Dipole-director	38	A	565.	6,750.
26	4.4	Rhombic	32	A	142.	4,500.
27	5	Rhombic	38	A	474.	16,250.
28	0.2	Fan	50	A	19,800.	32,500.
29	4.7	Fan	38	A	263.	4,000.
30	3.5	Fan	50	A	417.	9,500.
31	3.4	Fan	40	B	3,080.	21,300.
32	6	Fan	28	A	475.	4,000.
33	9.6	Broad-band array	50	A	256.	11,000.
34	5	Fan	10	A	396.	3,750.
35	5.4	Rhombic	35	B	550.	10,500.
36	5.6	Fan	28	A	680.	10,750.
37	1.1	Rhombic	8 fl. bldg.	B	19,800.	250,000.
38	3.5	Fan	45	B	110.	7,500.
39	4.8	Rhombic	40	A	900.	4,000.
40	4.3	Fan	40	B	1,350.	10,250.
41	5	Fan	35	A	1,320.	18,800.
42	9.7	Fan	35	B	1,140.	1,250.
43	9	Rhombic	40	A	210.	5,000.
44	4	Fan	25	A	450.	5,750.

be as great as the receiver voltages obtained with 20.5 kilowatts of effective radiated power on Channel 4. It may be seen that with the present radiated power of 3.6 kilowatts at 505.25 megacycles, only 4 per cent of the locations achieve a signal strength as great as that obtained on Channel 4. In order that 50 per cent of the locations realize this goal, the power requirements at 505.25 megacycles would be 1200 kilowatts. To obtain the same result for 70 per cent of the locations, a radiated power of 5000 kilowatts would be required.

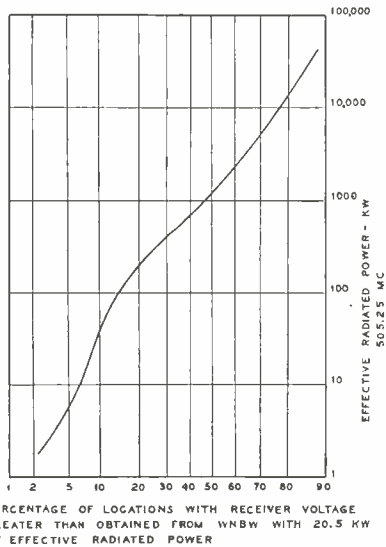

Fig. 18—A statistical analysis of the voltages on receiver terminals in home locations, expressed in terms of power requirements at 505.25 megacycles in order that a given percentage of locations shall have as great a signal as obtained from WNBW with 20.5 kilowatts of effective radiated power.

It may be of interest to return for a moment to the survey in the New York area. Using Figure 20 of the Reference 1, and assuming that a half-wave dipole was used for the receiving antenna, it was estimated that the power required at 505.25 megacycles should be 210 times the power of the Channel 4 station WNBT to obtain equality of receiver voltages for the two frequencies at 50 per cent of the locations. Multiplying 210 by the effective radiated power of WNBW, 20.5 kilowatts gives 4300 kilowatts. Again using the results of Reference 1, it is found that the power required to achieve the same result at 70 per cent of the locations would be 10,660 kilowatts. The following comparison of the Washington tests and the New York survey can then be made.

Percentage of receiving locations with receiver voltage equal to the Channel 4 signal.	Power requirements estimated from the Washington tests. (kilowatts)	Power requirements estimated from the New York tests. (kilowatts)
50	1,200	4,300
70	5,000	10,660

The agreement between the power estimates obtained from these experiments in two different areas of somewhat different topography is well within the limits of experimental accuracy for this type of data.

In addition, it should be remembered that in many installations in the Washington area directive receiving antennas were used effectively while the estimates from the New York data were based on the use of a dipole.

Since at most of the receiver locations in the Washington tests the Channel 4 signal is far in excess of the value required to give a completely noise-free picture, it may be more appropriate to examine the power requirements at 505.25 megacycles to obtain a noise-free picture or at least a marginal picture. With this objective in mind, Figure 19 was constructed from the data in Table III. The lower curve in this figure shows the power requirements to obtain 219 microvolts on the receiver terminals at a given number of locations. This is the value of voltage which was estimated earlier in this paper as being necessary to give the minimum acceptable signal-to-noise ratio on the Model A converter. Examination of the lower curve reveals the following power requirements when the Model A converter is used.

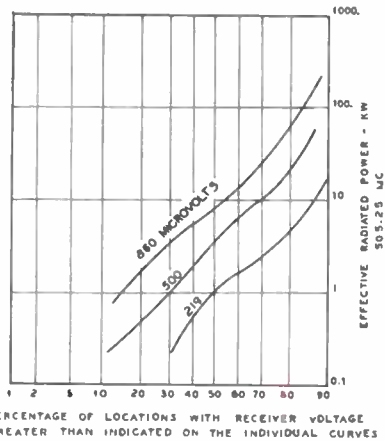

Fig. 19 — Power requirements at 505.25 megacycles in order that a given percentage of the receiving locations shall have a receiver terminal voltage as great as the values indicated on the individual curves.

Percentage of receiving locations with a receiver voltage of at least 219 microvolts	Power estimate (kilowatts)
50	1
70	2.4
78	3.6
80	4.7

The middle curve on Figure 19 holds for a receiver voltage of 500 microvolts. This would give a noticeably better picture than the minimum acceptable value of 219 microvolts. From this middle curve, the following power requirements are found to yield at least 500 microvolts on the receiver terminals.

Percentage of receiving locations with a receiver voltage of at least 500 microvolts	Power estimate (kilowatts)
51	3.6
70	10.2
80	22.0

The upper curve in Figure 19 is an attempt to estimate the power requirements to obtain a minimum usable signal on the Model B converter, that is, with 860 microvolts on the receiver terminals. Examination of this curve shows the following power requirements.

Percentage of receiving locations with a receiver voltage of at least 860 microvolts	Power estimate (kilowatts)
32	3.6
50	8.2
70	26.0
80	66.0

In an attempt to correlate the voltage measurements made in home receiving locations with the field intensity measurements, the field intensity data for the northnorthwest radial of Figure 19 has been transferred to Figure 20 where it is shown by the circles. A study of Figure 17 shows that the home locations numbered 4, 5, 7, 10, 11, 16, 29, 30, 34, 36, 38, and 39 are within reasonable distance of the northnorthwest radial. At two-thirds of these home locations, fan dipoles were used. It has been shown earlier that to convert receiver voltage to field intensity, for a dipole receiving antenna, a factor of 5.3 should be used. Hence the receiver voltage for the above twelve locations was converted in this manner, with the results shown by the crosses on Figure 20. A reasonable correlation may be seen with the limited data.

Conclusion

Contrary to experience in the New York area, multipath interference was found to be of little consequence in the Washington installations. Multipath signals were in evidence and it was necessary to move the receiving antenna to eliminate it. However, the major problem in many installations was to find a spot where the main signal was strong enough. The difference may be due to two factors. The signals observed on the west radial in the New York tests were radiated from the Empire State Buliding, with many tall buildings surrounding the source, but

at lower level. However, it was felt that the use of a directional transmitting antenna in the New York tests had minimized the multipath effects. The second factor may be due to the relative powers used in the two tests. In New York, high values of radiated power were used so that both the main signal and the reflected signals were well above the noise. In many cases in Washington, the main signal was only marginal and it may well be that the multipath signals were obscured because they were below noise level.

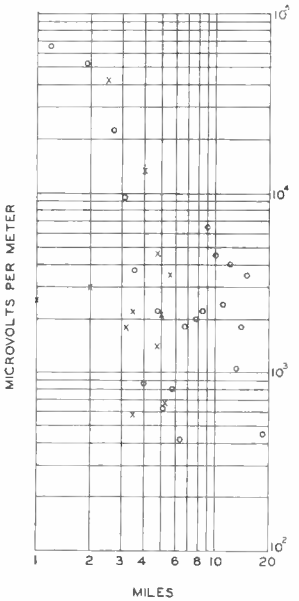

Fig. 20—A comparison of field intensity data with voltage on receiver terminals. The circles are the measured field intensities along the northnorthwest radial. The crosses are the apparent field intensity obtained from the receiver terminal voltages at home locations divided by the effective height of a dipole antenna.

A literal interpretation of Figure 18 shows that enormous amounts of power are required at 500 megacycles to give the same coverage as obtained on the Channel 4 station. It should be remembered, however, that in the area of the measurements, the Channel 4 station furnishes practically blanket coverage. Hence, not too extravagant amounts of power at 500 megacycles will furnish a reasonable coverage over a limited area, without providing the large area coverage of the low channels. When studying Figure 19 which indicates moderate power levels for reasonable coverage of a large percentage of the home locations, one should, nevertheless, not fail to consult Figure 17 and take note of the fact that the majority of the home locations used in this analysis were grouped in areas rather close to the transmitter.

The analysis of data shown in Figure 16 indicates a greater departure from theoretical values in the Washington area than was found in the New York tests. Two factors may account for the difference. In New York, the transmitting antenna was over 1000 feet above ground, while in Washington the transmitting antenna was only about 350 feet above the immediately surrounding terrain. In addition, the probability curve for the New York tests was formed by averaging the results from the hilly west radial which passed through residential districts with the results from the southwest radial which passed over

relatively barren territory. The terrain on all eight radials in Washington was not unlike the west radial of the New York tests.

ACKNOWLEDGMENT

Under usual circumstances of publication of scientific results, recognition of creative contributions to a project is established by joint authorship and assistance of a valuable but more routine nature is acknowledged by a formal statement incorporated as part of the paper, with individual names cited. In a project of the scope and magnitude of the Washington field test, neither procedure seemed practical since various phases of the work were carried out by several groups in the RCA organization. The author appears solely in the role of correlator and narrator and he wishes to emphasize the importance of the enthusiastic cooperation of the numerous engineers of RCA Laboratories Division who developed and designed the transmission equipment, the receiving antennas, and converters and who made all the measurements displayed in this paper; the engineers of the National Broadcasting Company, Inc., who contributed greatly to the installation and operation of the transmission equipment; the staff of RCA Victor Division which cooperated in the manufacture of the converters and transmitting tubes; and the RCA Service Company, Inc., which carried out the task of installing converters and receiving antennas in the Washington area.

ANALYSIS OF A SIMPLE MODEL OF A TWO-BEAM GROWING-WAVE TUBE*

By

Leon S. Nergaard

Research Department, RCA Laboratories Division,
Princeton, N. J.

Summary—*The gain and bandwidth of a mathematical model of a tube in which a growing wave is produced by the interaction of two electron beams is investigated. The model consists of two admixed beams, infinite in extent, and uniform except in the common direction of their velocities. The gain per unit length of the model is found to depend on the operating frequency, the current densities and the dc velocities of the two beams. The fractional bandwidth is found to depend on the total gain as well as on the parameters which determine the gain per unit length. With physically realizable current densities and velocities, adjusted for maximum gain, and an interaction space 30 centimeters long, the model yields a gain of 120 db at 3000 Mc with a bandwidth of 860 Mc.*

Introduction

SOME time ago C. W. Hansell of these laboratories proposed a growing-wave tube in which a wave is made to grow by the interaction of two electron beams of different velocities.[1] This proposal, in effect, substitutes a second electron beam for the helix in the conventional traveling-wave tube. There are several attractive features in this proposal. One is that the tube is all electronic and need contain none of the circuitry required with the traveling-wave tube. Another is that, because of the forward motion of the two beams, it seems unlikely that there will be a backward wave. The absence of a backward wave would render unnecessary the use of the circuit attenuation now used in conventional traveling-wave tubes to keep regeneration within reasonable bounds. The attractiveness of these features is, however, contingent upon the gain per unit length of tube which can be achieved with practical beam currents and voltages.

---

* Decimal Classification: R338.

[1] Subsequent to the analysis presented here and while the present paper was in preparation, a classified report by Dr. A. V. Haeff was received from the Naval Research Laboratory entitled "The Electron Wave Tube—A Novel Method of Amplification and Generation of Microwave Energy." Dr. Haeff's report (now declassified) contains a similar analysis of the interaction between streams of electrons and describes experimental results obtained with amplifying tubes based on this principle.

The writer has learned that the principle of the growing-wave tube was also conceived at the Bell Telephone Laboratories and that work on the tube is in progress there.

It is the purpose of this paper to present the results of an analysis of the gain per unit length of tube which can be achieved with the beam current densities and beam velocities which can be realized in practice. The tube model chosen for analysis is that of two admixed beams, infinite in extent, with arbitrary current densities and velocities. The velocity vectors of the two beams are assumed to be in the same direction. All dc space charge effects are neglected. The analysis then consists in finding the current densities and beam velocities for which growing waves exist, and the circumstances under which the growing waves increase most rapidly. This model is idealized and yields results better than can be achieved in practice where dc space charge effects and field fringing at the edges of the beam will act to reduce the gain. At the same time, it is practical in the sense that practical values of beam current densities and drift velocities can be used to calculate the performance.

The Mathematical Problem

Consider the model described in the Introduction. Let the beams be designated as beams 1 and 2, and let the symbols pertaining to beams 1 and 2 carry the subscripts 1 and 2, respectively. Further, let

ρ = dc space-charge density of electrons

σ = ac space-charge density of electrons

u = dc velocity of electrons $\qquad$ E = ac electric field

v = ac velocity of electrons

$$\omega = \sqrt{\frac{4\pi e\rho}{m}} = \text{plasma frequency}$$

Let the velocities of both beams be directed in the x direction. Then the equations of motions of the electrons in the two beams are

$$\frac{\partial v_1}{\partial t} + u_1\frac{\partial v_1}{\partial x} = \frac{eE}{m} \qquad (1)$$

$$\frac{\partial v_2}{\partial t} + u_2\frac{\partial v_2}{\partial x} = \frac{eE}{m} \qquad (2)$$

The equations of continuity in the two beams are

$$\rho_1\frac{\partial v_1}{\partial x} + u_1\frac{\partial \sigma_1}{\partial x} + \frac{\partial \sigma_1}{\partial t} = 0 \qquad (3)$$

$$\rho_2\frac{\partial v_2}{\partial x} + u_2\frac{\partial \sigma_2}{\partial x} + \frac{\partial \sigma_2}{\partial t} = 0 \qquad (4)$$

Finally, the divergence theorem is $$\frac{\partial E}{\partial x} = 4\pi (\sigma_1 + \sigma_2) \tag{5}$$

This equation introduces the interaction between the two beams.

It should be noted that all second order terms have been dropped in the above equations.

Now assume that all the ac quantities are periodic in time with a frequency $\omega/2\pi$ and also assume that the space distribution of the ac quantities may be represented by $e^{i\Gamma x}$. Then the above questions become

$$j(\omega + \Gamma u_1) v_1 = \frac{eE}{m} \tag{6}$$

$$j(\omega + \Gamma u_2) v_2 = \frac{eE}{m} \tag{7}$$

$$\Gamma \rho_1 v_1 + (\omega + \Gamma u_1) \sigma_1 = 0 \tag{8}$$

$$\Gamma \rho_2 v_2 + (\omega + \Gamma u_2) \sigma_2 = 0 \tag{9}$$

$$j \Gamma E = 4\pi (\sigma_1 + \sigma_2) \tag{10}$$

This is a set of five equations in five unknowns. The condition that a solution to these equations exists is that the determinant of the coefficients of the unknowns vanishes. Setting the determinant equal to zero leads to a secular equation, which in this case is easily found to be

$$1 = \left(\frac{\omega_1}{\omega + \Gamma u_1} \right)^2 + \left(\frac{\omega_2}{\omega + \Gamma u_2} \right)^2 \tag{11}$$

This equation gives the values of Γ for which solutions to the set of equations (6)-(10) exist. Because the equation (11) is a quartic, there will be four possible values of Γ. Let these values be Γ_n; $n = 1, 2, 3, 4$. Then the ac quantities may be written

$$v_m = \sum_n a_{mn} e^{j\Gamma_n} \tag{12}$$

$$E = \sum_n b_n e^{j\Gamma_n} \tag{13}$$

$$\sigma_m = \sum_n c_{mn} e^{j\Gamma_n} \tag{14}$$

where a_{mn}, b_n, c_{mn} are constants. There are a total of 20 such constants. The equations (6)-(10) provide 16 relations between these constants. Hence, the number of arbitrary constants is four. The four arbitrary constants serve to match boundary conditions on the beams. For example, a likely set of boundary conditions arises as follows: Suppose that both beams are unmodulated to the left of $x = 0$; and that the first beam has impressed upon it a velocity variation v_{10} at $x = 0$. Then

the set of boundary conditions on the beams is

$$v_1 = v_{10} \quad ; x = 0 \qquad\qquad v_2 = 0 \quad ; x = 0$$

$$\sigma_1 = -\frac{\rho_1}{u_1} v_{10}; \; x = 0 \qquad\qquad \sigma_2 = 0 \quad ; x = 0$$

These four relations determine the four arbitrary constants.

The character of Γ_n is of particular interest. If all Γ_n are real quantities, a tube employing two beams will behave like a velocity-modulation tube of somewhat greater complexity than the usual modulation tube. If two of the Γ_n are zero and the remaining two are real, the tube will behave like a conventional velocity modulation tube. However, if one or more of the Γ_n are complex, there is a possibility that the waves typified by $e^{i(\omega t + \Gamma_n x)}$ may increase in amplitude with increasing x. As it turns out, if any one Γ_n is complex, another Γ_n is is conjugate. Hence, if any Γ_n is complex, a "growing-wave" will exist. The remainder of this paper is concerned with the circumstances under which there are complex Γ_n, and what their magnitudes are.

Because the solution of the secular equation (11) is straightforward but tedious, the solution has been relegated to Appendix A at the end of the paper. A summary of the results will suffice here:

The possible values of Γ depend on two parameters. These parameters involve the ratios of the dc velocities of the two beams and the ratios of the propagation constants in the two beams. The two parameters are

$$\alpha = \frac{\sqrt{\omega_1 \, \omega_2}}{\omega \, s} \qquad (15)$$

$$\beta = \sqrt{\frac{\omega_1}{u_1} \frac{u_2}{\omega_2}} \qquad (16)$$

where

$$s = \frac{1}{2}\left(\sqrt{\frac{u_1}{u_2}} - \sqrt{\frac{u_2}{u_1}}\right) \qquad (17)$$

$$\frac{\omega_n}{u_n} = \text{propagation constant in beam } n.$$

The values of Γ are $\Gamma_n = \frac{\omega}{\sqrt{u_1 \, u_2}}\left[\gamma_n s - \frac{1}{2}\left(\sqrt{\frac{u_1}{u_2}} + \sqrt{\frac{u_2}{u_1}}\right)\right]$

in which

$$\gamma_n = \begin{cases} -\sqrt{t_1} \pm (\sqrt{t_2} + \sqrt{t_3}) \\ +\sqrt{t_1} \pm (\sqrt{t_2} - \sqrt{t_3}) \end{cases} ; \beta^2 < 1$$

$$\gamma_n = \begin{cases} +\sqrt{t_1} \pm (\sqrt{t_2} - \sqrt{t_3}) \\ -\sqrt{t_1} \pm (\sqrt{t_2} + \sqrt{t_3}) \end{cases} ; \beta^2 > 1$$

$$t_n = Z_n + 1 - \mu$$

$$Z_n = \begin{cases} A + B \\ -\dfrac{A+B}{2} \pm \dfrac{A-B}{2}\sqrt{-3} \end{cases}$$

$$\left.\begin{matrix} A \\ B \end{matrix}\right\} = \frac{1}{2}\left\{(\mu^3 - \alpha^4) \pm \alpha^2\sqrt{\alpha^4 - 2\mu^3}\right\}^{1/3}$$

$$\mu = \frac{2}{3}\left[1 - \frac{\alpha^2}{4}\left(\beta^2 + \frac{1}{\beta^2}\right)\right]$$

The nature of Γ_n is investigated in Appendix B. In particular, it is shown that there are complex roots only if

$$\alpha^4 > 2\mu^3 \qquad (18)$$

The condition

$$\alpha^4 = 2\mu^3 \qquad (19)$$

gives the minimum value of $|\alpha|$ as a function of β for which complex roots exist. The relation between $|\alpha|$ and β is shown in Figure 1.

It is shown in Appendix B that, if $\alpha^4 > 2\mu^3$, $\sqrt{t_1}$ is real and $\sqrt{t_2}$ and $\sqrt{t_3}$ are complex conjugates. Hence, the difference between $\sqrt{t_2}$ and $\sqrt{t_3}$ may be written $\sqrt{t_2} - \sqrt{t_3} = i\,\gamma_i$. All other terms entering into Γ_n are phase factors. Hence, for purposes of investigating the rate of increase of a growing wave, an investigation of

$$\Gamma_i \equiv \frac{\omega}{\sqrt{u_1\,u_2}}\,\gamma_i\,s$$

or, in dimensionless terms, of

$$\sqrt{\frac{u_1\,u_2}{\omega_1\,\omega_2}}\,\Gamma_i = \frac{\gamma_i}{\alpha} \equiv X \qquad (20)$$

will suffice.

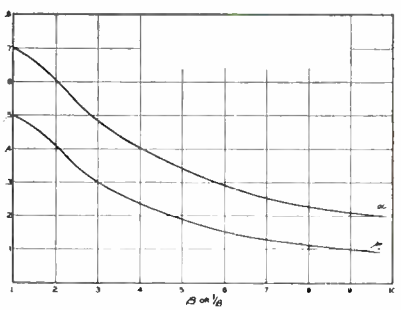

Fig. 1—Minimum value of α for which complex roots exist and the corresponding μ.

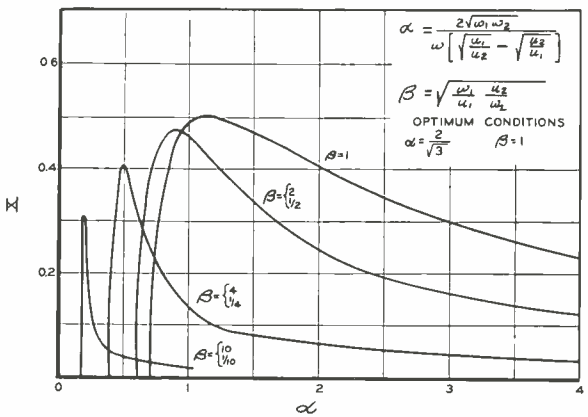

Fig. 2—Gain factor vs. α.

The behavior of X as a function of α for various values of β has been computed and is shown in Figure 2.

Gain and Bandwidth

In this section, formulas for the gain and electronic bandwidth of the model will be derived and expressed in practical terms. Having obtained these formulas, it will be possible to discuss the gain and bandwidth of model tubes with practical current densities and voltages.

First consider the gain of the model. The convection current density may be used as a measure of the gain. In accordance with equations (12) and (13), the convection-current density in beam 1 may be written $\psi_1 = \rho_1 v_1 + u_1 \sigma_1 = \sum_n (\rho_1 a_{1n} + \sigma_1 c_{1n})\, e^{j\Gamma_n x}$. Suppose a pair of the Γ_m, say Γ_1 and Γ_2, are complex conjugates of the form $\Gamma_1 = \Gamma_r \pm j\Gamma_i$ and the other pair are real. Then, if the tube is of substantial length, the term having the factor $e^{(j\Gamma_r + \Gamma_i)x}$ will far outweigh the other terms and ψ_1 may be written approximately

$$\psi_1 = (\rho_1 a_{21} + \sigma_1 c_{21})\, e^{(j\Gamma_r + \Gamma_i)x}.$$

The power output obtainable from the tube at x is measured by

$$\psi_1 \psi_1^* = |\rho_1 a_{21} + \sigma_1 c_{21}|^2\, e^{2\Gamma_i x}.$$

Hence, the gain of the model per unit length is

$$G = 10 \log \frac{\psi_1 (x+1)\, \psi_1^* (x+1)}{\psi_1 (x)\, \psi_1^* (x)} = 8.686\, \Gamma_i$$

$$= 8.686 \sqrt{\frac{\omega_1 \omega_2}{u_1 u_2}}\, X \text{ decibels per centimeter} \qquad (21)$$

where X is the function shown in Figure 2. For practical purposes, it

is convenient to have ω_n/u_n expressed in terms of the current density in the beam and of the electron velocity in volts. The required relation is

$$\frac{\omega_n}{u_n} = 3.09 \times 10^2 \sqrt{\frac{j_n}{V_n^{3/2}}} \tag{22}$$

where j_n = current density in amperes per square centimeter
V_n = beam velocity in volts.

For purposes of subsequent computation, it is worthwhile to note some further relations in the same terms and units

$$\omega_n = 1.85 \times 10^{10} \sqrt{\frac{j_n}{V_n^{1/2}}} \tag{23}$$

$$\alpha = \frac{3.70 \times 10^{10} \sqrt{\dfrac{j_1}{V_1^{1/2}}}}{\omega \sqrt{\dfrac{j_1}{j_2}\left(\dfrac{V_2}{V_1}\right)^{3/2}\left[\sqrt{\dfrac{V_1}{V_2}} - 1\right]}} \tag{24}$$

$$\beta = \sqrt{\frac{j_1}{j_2}\left(\frac{V_2}{V_1}\right)^{3/2}} \tag{25}$$

When $\alpha = 2\sqrt{3}$ and $\beta = 1$, the ratio of voltages is given by

$$\left|\sqrt{\frac{V_1}{V_2}} - 1\right| = \frac{3.20 \times 10^{10}}{\omega} \sqrt{\frac{j_1}{V_1^{1/2}}}. \tag{26}$$

It is interesting to note that relation (25) shows that if j_1 and j_2 are obtained from planar "diodes" of the same spacing or, more generally, from diodes of the same perveance per unit area, then $\beta = 1$ whatever the voltages V_1 and V_2.

Because the gain is proportional to X, the general behavior of the gain as a function of the parameters α and β is immediately apparent. X has a maximum value of one-half when $\alpha = 2/\sqrt{3}$ and $\beta = 1$. For each value of β, the gain falls off slowly from the maximum in the direction of increasing α, and quite abruptly in the direction of de-

creasing α. The more β departs from unity, the lower is the maximum value of gain and the more rapidly the gain falls as α departs from the optimum value. The variation in gain with α, particularly the variation with ratio of velocities, may portend a certain criticalness in the adjustment of the beam voltages. The logarithmic rate of change of α with $\frac{u_1}{u_2}$ is

$$\epsilon \equiv \frac{1}{\alpha}\frac{d\alpha}{d\left(\frac{u_1}{u_2}\right)} = -\frac{1}{2}\sqrt{\frac{u_2}{u_1}}\,\frac{\frac{u_1}{u_2}+1}{\frac{u_1}{u_2}-1}. \tag{27}$$

If u_1/u_2 is near unity, as it well may be in a practical case, the variation of gain with variations in either or both of the beam velocities will be quite marked. The rate of variation of α with $\sqrt{\omega_1\,\omega_2}$ is much less rapid than the variation with u_2/u_1, and the variation with ω is a measure of the bandwidth.

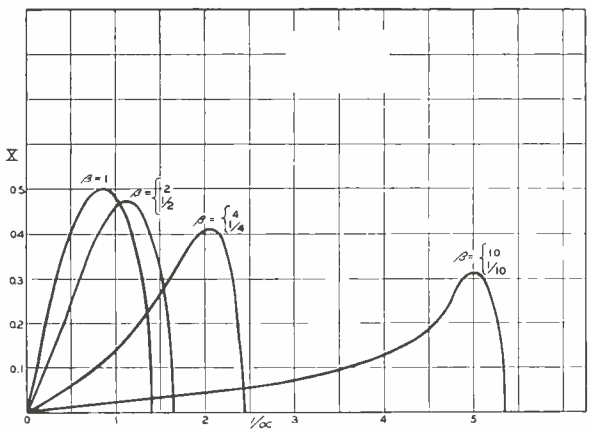

Fig. 3—Gain factor vs. $1/\alpha$.

Consider the bandwidth of the model, i.e., the variation of X as α is varied by varying ω. For this purpose, it is convenient to have X plotted as a function of ω or as a function of $1/\alpha$, which is directly proportional to ω. Such a plot is shown in Figure 3. The curves are asymmetrical about their maxima. However, near the maxima, the curves are very nearly parabolic. Within the accuracy of the present computations, the behavior of X with $1/\alpha$ may be represented by

$$X = X_{\max} - 0.805\,[(1/\alpha) - (1/\alpha_m)]^2 \tag{28}$$

in the neighborhood of a maximum; where α_m is the α corresponding to $X_{\max}$. This formula holds approximately for all four curves shown in Figure 3. Hence, it will be assumed that it holds for all values of β. Let

$$\omega = \omega_m + \Delta\omega/2 \tag{29}$$

where ω_m is the ω corresponding to $X_{\max}$ and $\Delta\omega$ is the bandwidth. Substituting equation (29) in equation (28) gives

$$X = X_{\max} - 0.805\left(\frac{\Delta\omega s}{2\sqrt{\omega_1\,\omega_2}}\right)^2$$

Hence, the total gain in db is

$$g = 8.686\sqrt{\frac{\omega_1\,\omega_2}{u_1\,u_2}}\,l\left[X_{\max} - 0.805\left(\frac{\Delta\omega s}{2\sqrt{\omega_1\,\omega_2}}\right)^2\right]$$

where l is the length of the interaction space. Because $\Delta\omega$ was defined as the bandwidth,

$$6.99\sqrt{\frac{\omega_1\,\omega_2}{u_1\,u_2}}\,l\left(\frac{\Delta\omega s}{2\sqrt{\omega_1\,\omega_2}}\right)^2 = 3\text{ db}$$

or

$$\Delta\omega = 1.31\sqrt{\frac{1}{l}\sqrt{\frac{u_1\,u_2}{\omega_1\,\omega_2}}\,\frac{\sqrt{\omega_1\,\omega_2}}{s}}. \tag{30}$$

This formula may be put in a more lucid form by expressing the fractional bandwidth in terms of the maximum gain.

$$\frac{\Delta\omega}{\omega_m} = 3.86\,\frac{\alpha_m\sqrt{X_{\max}}}{\sqrt{g_{\max}}}. \tag{31}$$

Hence the fractional bandwidth varies inversely as the square root of the total gain. The variation of bandwidth with β is shown in Figure 4. The bandwidth decreases rapidly as β departs from the optimum value of unity.

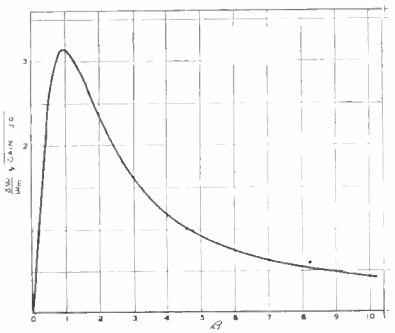

Fig. 4—Bandwidth vs. β.

Examples

Some examples will now be considered. In all of these examples it will be assumed that $\alpha = 2\sqrt{3}$ and $\beta = 1$, i.e., that optimum conditions obtain.

Example 1

An early traveling-wave tube was reported to operate at 3000 Mc with a current density of about 0.050 amperes per square centimeter and with a beam voltage of 1600 volts. The reported gain was 1.14 db per centimeter length of tube. It is interesting to compare the gain of a two-beam tube operating at the same total current and the same average voltage. To this end, let

$$j_1 = 0.025 \text{ ampere per square centimeter}$$
$$V_1 = 1600 \text{ volts}$$
$$\omega = 1.88 \times 10^{10} \text{ radians per second.}$$

The gain is then $G = 1340\sqrt{\dfrac{j_1}{V_1^{3/2}}} = 0.84$ decibels per centimeter.

The voltage ratio is $\dfrac{V_1}{V_2} = 1.087$

and j_2 is $j_2 = j_1\left(\dfrac{V_2}{V_1}\right)^{3/2} = 0.022$ amperes per square centimeter.

Hence, the gain of the growing-wave tube is substantially less than the gain of the traveling-wave tube. It is also interesting to compute the stability factor ϵ as given by equation (26).

$$\epsilon = -\frac{1}{2}\left(\frac{V_1}{V_2}\right)^{1/4}\frac{\sqrt{\dfrac{V_1}{V_2}}+1}{\sqrt{\dfrac{V_1}{V_2}}-1} = -\frac{1}{1.0426-1} = -23.5.$$

Hence a 2 percent change in the voltage ratio will result in a 24 percent change in α. This is a rather drastic change. An increase of a few percent in the voltage ratio V_1/V_2 would considerably reduce the gain. An examination of equation (25) shows that the stability requirement becomes more severe as the frequency increases and less severe as the ratio $j_1 V_1^{1/2}$ increases. As usual, an increase in current density pays dividends. It is obvious that the ratio of V_1 to V_2 may be held fixed by deriving both voltages from a common voltage source.

If the tube is assumed to be 30 cm long, the total gain will be 25.2 db. According to equation (31), the fractional bandwidth will be $\Delta\omega/\omega_m = 0.627$ and the actual bandwidth will be $\Delta\omega = 1880$ Mc. It seems likely that usable bandwidth will be determined by the circuitry at the input and output "terminals" of the beams.

Example 2

As an example of what might be done in a practical tube, let

$$j_1 = 0.100 \text{ amperes per square centimeter}$$

$$V_1 = 500 \text{ volts}$$

$$\omega = 1.88 \times 10^{10} \text{ radians per second}$$

These values are reasonable for a tube 30 cm long. In this case, the gain is $G = 1340 \sqrt{\dfrac{j_1}{V_1^{3/2}}} = 4.0$ decibels per centimeter

The voltage ratio is $\dfrac{V_1}{V_2} = 1.240$

The current density in the second beam is

$$j_2 = 0.072 \text{ amperes per square centimeter}$$

The stability factor is $\epsilon = -8.80$

The use of the higher current density and lower voltage makes a marked improvement over the results in the previous example, with regard to both gain and stability. The gain in this case looks quite encouraging. Before the results are viewed in too optimistic a light, it is well to recall the remarks in the introduction which point out that the present model neglects dc space charge effects and fringing at the edges of the beam, both to other parts of the beam and to any enclosing metallic structure. All of these effects will probably tend to reduce the theoretical gain. There is a possibility that the distribution in velocities

resulting from space-charge depression of the voltage at the center of each of the beams may enhance the contributions to the gain of certain velocity groups. By the same token, certain other groups may load the useful parts of the beams. Whether the result is a net gain or loss is a matter of conjecture at the moment.

If this tube is also made 30 cm long, the total theoretical gain is 120 db and the bandwidth is 860 Mc.

Conclusion

The present model of the two-beam growing-wave tube suggests the possibility of obtaining very considerable power gains from such a tube. As has been pointed out, these estimates of gain must be tempered by the knowledge that the present model is not physically realizable Theoretical models which more closely resemble physically realizable tubes will no doubt be forthcoming. In the meantime, the present theory provides a rough guide to the design of practical structures.

Acknowledgment

The writer gratefully acknowledges the benefit derived from numerous discussions of this subject with D. O. North and C. W. Hansell.

APPENDIX A

Solution of the Secular Equation

The secular equation to be solved for Γ is

$$1 = \left(\frac{\omega_1}{\omega + \Gamma u_1} \right)^2 + \left(\frac{\omega_2}{\omega + \Gamma u_2} \right)^2 \tag{32}$$

This is a quartic in Γ and can be solved by Euler's method.[2] To reduce the equation to standard form, let

$$r = \frac{1}{2}\left(\sqrt{\frac{u_1}{u_2}} + \sqrt{\frac{u_2}{u_1}} \right) \tag{33}$$

$$s = \frac{1}{2}\left(\sqrt{\frac{u_1}{u_2}} - \sqrt{\frac{u_2}{u_1}} \right) \tag{34}$$

$$\alpha = \frac{\sqrt{\omega_1 \omega_2}}{\omega s} \tag{35}$$

$$\beta = \sqrt{\frac{\omega_1}{u_1}\frac{u_2}{\omega_2}} \tag{36}$$

[2] See, for example, Webster Wells, ADVANCED COURSE IN ALGEBRA, Heath and Co., New York, N. Y., 1904.

$$\gamma = \frac{\sqrt{u_1 u_2}}{\omega s}\Gamma + \frac{r}{s} \qquad (37) \qquad X = \sqrt{\frac{u_1 u_2}{\omega_1 \omega_2}}\Gamma_i \qquad (38)$$

Then the secular equation becomes $$1 = \left(\frac{\alpha\beta}{\gamma - 1}\right)^2 + \left(\frac{\alpha\beta}{\gamma + 1}\right)^2 \qquad (39)$$

This equation contains an unknown, γ; and two arbitrary parameters, α and β. The parameters, α and β, will determine the nature of the roots of the equation. On expansion, (39) becomes

$$\gamma^4 - \gamma^2\left[2 + \alpha^2\left(\beta^2 + \frac{1}{\beta^2}\right)\right] - 2\gamma\left[\alpha^2\left(\beta^2 - \frac{1}{\beta^2}\right)\right] + \left[1 - \alpha^2\left(\beta^2 + \frac{1}{\beta^2}\right)\right] = 0 \qquad (40)$$

This is of the form $\gamma^4 - a\gamma^2 + b\gamma + c = 0$

where $$a = -\left[2 + \alpha^2\left(\beta^2 + \frac{1}{\beta^2}\right)\right] \qquad (41)$$

$$b = -2\alpha^2\left(\beta^2 - \frac{1}{\beta^2}\right) \qquad (42) \qquad c = 1 - \alpha^2\left(\beta^2 + \frac{1}{\beta^2}\right) \qquad (43)$$

The auxiliary cubic is $$t^3 + \frac{a}{2}t^2 + \frac{a^2 - 4c}{6}t - \frac{b^2}{64} = 0 \qquad (44)$$

Substituting the values of a and b in the cubic gives

$$t^3 - \left[1 + \frac{\alpha^2}{2}\left(\beta^2 + \frac{1}{\beta^2}\right)\right]t^2 + \frac{1}{2}\alpha^2\left(\beta^2 + \frac{1}{\beta^2} - 1\right) + \frac{\alpha^2}{8}\left(\beta^2 + \frac{1}{\beta^2}\right)\Bigg]t - \frac{1}{16}\alpha^4\left(\beta^2 - \frac{1}{\beta^2}\right)^2 = 0. \qquad (45)$$

The cubic may be reduced to standard form by the substitution

$$t = Z + \frac{1}{3}\left[1 + \frac{\alpha^2}{2}\left(\beta^2 + \frac{1}{\beta^2}\right)\right] \qquad (46)$$

The result is

$$Z^3 - \frac{1}{3}\left[1 - \frac{\alpha^2}{4}\left(\beta^2 + \frac{1}{\beta^2}\right)\right]^2 Z + \frac{2}{27}\left\{\frac{27}{8}\alpha^4 - \left[1 - \frac{\alpha^2}{4}\left(\beta^2 + \frac{1}{\beta^2}\right)\right]^3\right\} = 0 \qquad (47)$$

The notation may be simplified further by writing

$$\mu = \frac{2}{3}\left[1 - \frac{\alpha^2}{4}\left(\beta^2 + \frac{1}{\beta^2}\right)\right] \qquad (48)$$

Then the cubic becomes

$$Z^3 - \frac{3}{4}\mu^2 Z + \frac{1}{4}[\alpha^4 - \mu^3] = 0. \qquad (49)$$

This equation may be solved by Cardan's method. The result is

$$Z_{\substack{1\\2\\3}} = \begin{cases} A + B \\ -\dfrac{A+B}{2} \pm \dfrac{A-B}{2}\sqrt{-3} \end{cases} \qquad (50)$$

where

$$\left.\begin{matrix} A \\ B \end{matrix}\right\} = \frac{1}{2}\{|\mu^3 - \alpha^4| \pm \alpha^2\sqrt{\alpha^4 - 2\mu^3}\}^{1/3}. \qquad (51)$$

The corresponding values of t are

$$t_{\substack{1\\2\\3}} = Z_{\substack{1\\2\\3}} + 1 - \mu \qquad (52)$$

Then the roots of the quartic are $\gamma_n = \begin{cases} -\sqrt{t_1} \pm (\sqrt{t_2} + \sqrt{t_3}) \\ +\sqrt{t_1} \pm (\sqrt{t_2} - \sqrt{t_3}) \end{cases}$ (53)

when $\beta^2 < 1$

and

$$\gamma_n = \begin{cases} \sqrt{t_1} \pm (\sqrt{t_2} + \sqrt{t_3}) \\ -\sqrt{t_1} \pm (\sqrt{t_2} - \sqrt{t_3}) \end{cases} \qquad (54)$$

when $\beta^2 > 1$.

An examination of equation (44) reveals an interesting special case. It will be noted that when $\beta = 1$, one of the roots, say t_1, is zero.

The other roots are obviously $$t_{\frac{2}{3}} = \frac{1}{2}[1 + \alpha^2 \pm \sqrt{1 - 2\alpha^2}]. \tag{55}$$

Hence, the roots of the

quartic in γ are $$\gamma_n = \pm [(1 + \alpha^2) \pm \alpha \sqrt{4 + \alpha^2}]^{1/2}. \tag{56}$$

One pair of roots is imaginary when $$\alpha \sqrt{4 + \alpha^2} \geq 1 + \alpha^2$$

i.e., when $$|\alpha| \geq 1/\sqrt{2}.$$

Because of the simplicity of this case, it is possible to maximize X

$$X = \frac{\gamma_i}{\alpha} = \frac{1}{\alpha}[\alpha \sqrt{4 + \alpha^2} - (1 + \alpha^2)]^{1/2}; \alpha > \frac{1}{\sqrt{2}}.$$

It is found that the maximum value of X_i is $1/2$ and occurs when $|\alpha| = 2/\sqrt{3}$. Subsequent computation shows that no other choice of α and β yields a higher value of X.

In the case when $\alpha = 2/\sqrt{3}$ and $\beta = 1$, a simple relation between the operating frequency and the plasma frequencies may be found. This is

$$\frac{\sqrt{3}}{\omega} = \left| \frac{1}{\omega_1} - \frac{1}{\omega_2} \right| \tag{57}$$

APPENDIX B

The Nature of the Roots of the Secular Equation

The computation of the roots of a quartic equation is laborious under the best of circumstances. Because the roots of the present quartic are functions of two parameters, the computation of the roots over the entire ranges of the two parameters could be quite time-consuming. To reduce the amount of computation to a minimum, it is advantageous to explore the nature of the roots as far as possible without resort to computation. In particular, it is advantageous to determine over what ranges of the parameters α and β the roots of the quartic are complex.

First consider the cubic (45). All the coefficients are real. Therefore, the roots may be

Case 1.) All real

Case 2.) One real; two, complex conjugates.

Because the last coefficient on the right of (45) is negative, the two cases above may be further specified.

Case 1.) All roots real; one positive, the others with the same sign.

Case 2.) One root real and positive; the others, complex conjugates.

It would greatly simplify matters, if one of these cases could be shown to be of no interest, i.e., if it could be shown that it does not lead to complex roots for γ. Case 1. seems most promising in this regard.

To show that Case 1. is of no interest, it is necessary to show that in this case all of the roots are positive. Consider equations (49) and (52):

$$Z^3 - \frac{3}{4}\mu^2 Z + \frac{1}{4}|\alpha^4 - \mu^3| = 0 \tag{49}$$

$$t_n = Z_n + 1 - \mu; \; n = 1, 2, 3. \tag{52}$$

It is obvious that $t_n \geqslant 0$ if $Z_n \geqslant \mu - 1$. (58)

The discriminant of (49) is $\alpha^4 - 2\mu^3$. The condition that all the roots be real is that the discriminant be negative, i.e., that

$$0 < \alpha^4 < 2\mu^3. \tag{59}$$

Consider the function $Y = Z^3 - \frac{3}{4}\mu^2 Z + \frac{1}{4}|\alpha^4 - \mu^3|$. (60)

It has stationary values when $Z = \pm \mu/2$, approaches $+\infty$ when Z approaches $+\infty$, and approaches $-\infty$ when Z approaches $-\infty$. Therefore, its general character is as shown in Figure 5. An examination of (48) shows that μ cannot exceed 2/3. It follows that $\mu - 1$ lies to the left of $-\mu/2$ in the sketch. Substitute $Z = \mu - 1$ in (59). The result is

$$Y_1 = -\left[1 - 3\mu + \frac{9}{4}\mu^2\right] + \frac{\alpha^4}{4} \tag{61}$$

By eliminating μ through the use of (48), this may be reduced to

$$Y_1 = -\frac{\alpha^4}{4}\left[\frac{1}{4}\left(\beta^2 + \frac{1}{\beta^2}\right)^2 - 1\right] \tag{62}$$

The minimum value of $\beta^2 + 1/\beta^2$ is 2. Hence, Y_1 is negative and all the roots of $Y = 0$ exceed $\mu - 1$, except in the limiting case $\beta = 1$, when one root may equal $\mu - 1$.

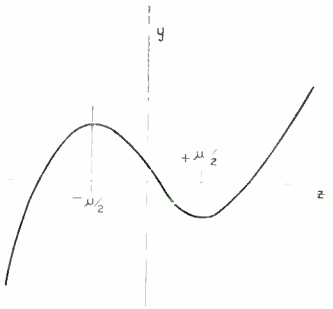

Fig. 5—General character of Equation (60).

Therefore, γ cannot be complex in Case 1, i.e., when

$$0 < \alpha^4 < 2\,\mu^3 \tag{59}$$

Now consider Case 2 in which one root is real and positive and the remaining pair are complex conjugates. The real positive root cannot contribute to an imaginary term in γ, so it remains to examine the complex roots. The complex roots occur when the discriminant is positive, i.e., when $\alpha^4 > 2\,\mu^3$. (63)

Suppose the complex roots are $Z_{\frac{2}{3}} = \mu\,(a \pm ib)$. (64)

Then, $\gamma_{\frac{2}{3}} = 1 - \mu + \mu\,(a \pm ib) = 1 - \mu\,(1 - a) \pm i\mu b = C \pm iD$ (65)

and $$\sqrt{\gamma_{\frac{2}{3}}} = \sqrt{\frac{1}{2}\left[\sqrt{C^2 + D^2} + C\right]} \pm i\sqrt{\frac{1}{2}\left[\sqrt{C^2 + D^2} - C\right]}. \tag{66}$$

It is the term $$\gamma_i = 2\sqrt{\frac{1}{2}\left[\sqrt{C^2 + D^2} - C\right]}. \tag{67}$$

which is of particular interest in the present problems.

The Cases 1 and 2 are separated by the critical case in which the discriminant vanishes, i.e., $\alpha^4 = 2\mu^3$. (68)

This is the condition that all the roots be real and two of them equal.

Because equation (68) sets a lower limit to the values of α for which complex roots exist, it is of interest to compute the values of α which satisfy this relation in terms of β, the other primary parameter. The results of this computation are shown in Figure 1.

RELATION BETWEEN AMPLITUDE AND PHASE IN ELECTRICAL NETWORKS*†

By

T. Murakami and Murlan S. Corrington

Home Instrument Department, RCA Victor Division, Camden, N. J.

Summary—*A simple graphical method is presented for computing the phase curve from a given amplitude characteristic, and the attenuation characteristic from a given phase curve in a minimum phase shift network. The effect of any change in one characteristic on the other can be computed directly. A large number of universal curves are given, to simplify the application of the theory.*

Introduction

FOR many years the relations that are satisfied by most passive electric networks have been known. In early papers, Campbell[1] and Foster[2] showed that, in a network composed of a finite number of self-inductances, mutual inductances, and capacities, the impedance is a pure reactance with a number of resonant and anti-resonant frequencies which alternate with each other. For every impedance the reactance increases with the frequency, except for the discontinuities which carry it back from a positive infinite value to a negative infinite value at the anti-resonant points. They obtained formulas for the design of such networks, and showed that the free oscillations of the system were equivalent to the dynamical problem of the small oscillations of a system about a position of equilibrium, with no frictional forces acting.[3]

Soon after this, Carson[4] recognized the relations between the real and imaginary parts of the impedance of a network which includes

---

* Decimal Classification: R140.

† A substantial part of this paper was presented by T. Murakami as a thesis in partial fulfillment of the requirement of a Masters Degree at the Moore School of Electrical Engineering, University of Pennsylvania.

[1] George A. Campbell, "Physical Theory of the Electric Wave Filter," *Bell Sys. Tech. Jour.*, Vol. 1, pp. 1-32, November, 1922.

[2] Ronald M. Foster, "A Reactance Theorem," *Bell Sys. Tech. Jour.*, Vol. 3, pp. 259-267, April, 1924.

[3] E. J. Routh, ADVANCED RIGID DYNAMICS (sixth edition), Cambridge University Press, London, 1905 (pp. 44-55).

[4] John R. Carson, ELECTRIC CIRCUIT THEORY AND THE OPERATIONAL CALCULUS, McGraw-Hill Book Company, Inc., New York, N. Y., 1926 (p. 180).

dissipation and showed that the behaviour of a network under all circumstances is completely determined if either the real or imaginary component of the complex steady state admittance is specified over the entire frequency range. Bush[5] obtained similar results.

In 1925, H. A. Kramers[6] obtained relations between the real and the imaginary parts of the coefficient of polarization of the atom for incident rays, in the form of integral transformations which made it possible to compute either one from the other. He pointed out that this coefficient behaves like an analytic function of frequency and that the results were supported by the experimental work of van der Plaats[7] with colored liquids. The application to the atomic absorption coefficient and the index of refraction of X-rays was made by Kronig[8] and by Kallman and Mark[9].

Further studies led to a statement of the necessary conditions that must be satisfied by the impedance function of a passive network, the properties of positive real functions, and a method for synthesis of networks[10].

The results obtained by Carson[1] and Bush[5] were used by Lee[11] to show that the conductance and susceptance of the admittance of a network are Hilbert transforms or conjugate integrals of each other. He used these transforms to compute one from the other, and also established relations between the modulus and the phase of an admittance function. Additional relations were obtained by Bayard[12]. He discussed the minimum reactance requirements and the physical meaning of the fact that the integral transforms include an arbitrary

---

[5] Vannevar Bush, OPERATIONAL CIRCUIT ANALYSIS, John Wiley & Sons, Inc., New York, N. Y., 1929 (p. 180).

[6] H. A. Kramers, "La Diffusion de la Lumière par les Atomes," Atti del Congresso Internazionale dei Fisici, Sept. 11-20, 1927, Como-Pavia-Roma, Vol. 2, Nicola Zanichelli, Bologna, 1928 (pp. 545-557).

[7] Bern. J. van der Plaats, "Untersuchung über Absorption und Dispersion des Lichtes in Farbstofflösungen," *Annalen der Physik*, Ser. 4, Vol. 47, pp. 429-462, July, 1915.

[8] R. de L. Kronig, "On the Theory of Dispersion of X-rays," *Jour. Opt. Soc. Amer.*, Vol. 12, pp. 547-557, June, 1926.

[9] H. Kallman and H. Mark, "Über die Dispersion und Streuung von Röntgenstrahlen," *Annalen der Physik*, Ser. 4, Vol. 82, pp. 585-604, March, 1927.

[10] Otto Brune, "Synthesis of a Finite Two-terminal Network whose Driving-point Impedance is a Prescribed Function of Frequency," *Jour. Math. and Phys.* (M.I.T.), Vol. 10, pp. 191-236, 1930-1931.

[11] Y. W. Lee, "Synthesis of Electric Networks by Means of the Fourier Transforms of Laguerre's Functions," *Jour. Math. and Phys.* (M.I.T.), Vol. 11, pp. 83-113, 1931-1932.

[12] M. Bayard, "Relations Entre les Parties Réelles et Imaginaires des Impédances et Détermination des Impédances en Fonction de l'une des Parties," *Revue Générale de l'Électricité*, Vol. 37, No. 21, pp. 659-664, May 25, 1935.

constant. Leroy[13] and Guillemin[11] discussed the fact that arbitrary assumptions of independent amplitude and phase characteristics of an ideal filter lead to inconsistencies, and the solution for such a circuit may respond before the disturbing force is applied.

Work continued in other branches of physics, and Gorter and Kronig[15-17] obtained relations between the real and imaginary parts of the dielectric constant and of the permeability. Similar relations between sound absorption and dispersion in fluids and gases were obtained by Kneser[18].

Some further results for electrical circuits were stated by van der Pol[19], and Cauer[20,21] discussed the theory from the complex variable theory. Up to this point there were few actual solutions of the integrals, and few applications to practical engineering problems. Bode applied the results to the design of amplifiers[22,23] and later in his book[24] he gave many more pairs of solutions and a graphical method for solving such problems. Since the solution of such problems requires the use

---

[13] R. Leroy, "Relationship Between Attenuation and Phase of a Linear Transmission System," *Annales des Postes, Télégraphes et Téléphones*, Vol. 24, No. 8, pp. 733-740, August, 1935.

[14] E. A. Guillemin, COMMUNICATION NETWORKS (Vol. II), John Wiley & Sons, New York, N. Y., 1935 (pp. 480, 501-04).

[15] C. J. Gorter and R. de L. Kronig, "On the Theory of Absorption and Dispersion in Paramagnetic and Dielectric Media," *Physica*, Vol. 3, pp. 1009-1020, 1936.

[16] C. J. Gorter, "Paramagnetische Dispersion und Absorption," *Zeitschrift für Technische Physik*, Vol. 19, pp. 501-509, 1938. Also, *Physikalische Zeitschrift*, Vol. 39, pp. 815-823, December, 1938.

[17] R. de L. Kronig, "Zur Theorie der Relaxationserscheinungen," *Zeitschrift für Technische Physik*, Vol. 19, pp. 509-516, 1938. Also, *Physikalische Zeitschrift*, Vol. 39, pp. 823-830, December, 1938.

[18] H. O. Kneser, "Die Akustischen Relaxationserscheinungen," *Zeitschrift für Technische Physik*, Vol. 19, pp. 486-492, 1938. Also, *Physikalische Zeitschrift*, Vol. 39, pp. 800-806, December, 1938.

[19] Balth. van der Pol, "Discontinuous Phenomena in Radio Communication," *Jour. Inst. Elec. Eng.*, Vol. 81, pp. 381-398, 1937.

[20] W. Cauer, "The Poisson Integral for Functions with Positive Real Part," *Bull. Amer. Math. Soc.*, Vol. 38, pp. 713-717, October, 1932.

[21] W. Cauer, "Das Poissonsche Integral und seine Anwendungen auf die Theorie der Linearen Wechselstromschaltungen (Netzwerke)," *Elektrische Nachrichten-Technik*, Vol. 17, No. 1, pp. 17-30, January, 1940.

[22] Hendrik W. Bode, United States Patent 2,123,178, July 12, 1938.

[23] H. W. Bode, "Relations Between Attenuation and Phase in Feedback Amplifier Design," *Bell Sys. Tech. Jour.*, Vol. 19, pp. 421-454, July, 1940.

[24] Hendrik W. Bode, "NETWORK ANALYSIS AND FEEDBACK AMPLIFIER DESIGN", D. van Nostrand Company, Inc., New York, N. Y., 1945 (Chapters 13, 14, 15).

of the theory of integral equations, Gross[25], Gama[26], and Levi[27] discussed the solution of such equations, the inversion of the integrals, and the derivatives of the functions, as well as the application to the conductance and capacitance of a capacitor[28-30]. Gross has given an English summary[31] of papers[25-27]. Since many authors apparently did not fully appreciate the fact that these equations apply to most linear systems of physics, Takahasi[32] reviewed several of the above papers and showed that the results have analogs in many branches of physics. In a recent paper[33] he considers the problem of making a given linear unstable system stable by coupling it to a second circuit, using the results of the first paper. Fränz[34] has generalized the Foster reactance theorem to arbitrary impedances and a recent article by Antokoljskij[35] reviews the transformation equations. A paper by Gross[36] discusses the relations between loss factor and storage factor in the theory of elasticity.

Since these integral relations between the components apply to nearly all systems where there is a linear relation between cause and effect and where the constants do not change with time, the integrals

---

[25] B. Gross, "Sobre uma Transformação Integral que Interessa a' Eletrotecnica," *Annaes da Academia Brasileira de Sciencias, Rio de Janeiro*, Vol. 13, No. 1, pp. 31-50, 1941. Part II, *Anais da Academia Brasileira de Ciencias*, Vol. 13, No. 3, pp. 163-164, 1941.

[26] Lelio I. Gama, "Nota Sobre a Integral Impropria $\int_0^{+\infty} \frac{B(\alpha)\,d\alpha}{\omega^2 - \alpha^2}$," *Annaes da Academia Brasileira de Sciencias, Rio de Janeiro*, Vol. 13, No. 1, pp. 51-55, 1941.

[27] Beppo Levi, "Sobre una Transformación Integral," *Anais da Academia Brasileira de Ciencias, Rio de Janeiro*, Vol. 13, No. 3, pp. 185-194, 1941.

[28] B. Gross, "On the Theory of Dielectric Loss," *Phys. Rev.*, Vol. 59, pp. 748-750, May 1, 1941.

[29] Robert H. Cole, "Correlations in Dielectric Data," (Abstract) *Phys. Rev.*, Vol. 60, p. 172, July 15, 1941.

[30] H. Silva and B. Gross, "Some Measurements on the Validity of the Principle of Superposition in Solid Dielectrics," *Phys. Rev.*, Vol. 60, pp. 684-687, Nov. 1, 1941.

[31] Bernard Gross, "On an Integral Transformation of General Circuit Theory," *Amer. Math. Monthly*, Vol. 50, pp. 90-93, 1943.

[32] Hidetosi Takahasi, "Über die Beziehungen Zwischen dem Reellen und dem Imaginären Teil einer Frequenzabhängigen Komplexen Grösse," *Proc. Physico-Math. Soc., Japan*, Ser. 3, Vol. 24, pp. 63-75, January, 1942.

[33] Hidetosi Takahasi, "Das Problem der Stabilisierung," *Proc. Physico-Math. Soc., Japan*, Ser. 3, Vol. 24, pp. 412-433, 1942.

[34] Kurt Fränz, "Eine Verallgemeinerung des Fosterschen Reaktanztheorems auf Beliebige Impedanzen," *Elektrische Nachrichten-Technik*, Vol. 20, pp. 113-115, May, 1943.

[35] M. L. Antokoljskij, "On the Relation Between Frequency and Phase Characteristics," *Jour. Tech. Phys., U.S.S.R.*, Vol. 17, No. 2, pp. 203-210, 1947. (In Russian).

[36] B. Gross, "On Creep and Relaxation, II," *Jour. Appl. Phys.*, Vol. 19, pp. 257-264, March, 1948.

will be evaluated for a large number of cases to facilitate the practical applications.

Bode* gives a graphical technique for finding the imaginary component when the real component of a network function is known. This paper will extend his results, and add the inverse problem, the graphical computation of the real component when the imaginary component is given.

The general expression for a network function, which may be an input impedance or admittance, a transfer impedance or admittance, or many other network functions, can be written as the ratio of two polynominals, as shown by Equation (1),

$$\theta = \frac{A_m p^m + A_{m-1} p^{m-1} + \cdots + A_1 p + A_o}{B_n p^n + B_{n-1} p^{n-1} + \cdots + B_1 p + B_o} \tag{1}$$

whenever the tubes, network elements, and wiring can be considered to obey a lumped-constant analysis. The immittance (a word which means either impedance or admittance), θ, is a rational function of $p = i\omega$, where ω is the angular frequency, and is used to represent any network function which can be written in the complex form $A + iB$, where A and B may be functions of frequency. In the factored form the equation can be rewritten as

$$\theta = \frac{A_m (p - a_1)(p - a_2) \cdots (p - a_m)}{B_n (p - b_1)(p - b_2) \cdots (p - b_n)} \tag{2}$$

where $a_1, a_2, \cdots a_m$ are the zeros and $b_1, b_2, \cdots b_n$ are the poles of the function θ.

Properties of Input Immittance

In order that Equation (2) represent a physically realizable and stable network, certain restrictions on θ are necessary. Since the coefficients $A_o, \cdots A_m$ and $B_o, \cdots B_n$ are determined by the differential equations for the meshes and nodes of the network, they are functions of R, L, and C and hence must be real constants, but not necessarily positive; negative quantities can be synthesized by appropriate vacuum-tube circuits. Because they are constants, this restricts the following discussion to linear systems. By the ordinary rules for algebraic equations with real coefficients, the zeros and poles are either real or occur in complex conjugate pairs. If p is replaced by its conjugate, all

* See Reference 24, p. 337 et seq.

powers of p are changed to their conjugates, and thus θ is changed to its conjugate This means that the real component of the network function must have even symmetry on the real-frequency axis, and the imaginary component must have odd symmetry. This fact is well known in alternating-current theory where the resistive component of an impedance has even symmetry with respect to frequency and the reactance has odd symmetry.

In order that the immittance be stable, the system must not be capable of an oscillation that increases with time. This means that any transient that is produced must be damped, or at most remain as an oscillation of fixed amplitude. Since a positive real component of p corresponds to an amplitude that increases with time, it is then evident that all zeros and poles of θ must be confined to the left half of the p-plane or to the real-frequency axis; the system must not have a negative resistance component.

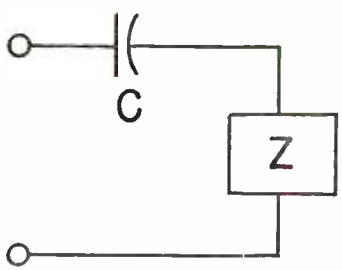

Fig. 1—Series reactance.

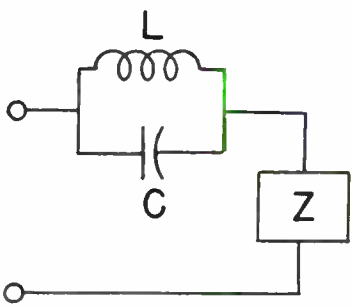

Fig. 2—Series reactive circuit.

Minimum Reactance Condition

If the network has a pure reactance in series, as in Figure 1, the input impedance will be $Z_{in} = \dfrac{1}{i\omega C} + Z$. This has a pole on the real-frequency axis when $\omega = 0$. If C were changed to L, the pole would be at $\omega = \infty$. Likewise in Figure 2 the input impedance is $Z_{in} = \dfrac{i\omega L}{1 - \omega^2 LC} + Z$, which has poles when $\omega = \pm 1/\sqrt{LC}$, again on the real-frequency axis. In the derivation that follows, it will be assumed that there are no poles on the real-frequency axis. This means either that all reactances must have some dissipation, or that in an impedance all series pure reactances are subtracted from the network under discussion. The network that remains when all the real-frequency poles have been removed by subtracting all series pure reactances is the minimum

reactance structure. Likewise if all the real-frequency zeros have been removed from an admittance, the remaining structure will be called a minimum susceptance network.

Properties of Transfer Impedances

Since the transfer impedance of a network of lumped constants can be written as the ratio of two polynomials, many of its properties will be the same as for an input immittance. The zeros and poles are either real or occur in conjugate complex pairs. The real and imaginary components are respectively even and odd functions of frequency on the real frequency axis. None of the zeros can be found in the right half plane. Poles of the transfer impedance may be found anywhere in the p-plane. It is not necessary that the phase angle of a transfer impedance be limited to ± 90 degrees, since phase shifts can be made as large as desired by adding more circuits for the signal to pass through. This means that the real part can be negative in a physically realizable stable network. It is necessary, however, that the network not be a source of power; the real component of the transfer loss cannot be negative at real frequencies.

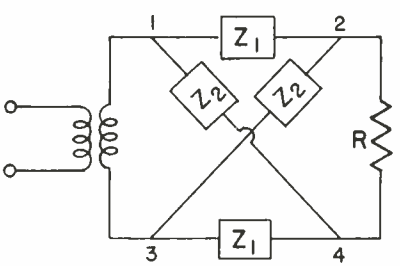

Fig. 3—Symmetrical lattice network.

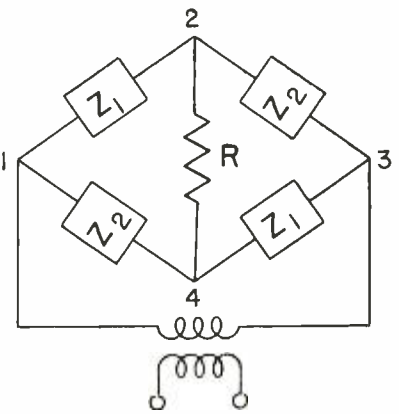

Fig. 4—Equivalent bridge circuit.

Minimum Net Phase Shift Condition

In the discussion which follows, it will be assumed that there are no poles of the transfer impedance in the right half plane. This means that for a given input voltage, the output current must not be zero for any p with a real part greater than zero. This excludes many circuits where the signal can reach the output by more than one path to produce cancellation of the output current.

Figure 3 shows a transfer impedance composed of a symmetrical lattice structure, and in Figure 4 the circuit is redrawn in the form

of a Wheatstone bridge. It is clear that for certain values of Z_1 and Z_2 the current in R will be zero. This corresponds to a pole of the transfer impedance for a value of p in the right half plane.

A second circuit which can have a pole of the transfer impedance in the right half plane is the bridged-T structure of Figure 5. Such a circuit is sometimes used to produce sharp rejection frequencies. As shown by Figure 6, this is not exactly equivalent to Figure 4 but it does depend upon a balance at a certain frequency.

A network that has no poles in the right half plane is called a minimum net phase shift structure. Since a mere reversal of polarity of the output terminals of a transfer network is not a significant change, it is the net change with frequency that is important.

It is not possible to give a general rule as to whether the bridged-T network is of minimum net phase shift type. It is sometimes necessary to actually compute the poles to decide.

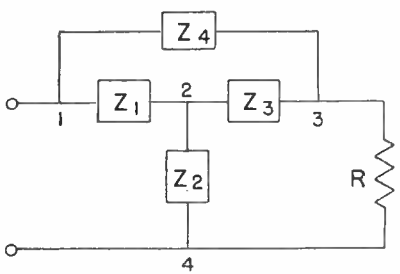

Fig. 5—Bridged-T network.

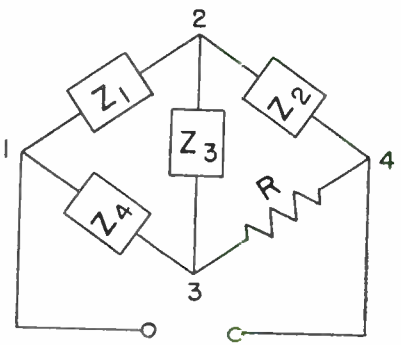

Fig. 6—Equivalent bridge circuit.

Most engineering applications in the radio field use series or shunt type circuits in a ladder network, and these are the minimum net phase shift type. The unilateral amplifying tubes merely change the level of the signal, so can be included in the circuit without affecting the validity of the results.

Relations Between the Components

Computation of the Phase Curve from the Attenuation Characteristic

The following discussion is very similar to that given by Bode, and is given in order to clarify the restrictions on the circuits which can be treated by the method to be presented.

Let θ be an input impedance or admittance, the logarithm of the transfer impedance (attenuation and phase angle) or a similar network

function. Then $\theta = A + iB$ where A is the real part of θ and B is the imaginary component. Let the values at ω_x be $A(x)$ and $B(x)$. In order to find the relation between $B(x)$ and $A(x)$, create a pole at ω_x and, since the poles occur in conjugate pairs, create a second pole at $-\omega_x$, to retain symmetry. To simplify the derivation, the analytic function will be taken as $\theta - A(x)$. Then by Cauchy's integral theorem, the integral of an analytic function around a contour which contains no poles is zero.

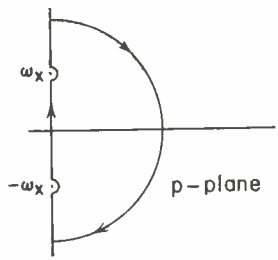

Fig. 7—Contour for integration.

Let the contour be that shown by Figure 7, where the very small semicircles exclude the poles at $\pm \omega_x$, and the large semicircle has an infinite radius. The integral becomes

$$\oint \left\{ \frac{\theta - A(x)}{\omega - \omega_x} - \frac{\theta - A(x)}{\omega + \omega_x} \right\} d\omega =$$

$$\oint \frac{2\omega_x}{\omega^2 - \omega_x^2} [\theta - A(x)] \, d\omega = 0. \qquad (3)$$

Since the integrand vanishes as ω^{-2} at high frequencies, the integral along the infinite semicircle is zero. If the values of θ on the very small indentations are assumed to be constant and equal to $A(x) \pm iB(x)$, the integral becomes

$$\int_{\infty}^{\infty} \frac{2\omega_x}{\omega^2 - \omega_x^2} [A + iB - A(x)] \, d\omega + \oint_{\omega_x} iB(x) \left\{ \frac{1}{\omega - \omega_x} - \frac{1}{\omega + \omega_x} \right\} d\omega$$

$$- \oint_{\omega_x} iB(x) \left\{ \frac{1}{\omega - \omega_x} - \frac{1}{\omega + \omega_x} \right\} d\omega = 0 \qquad (4)$$

where the second and third integrals are taken around the upper and lower small semicircles respectively.

Since B is an odd function of frequency, the imaginary component of the first term can be set equal to zero. In the second integral $1/(\omega + \omega_x)$ can be neglected in comparison with $1/(\omega - \omega_x)$ since ω is very nearly equal to ω_x. The residue at ω_x is $iB(x)$, so the second

integral equals $-\pi B(x)$. By a similar argument, the third integral is evaluated at $-\omega_x$ to give $-\pi B(x)$. This gives the result

$$\int_{-\infty}^{\infty} \frac{2\omega_x}{\omega^2 - \omega_x^2} [A - A(x)]\, d\omega = 2\pi B(x) \quad \text{or}$$

$$B(x) = \frac{2\omega_x}{\pi} \int_0^{\infty} \frac{A - A(x)}{\omega^2 - \omega_x^2}\, d\omega, \tag{5}$$

the desired relation.

To obtain a result more useful for the particular problem to be considered, transform to a logarithmic scale; let $\alpha = \log(\omega/\omega_x)$. Then

$$B(x) = \frac{2}{\pi} \int_0^{\infty} \frac{A - A(x)}{\omega/\omega_x - \omega_x/\omega} \frac{d\omega}{\omega} = \frac{2}{\pi} \int_{-\infty}^{\infty} \frac{A - A(x)}{e^{\alpha} - e^{-\alpha}}\, d\alpha$$

$$= \frac{1}{\pi} \int_{-\infty}^{\infty} \frac{A - A(x)}{\sinh \alpha}\, d\alpha. \tag{6}$$

Integrate by parts, using the result $\int \frac{d\alpha}{\sinh \alpha} = -\log \coth |\tfrac{1}{2}\alpha| + C$.

This gives

$$B(x) = \frac{1}{\pi} \left[-[A - A(x)] \log \coth |\tfrac{1}{2}\alpha| \right]_{-\infty}^{\infty}$$

$$+ \frac{1}{\pi} \int_{-\infty}^{\infty} \frac{dA}{d\alpha} \log \coth |\tfrac{1}{2}\alpha|\, d\alpha.$$

The first term can be shown to vanish*, so

$$B(x) = \frac{1}{\pi} \int_{-\infty}^{\infty} \frac{dA}{d\alpha} \log \coth |\tfrac{1}{2}\alpha|\, d\alpha$$

$$= \frac{1}{\pi} \int_0^{\infty} \frac{dA}{d\omega} \log \left| \frac{\omega + \omega_x}{\omega - \omega_x} \right| d\omega. \tag{7}$$

* See Reference 24, p. 312.

This result applies to an input immittance with no poles in the right half plane or on the real frequency axis. If the immittance is not of the minimum reactance type and does have one or more poles on the real frequency axis, the residues at the poles must be determined and included in the evaluation of the contour integral. In the case of a transfer impedance, there must be no poles in the right half plane or on the real frequency axis. If the network is not of a minimum net phase shift type, the phase shifting network must be removed before applying the formula, or a correction term must be added to the formula, which is found from the residues of the poles in the right half plane.

Computation of the Attenuation Characteristic from the Phase Curve

To find the real component in terms of the imaginary component, the function to be integrated around the contour is

$$\phi = \left\{ \frac{\theta - A(o)}{i\omega} - \frac{B(x)}{\omega_x} \right\} \left\{ \frac{1}{\omega - \omega_x} - \frac{1}{\omega + \omega_x} \right\} \tag{8}$$

where ω_x corresponds to some arbitrary real frequency at which the real component is to be determined and $B(x)$ is the corresponding imaginary component. $A(o)$ is the value of the real component at zero frequency. The function ϕ will have singularities at the frequencies $+\omega_x$ and $-\omega_x$, but not at the origin, since θ is analytic at the origin and can be expanded in the series $\theta = A_o + iB_o\omega + A_1\omega^2 + \ldots$.

The contour around which ϕ will be integrated is shown in Figure 7, where the radius of the semicircular path is infinitely large. The contour integral to be considered in this case is

$$\oint \left[\frac{\theta - A(o)}{i\omega} - \frac{B(x)}{\omega_x} \right] \left[\frac{1}{\omega - \omega_x} - \frac{1}{\omega + \omega_x} \right] d\omega = 0. \tag{9}$$

It is seen that for ω very large the integrand approaches zero at least as rapidly as ω^{-2} and the contribution of the infinitely large semicircular path to the complete integral can be neglected. This leaves the path along the real frequency axis between plus and minus infinity and the two small semicircular paths at the points ω_x and $-\omega_x$. The indentations at ω_x and $-\omega_x$ will be assumed very small so that θ can be assumed to be constant and equal to $A(x) + iB(x)$ and $A(x) - iB(x)$ at ω_x and $-\omega_x$ respectively. Equation (9) can then be written

$$\int_{-\infty}^{\infty} \left[\frac{A - A(o)}{i\omega} + \frac{B}{\omega} - \frac{B(x)}{\omega_x} \right] \left[\frac{2\omega_x}{\omega^2 - \omega_x^2} \right] d\omega$$

$$+ \oint_{+\omega_x} \left[\frac{A(x) - A(o)}{i\omega} + \frac{B(x)}{\omega} - \frac{B(x)}{\omega_x} \right] \left[\frac{1}{\omega - \omega_x} - \frac{1}{\omega + \omega_x} \right] d\omega$$

$$+ \oint_{-\omega_x} \left[\frac{A(x) - A(o)}{i\omega} - \frac{B(x)}{\omega} - \frac{B(x)}{\omega_x} \right] \left[\frac{1}{\omega - \omega_x} - \frac{1}{\omega + \omega_x} \right] d\omega = 0 \tag{10}$$

where the integrals around the small semicircular paths are denoted by $\oint_{\pm \omega_x}$.

Since A is an even function of frequency, the first term of the first integral cancels out in the integration. The second integral is to be evaluated on the small semicircular contour near $+\omega_x$, so the term $1/(\omega + \omega_x)$ can be neglected in comparison with $1/(\omega - \omega_x)$. By Cauchy's theorem

$$\oint_{+\omega_x} \left[\frac{A(x) - A(o)}{i\omega} + \frac{B(x)}{\omega} - \frac{B(x)}{\omega_x} \right] \left[\frac{1}{\omega - \omega_x} \right] d\omega$$

$$= \frac{\pi}{\omega_x} [A(x) - A(o)]. \tag{11}$$

By the same process, this is also the value of the third integral. This gives the result

$$2\omega_x \int_{0}^{\infty} \frac{B/\omega - B(x)/\omega_x}{\omega^2 - \omega_x^2} d\omega + \frac{2\pi}{\omega_x} [A(x) - A(o)] = 0$$

$$\text{or } A(x) - A(o) = -\frac{2\omega_x^2}{\pi} \int_{0}^{\infty} \frac{B/\omega - (B/\omega)_x}{\omega^2 - \omega_x^2} d\omega. \tag{12}$$

Equation (12) relates the real component to the imaginary component of a network function, with the value of the real component at zero frequency as reference.

For convenience, Equation (12) can be written using a logarithmic frequency scale.

$$A(x) - A(o) = -\frac{2\omega_x}{\pi}\int_o^\infty \frac{B/\omega - (B/\omega)_x}{\omega/\omega_x - \omega_x/\omega}\cdot\frac{d\omega}{\omega}$$

let $\omega/\omega_x = e^\alpha$, $\alpha = \log \omega/\omega_x$, then

$$A(x) - A(o) = -\frac{2\omega_x}{\pi}\int_\infty^\infty \frac{B/\omega - (B/\omega)_x}{e^\alpha - e^{-\alpha}}\,d\alpha$$

$$= -\frac{\omega_x}{\pi}\int_{-\infty}^\infty \frac{B/\omega - (B/\omega)_x}{\sinh\alpha}\,d\alpha. \qquad (13)$$

Integrating Equation (13) by parts and noting that

$$\int \frac{d\alpha}{\sinh\alpha} = -\log\coth|\tfrac{1}{2}\alpha| + C$$

$$A(x) - A(o) = \left[\frac{\omega_x}{\pi}\{B/\omega - (B/\omega)_x\}\log\coth|\tfrac{1}{2}\alpha|\right]_{-\infty}^{\infty}$$

$$-\frac{\omega_x}{\pi}\int_{-\infty}^\infty \frac{d(B/\omega)}{d\alpha}\log\coth|\tfrac{1}{2}\alpha|\,d\alpha.$$

It can be shown that the first term on the right is equal to zero, so the equation reduces to

$$A(x) - A(o) = -\frac{\omega_x}{\pi}\int_{-\infty}^\infty \frac{d(B/\omega)}{d\alpha}\log\coth|\tfrac{1}{2}\alpha|\,d\alpha \qquad (14)^*$$

$$= -\frac{\omega_x}{\pi}\int_o^\infty \frac{d(B/\omega)}{d\omega}\log\left|\frac{\omega+\omega_x}{\omega-\omega_x}\right|\,d\omega. \qquad (15)$$

The Semi-Infinite Constant Slope Characteristic for Attenuation

Consider the ideal low-pass filter, which has zero attenuation from zero frequency to cutoff frequency, ω_o, and rolls off at a constant number of decibels per octave thereafter. This can be specified as

* Reference 24, equation 14-24.

$$\frac{dA}{du} = 0 \quad -\infty < u \leq 0 \qquad \frac{dA}{du} = k \quad 0 \leq u < \infty \tag{16}$$

where $u = \log \omega / \omega_o$.

This gives the result, using Equation (7),

$$B(x) = \frac{k}{\pi} \int_{\alpha_o}^{\infty} \log \coth \left| \tfrac{1}{2}\alpha \right| d\alpha$$

$$= \frac{k}{\pi} \int_o^x \log \left| \frac{1+t}{1-t} \right| \frac{dt}{t} = \frac{2k}{\pi} \int_o^x \tanh^{-1} t \, \frac{dt}{t} \tag{17}$$

where $\alpha_o = \log \omega_o / \omega_x$, $x = \omega_x - \omega_o$ and $t = \omega_x / \omega$.

A graph of this integral is given by Bode#, p. 316, and is shown by curve D of Figure 10, corresponding to the semi-infinite constant slope characteristic, curve D of Figure 9. Complete tables are given by Corrington[37] and Thomas[38].

This integral can also be expressed in terms of Spence's integral (see Appendix I). Since

$$L(1+x) = \int_o^x \log (1+t) \, \frac{dt}{t} \tag{19}$$

and

$$L(1-x) = \int_o^x \log (1-t) \, \frac{dt}{t} \tag{20}$$

$$B(x) = \frac{k}{\pi} [L(1+x) - L(1-x)] = \frac{2k}{\pi} \phi(x), \ddagger \tag{21}$$

Reference 24, p. 316.

[37] Murlan S. Corrington, "Table of the Integral $\frac{2}{\pi} \int_o^x \tanh^{-1} t \, dt/t$," *RCA Review*, Vol. VII, No. 3, pp. 432-437; September, 1946. [$x = 0(.01).97(.005).99(.002)1;5D$]

[38] D. E. Thomas, "Tables of Phase Associated with a Semi-infinite Unit Slope of Attenuation," *Bell. Sys. Tech. Jour.*, Vol. 26, pp. 870-899, October, 1947. [$B(x)$ in degrees and radians, x, $1/x = 0(.001).996(.0005).998(.0001)1;5S$]

‡ This relation was also obtained by Dr. J. C. P. Miller of the Scientific Computing Service Limited, and communicated to the author by letter.

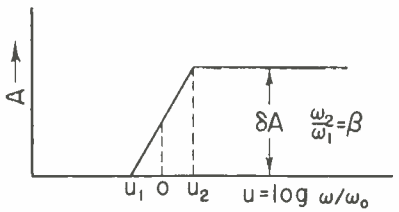

Fig. 8—Finite line segment real characteristic.

The known tables of $L(x)$ and $\phi(x)$ are listed in Appendix I.

Finite Line Segment Characteristic for Attenuation

If the difference of two semi-infinite constant slope characteristics, having different cutoff frequencies but equal slopes, is taken, the result is a finite line segment, as shown by Figure 8.

If the slope of the line segment is k, the total jump, $A_\infty - A_0$, is $k \log \omega_2/\omega_1 = k \log \beta$. A large number of curves have been computed for various values of β, Figures 19-27 inclusive, and the frequency range $0 \leq \omega/\omega_0 \leq 1$. Since the curves are symmetrical about the line $\omega = \omega_0$, on a logarithmic frequency scale, it is not necessary to plot the entire range. The curves have all been normalized for a jump of one decibel by dividing by $k \log \beta$, so that the vertical scale is in degrees per decibel. These curves are similar to those of Bode**, except that the parameter is the ratio of the end frequencies instead of the square, and the vertical scale is in decibels instead of nepers, since these are the units universally used by radio engineers. In addition, the functions have been cross-plotted with β as the variable instead of ω/ω_0, since this makes interpolation much easier.

An Example of the Computation of the Phase Curve from the Attenuation Characteristic

Let the attenuation curve be an ordinary deemphasis curve, as shown by Figure 9. As a first approximation, it can be represented by the semi-infinite constant slope characteristic D, which is asymptotically equal to the curve at infinity. An approximation can be made much better by adding the three line segments A, B, and C. For

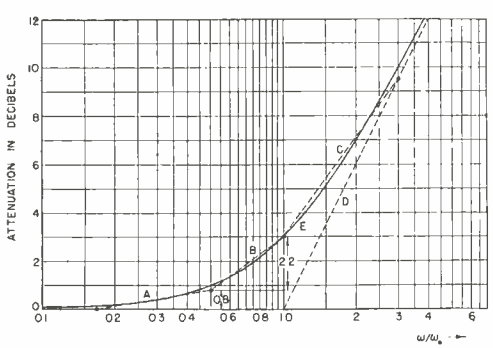

Fig. 9—Deemphasis characteristic.

** Reference 24, Chapter 15.

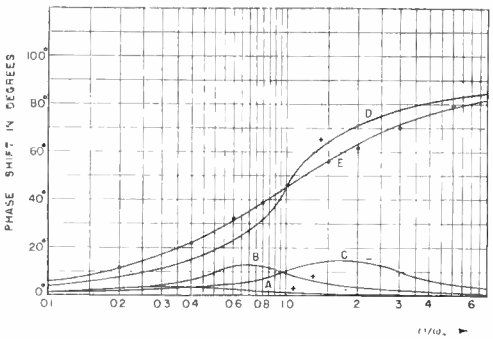

Fig. 10—Computed phase curve.

curves A and C, $\beta = 3$, and for curve B, $\beta = 2$. The phase curve corresponding to line segment A is obtained by multiplying the universal curve by 0.8, the jump in decibels. The phase curve for curve B is 2.2 times the universal curve for $\beta = 2$, and that for curve C is -3.0 times the universal curve for $\beta = 3$. Curve D corresponds to $k = 1$. These curves are plotted in Figure 10, and added graphically to give the resultant phase curve corresponding to the given deemphasis curve. It is helpful to use semi-log paper and to plot the individual curves with the proper multiple directly from the universal curves. These are then placed under the sheet of semi-log paper on which the final computations are made, and moved along until they center under the corresponding line segments. The curve is then traced on the final sheet. The small circles of Figure 10 show the results of the graphical solution and the solid line is the exact solution. The accuracy of the result can be made as high as desired by taking more line segments.

The Semi-Infinite Constant Slope Characteristic for the Phase

Figure 11 shows a graph of the imaginary component in which the value of the imaginary component is zero below some prescribed frequency ω_0 and has a constant slope thereafter when plotted to a logarithmic frequency scale. The derivation of the equation for the real component corresponding to the semi-infinite constant slope imaginary characteristic is given below.

Let $B = ku$, $0 \leq u < \infty$ $\qquad B = 0$, $-\infty < u \leq 0$.

By Equation (15)

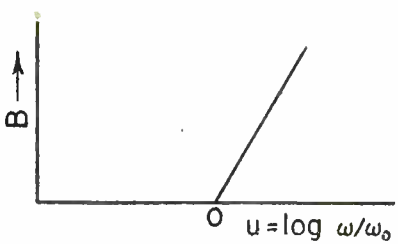

Fig. 11—Semi-infinite constant-slope characteristic.

$$A(x) - A(o) = -\frac{\omega_x}{\pi}\int_o^\infty \frac{d(B/\omega)}{d\omega}\log\left|\frac{\omega+\omega_x}{\omega-\omega_x}\right| d\omega. \qquad (22)$$

But $$\frac{d(B/\omega)}{d\omega} = \frac{d}{d\omega}\left(\frac{k}{\omega}\log\frac{\omega}{\omega_o}\right) = \frac{k}{\omega^2}\left(1-\log\frac{\omega}{\omega_o}\right)$$

so

$$A(x) - A(o) = -\frac{k\omega_x}{\pi}\int_{\omega_o}^\infty\left(1-\log\frac{\omega}{\omega_o}\right)\log\left|\frac{\omega+\omega_x}{\omega-\omega_x}\right|\frac{d\omega}{\omega^2}.$$

Let $t = \omega_x/\omega$, $\quad dt = -\frac{\omega_x}{\omega^2}d\omega$, $\quad x = \omega_x/\omega_o$

then

$$A(x) - A(o) = \frac{k}{\pi}\int_{\omega_x/\omega_o}^o\left(1+\log\frac{\omega_o}{\omega_x}t\right)\log\left|\frac{1+t}{1-t}\right| dt \qquad (23)$$

or

$$A(x) - A(o) = -\frac{k}{\pi}(1-\log x)\int_o^x \log\left|\frac{1+t}{1-t}\right| dt$$

$$-\frac{k}{\pi}\int_o^x \log t\log\left|\frac{1+t}{1-t}\right| dt.$$

Integrating the second integral by parts, let

$$u = \log t,\ du = dt/t,\ dv = \log\left|\frac{1+t}{1-t}\right| dt$$

$$v = t\log\left|\frac{1+t}{1-t}\right| + \log(1-t^2)$$

then

$$A(x) - A(o) = -\frac{k}{\pi}(1-\log x)\int_o^x \log\left|\frac{1+t}{1-t}\right| dt$$

$$-\frac{k}{\pi}\log x\int_o^x \log\left|\frac{1+t}{1-t}\right| dt + \frac{k}{\pi}\int_o^x\left[t\log\left|\frac{1+t}{1-t}\right| + \log|1-t^2|\right]\frac{dt}{t}$$

$$= \frac{k}{\pi} \int_0^x \frac{\log |1 - t^2|}{t}\, dt \tag{24}$$

$$= \frac{k}{\pi} \int_0^x \frac{\log |1 + t|}{t}\, dt + \frac{k}{\pi} \int_0^x \frac{\log |1 - t|}{t}\, dt$$

$$= \frac{k}{\pi} [L(1 + x) + L(1 - x)] = -\frac{2k}{\pi} \psi(x)^*$$

by Equations (19) and (20).

When $x \geq 1$, $A(x) - A(o) = \frac{k}{\pi} \int_0^x \frac{\log (t + 1)}{t}\, dt$

$$+ \frac{k}{\pi} \int_0^1 \frac{\log (1 - t)}{t}\, dt + \frac{k}{\pi} \int_1^x \frac{\log (t - 1)}{t}\, dt.$$

Integrating the third integral by parts

$$A(x) - A(o) = \frac{k}{\pi} L(1 + x) + \frac{k}{\pi} L(o)$$

$$+ \frac{k}{\pi} \left[\log |t - 1| \log t \right]_1^x - \frac{k}{\pi} \int_1^x \frac{\log t}{t - 1}\, dt$$

$$A(x) - A(o) = \frac{k}{\pi} \left[L(1 + x) - L(x) + \log (x - 1) \log x - \frac{\pi^2}{6} \right]$$

$$x \geq 1 \tag{26}$$

since $L(0) = -\pi^2/6$.

The function $\frac{\pi}{k} [A(x) - A(o)]$ is shown in Figure 12.

To derive a useful formula relating the function for $x > 1$ to the range for $x < 1$ for the semi-infinite constant slope characteristic, consider the real part at a frequency $x = \frac{\omega_x}{\omega_o}$ which is given by

$$A(x) - A(o) = \frac{k}{\pi} \left[L(1 + x) - L(x) - \frac{\pi^2}{6} + \log x \log |1 - x| \right]$$

* See Reference 41 for $\psi(x)$.

Similarly at a frequency $\frac{1}{x} = \frac{\omega_o}{\omega_x}$ the real component is

$$A\left(\frac{1}{x}\right) - A(o) = \frac{k}{\pi}\left[L\left(1+\frac{1}{x}\right) - L\left(\frac{1}{x}\right) - \frac{\pi^2}{6} + \log\frac{1}{x}\log\left|1-\frac{1}{x}\right|\right]$$

Substituting the expressions for $L\left(\frac{1}{x}\right)$ and $L\left(1+\frac{1}{x}\right)$ from Equations (35) and (37) in Appendix I,

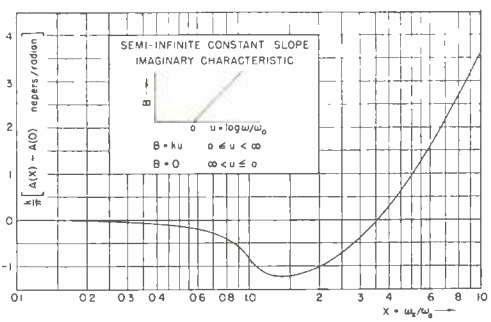

Fig. 12—Real component for semi-infinite constant slope imaginary characteristic.

$$A\left(\frac{1}{x}\right) - A(o) = \frac{k}{\pi}\left\{\tfrac{1}{2}(\log x)^2 + \frac{\pi^2}{6} - L(1+x) + L(x) - \tfrac{1}{2}(\log x)^2 - \frac{\pi^2}{6} - \log x\,[\log|x-1| - \log x]\right\}$$

$$A\left(\frac{1}{x}\right) - A(o) = \frac{k}{\pi}\left[-L(1+x) + L(x) - \log x \log|x-1| + (\log x)^2\right]$$

Adding the equations for $[A(x) - A(o)]$ and $\left[A\left(\frac{1}{x}\right) - A(o)\right]$

$$[A(x) - A(o)] + \left[A\left(\frac{1}{x}\right) - A(o)\right] = \frac{k}{\pi}\left[(\log x)^2 - \frac{\pi^2}{6}\right] \quad (27)$$

or

$$A(x) - A(o) = \frac{k}{\pi}\left[(\log x)^2 - \frac{\pi^2}{6}\right] - \left[A\left(\frac{1}{x}\right) - A(o)\right] \qquad (28)$$

$x > 0.$

Finite Line Segment Imaginary Characteristic for Phase

In the case of a step function or finite line segment of the imaginary component B, the real function is obtained by the addition of two semi-infinite constant slope characteristics as shown in Figure 13, where

$$\beta = \frac{\omega_2}{\omega_1}, \quad u_1 = -\tfrac{1}{2}\log\beta, \quad \text{and} \quad u_2 = \tfrac{1}{2}\log\beta.$$

The real component at the frequency $x = \omega_x/\omega_o$ is then given by Equation (24)

$$A(x) - A(o) = \frac{k}{\pi}\int_o^{x\sqrt{\beta}} \frac{\log|t^2-1|}{t}\,dt - \frac{k}{\pi}\int_o^{x/\sqrt{\beta}} \frac{\log|t^2-1|}{t}\,dt \qquad (29)$$

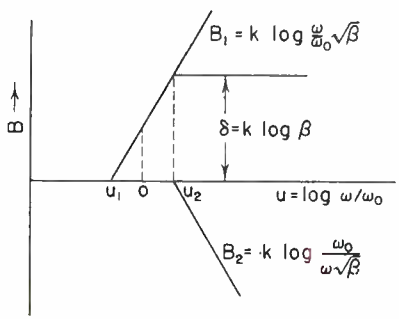

Fig. 13—Finite-line-segment imaginary characteristic.

$$A(x) - A(o) = [\{A(x\sqrt{\beta}) - A(o)\} - \{A(x/\sqrt{\beta}) - A(o)\}]$$

$$A(1/x) - A(o) = [\{A(\sqrt{\beta}/x) - A(o)\} - \{A(1/x\sqrt{\beta}) - A(o)\}]$$

subtracting the two equations

$$\{A(x) - A(o)\} - \{A(1/x) - A(o)\}$$
$$= [\{A(x\sqrt{\beta}) - A(o)\} + \{A(1/x\sqrt{\beta}) - A(o)\}]$$
$$- [\{A(x/\sqrt{\beta}) - A(o)\} + \{A(\sqrt{\beta}/x) - A(o)\}].$$

The use of Equation (27) gives the result

$$\{A(x) - A(o)\} = \left\{A\left(\frac{1}{x}\right) - A(o)\right\}$$

$$= \frac{k}{\pi}\left\{(\log x\sqrt{\beta})^2 - \frac{\pi^2}{6} - \left(\log\frac{x}{\sqrt{\beta}}\right)^2 + \frac{\pi^2}{6}\right\} = \frac{k}{\pi}\left[2\log\beta\log x\right]$$

let $\delta B = k\log\beta = 1$

$$A(x) - A(o) = \left\{A\left(\frac{1}{x}\right) - A(o)\right\} + \frac{2}{\pi}\log x \quad \text{where } x = \frac{\omega_x}{\omega_o} \qquad (30)$$

This equation shows that for the finite line segment of imaginary characteristic the real component need only be computed for the values of x between zero and unity. The function $A(x) - A(o)$ has been plotted for various values of β, these curves are shown in Figures 28 to 32 inclusive. Figures 33 to 35 show a plot of $A(x) - A(o)$ versus β for various values of ω_x/ω_o. The integrals in Equation (29) were evaluated from tables of the function using three-point Lagrangian interpolation coefficients[39].

Graphical Check of Derivation

Figure 14 shows the graph of $A(x) - A(o)$ for $\beta = 4$. The dashed line is the plot of $2/\pi \log \omega_x/\omega_o$; the function is symmetrical about this line and the $A(x) - A(o) = 0$ axis, as indicated by Equation (30).

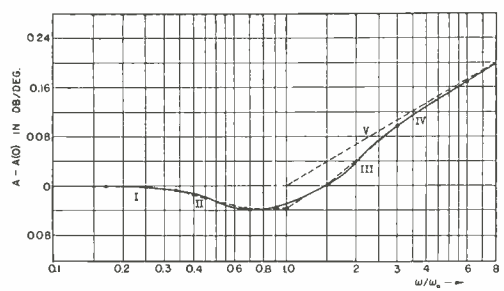

Fig. 14—Real characteristic for $\beta = 4$.

The corresponding finite line segment of imaginary characteristic is shown in Figure 15. Using the previously described method of finding the imaginary characteristic from the real characteristic the computed real characteristic was verified. The crosses in Figure 15 indicate the points obtained by the checking process. The accuracy can be increased as much as desired by taking more points on Figure 14.

---

[39] National Bureau of Standards, Mathematical Tables Project, TABLES OF LAGRANGIAN INTERPOLATION COEFFICIENTS, Columbia University Press, New York, N. Y., 1944.

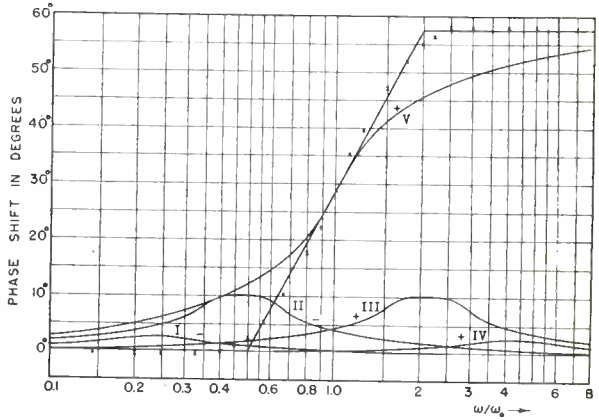

Fig. 15 — Imaginary characteristic for $\beta = 4$.

An Example of the Computation of the Attenuation Characteristic from the Phase Curve

In Figure 16 the transfer-impedance phase characteristic for a double-tuned transformer is shown. The equation which was used to compute the phase characteristic is derived in Appendix II. To find the amplitude characteristic from the given phase curve, the phase curve is divided into a number of finite line segments, 1, 2, 3, etc. The corresponding frequency ratio, β, and the change in phase δB are found for each of the line segments as shown below.

Segment	β	δB. *(degrees)*
1	1.6	—7.4
2	1.1	—8.0
3	1.08	—21.4
4	1.11	—268.
5	1.05	—33.2
6	1.18	—11.5
7	2.0	—5.7

Since the function $A(x) - A(o)$ was computed for $\delta B = 1$ degree, the values in the tables must be multiplied by the factor δB to obtain the amplitude curve for each line segment. The curves so obtained are then placed along the frequency axis so that the point $\omega/\omega_0 = 1$ for each amplitude curve lies at the geometric mean (the center on a logarithmic frequency scale) of the end frequencies of the particular line segment. When the curves are plotted on semi-log paper as shown,

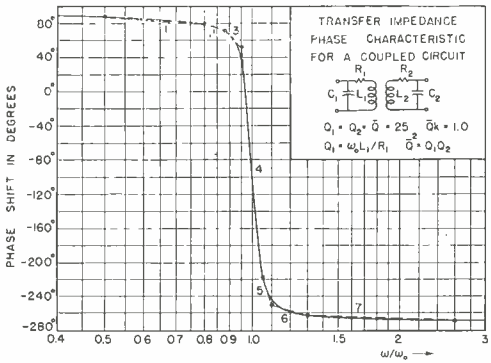

Fig. 16—Transfer impedance phase characteristic for a coupled circuit.

the amplitude curves are centered with respect to the finite line segments of the corresponding phase curve. Some of the curves of Figure 17 have been shifted vertically to avoid crowding. In all except No. 8, the reference axis is the line asymptotic to the curve on the left side. Curve No. 8 is referred to the dashed line. Curve 8 in Figure 17 corresponds to a phase shift of 90 degrees at $\omega = 0$ and is of unit slope (i.e., 6 decibels per octave). This is added due to the 90-degree initial phase shift in the transfer impedance of the coupled circuit.* The amplitude or attenuation characteristic is obtained by the algebraic summation of the ordinates of the individual amplitude curves; the points so obtained are indicated by the crosses in Figure 17. The solid curve *A* denotes the calculated curve for the transfer impedance.

Conclusions

A method has been developed that enables the computation of the phase curve from the attenuation characteristic of a network, or the inverse operation, the computation of the attenuation characteristic from the phase curve. The theory applies to any stable network of

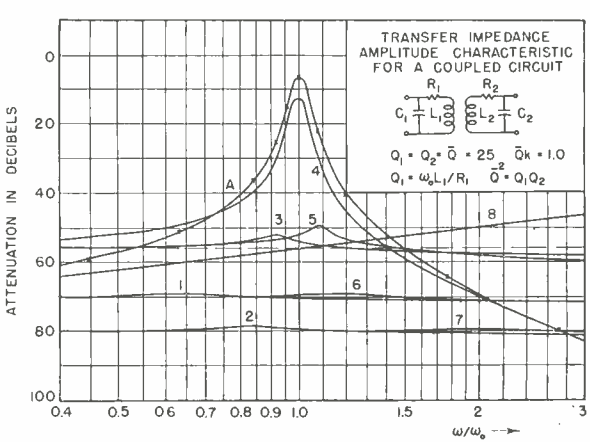

Fig. 17—Transfer impedance amplitude characteristic for a coupled circuit.

* See Reference 24, p. 315.

lumped constants, with two qualifications. An input immittance must be of the minimum reactance type, and a transfer impedance must be of the minimum net phase shift type. Nearly all networks used by radio engineers satisfy these requirements, so the analysis can be used directly in most cases.

The method is especially useful since it is not necessary to know the actual circuit used, but merely the experimental or otherwise prescribed selectivity curve. The effect of any change in the curve can be computed directly, and it is a simple procedure to determine what change in one characteristic is needed to cause a desired change in the other. Many universal curves are given, so the computations can all be made graphically.

APPENDIX I

Spence's Integral

One of the most elementary of the logarithmic transcendents was studied by Spence in 1809[10]. This function of the second order can be defined by

$$L(x) = \int_1^x \frac{\log t}{t-1}\, dt \tag{31}$$

or $L(1+x) = \int_0^x \log(1+t)\,\frac{dt}{t}$ and $L(1-x) = \int_0^x \log(1-t)\,\frac{dt}{t}$.

He has given tables and numerous relations for the function. Later Newman[11] again studied these functions and gave tables for $L(1+x)$ and $-L(1-x)$. Recently Powell[12] has given other tables which are especially helpful in this paper, and has developed most of the relations which are given below for convenient reference.

---

[10] William Spence, AN ESSAY ON THE THEORY OF THE VARIOUS ORDERS OF LOGARITHMIC TRANSCENDENTS; WITH AN INQUIRY INTO THEIR APPLICATIONS TO THE INTEGRAL CALCULUS AND THE SUMMATION OF SERIES, London and Edinburgh, 1809. Second edition 1820, in Spence's Mathematical Essays, edited by J. F. W. Herschel, with additions from Spence's papers. $L(x)$, $[x = 1(1)100;\ 9D]$ p. 24

[11] F. W. Newman, THE HIGHER TRIGONOMETRY, SUPERRATIONALS OF SECOND ORDER, Cambridge, 1892. $L(1+x)$, $-L(1-x)$, $[x = 0(.01).5;\ 12D]$, $\phi(x) = \frac{1}{2}[L(1+x) - L(1-x)]$, $[x = .01(.01).50;\ 12D]$, $\psi(x) = -\frac{1}{2}[L(1+x) + L(1-x)]$, $[x = .01(.01).50;\ 12D]$.

[12] E. O. Powell, "An Integral Related to the Radiation Integrals," *Phil. Mag.*, Ser. 7, Vol. 34, pp. 600-607; September, 1943. $L(x)$, $[x = 0(.01)2(.02)6;\ 7D]$. For errata see Alan Fletcher, "Note on tables of an integral," *Phil. Mag.*, Ser. 7, Vol. 35, pp. 16-17, 1944.

$$L(x) = \int_1^x \frac{\log t}{t-1}\,dt = \sum_{n=1}^{\infty} (-1)^{n+1}\,(x-1)^n\,n^{-2} \qquad 0 \leq x \leq 2 \qquad (32)$$

$$L(x) = \log x \log\,(x-1) - \tfrac{1}{2}\,(\log x)^2 + \frac{\pi^2}{6} - \sum_{n=1}^{\infty} n^{-2}\,x^{-n} \qquad x \geq 1 \qquad (33)$$

$$L(x) = \log x \log\,(1-x) - \frac{\pi^2}{6} + \sum_{n=1}^{\infty} n^{-2}\,x^n \qquad 0 \leq x \leq 1 \qquad (34)$$

$$L(x) + L\left(\frac{1}{x}\right) = \tfrac{1}{2}\,(\log x)^2 \qquad x > 0 \qquad (35)$$

$$L(x+1) - L(x) = \log x \log\,(x+1) + \frac{\pi^2}{12} - \tfrac{1}{2}\,L(x^2) \qquad x > 0 \qquad (36)$$

$$L(x+1) + L\left(\frac{1}{x}+1\right) = \tfrac{1}{2}\,(\log x)^2 + \frac{\pi^2}{6} \qquad x > 0 \qquad (37)$$

APPENDIX II

Transfer Impedance of Coupled Circuit

Assuming that R is constant across the entire frequency spectrum, and that there exists no capacitative coupling between the windings,

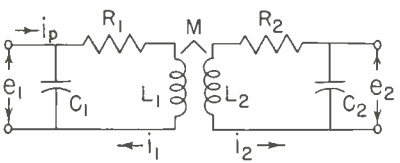

Fig. 18—Double-tuned transformer.

the transfer impedance can be found as follows:

$$e_1 = i_1\,(R_1 + \rho L_1) + i_2\,\rho M = (i_p - i_1)\,\frac{1}{\rho C_1} \qquad (38)$$

$$e_2 = -\,i_2\,\frac{1}{\rho C_2} = i_2\,(R_2 + \rho L_2) + i_1 \rho M \qquad (39)$$

where $\rho = j\omega$; $j^2 = -1$.

Let $\omega_o^2 = \dfrac{1}{L_1 C_1} = \dfrac{1}{L_2 C_2}$, $\dfrac{\omega}{\omega_o} = \dfrac{a + \overline{Q}}{\overline{Q}}$, $Q_1 = \dfrac{\omega_o L_1}{R_1}$, $Q_2 = \dfrac{\omega_o L_2}{R_2}$,

$k^2 = \dfrac{M^2}{L_1 L_2}$, $\overline{Q}^2 = Q_1 Q_2$, $Z_1 = Q_1\,\omega_o\,L_1$, $Z_2 = Q_2\,\omega_o\,L_2$ and $\overline{Z}^2 = Z_1 Z_2$.

If there is no secondary detuning and if the primary and secondary *Q's* are equal, the normalized transfer impedance reduces to

$$\frac{Z_T}{\overline{Z}} = \frac{j\dfrac{\overline{Q}}{a+\overline{Q}}\overline{Q}k}{\left\{-j+a+Q-\dfrac{\overline{Q}^2}{a+\overline{Q}}\right\}^2-\left\{\dfrac{a+\overline{Q}}{\overline{Q}}\right\}^2(\overline{Q}k)^2} \tag{40}$$

$$\frac{Z_T}{\overline{Z}} = \frac{j\dfrac{\omega_0}{\omega}\overline{Q}k}{\left[-j+\dfrac{\omega}{\omega_0}\overline{Q}-\dfrac{\omega_0}{\omega}\overline{Q}\right]^2-\left(\dfrac{\omega}{\omega_0}\overline{Q}k\right)^2} \tag{41}$$

$$\text{let } \overline{Q}k = 1.0;\ \overline{Q} >> 1 \text{ as } \frac{\omega}{\omega_0} \to \infty,\ \frac{Z_T}{\overline{Z}} \to \frac{j}{\left(\dfrac{\omega}{\omega_0}\right)^3\overline{Q}^2}$$

showing that the transfer impedance for a coupled circuit decreases 18 decibels per octave as the frequency becomes large compared to the resonant frequency of the circuit.

$$\text{as } \frac{\omega}{\omega_0} \to 0,\ \frac{Z_T}{\overline{Z}} \to \frac{j}{\dfrac{\omega}{\omega_0}\overline{Q}^2}$$

On the low frequency side the transfer impedance decreases 6 decibels per octave.

Figs. 19-27 — Imaginary component for finite line segment real characteristic.

Figs. 28-35 — Real component for finite line segment imaginary characteristic.

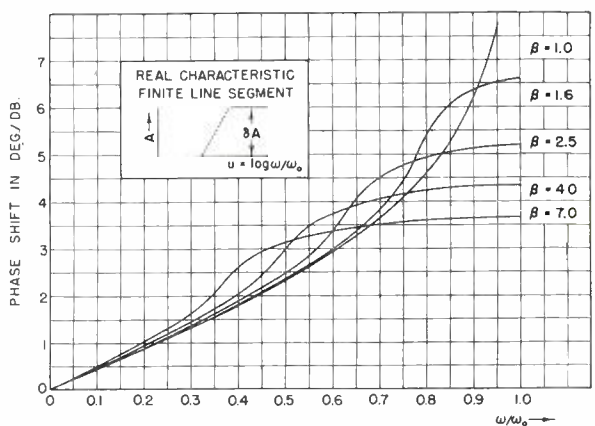

Fig. 19

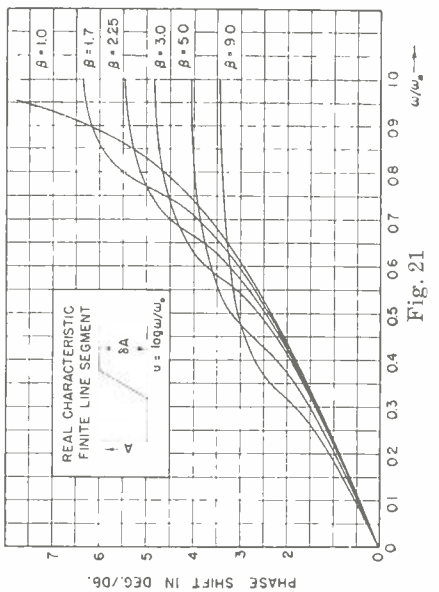

Fig. 21

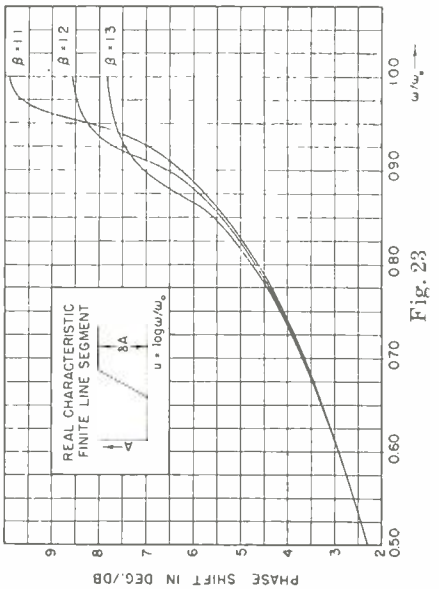

Fig. 23

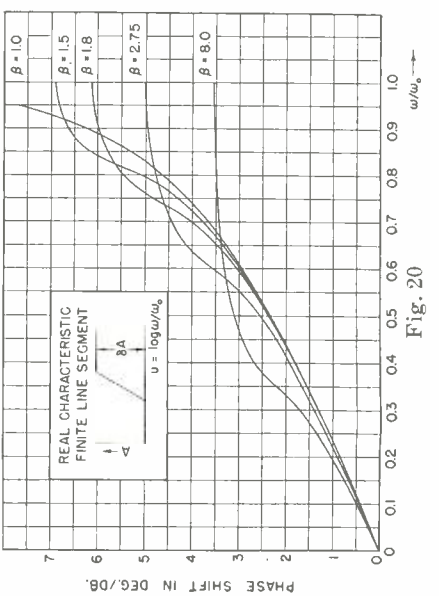

Fig. 20

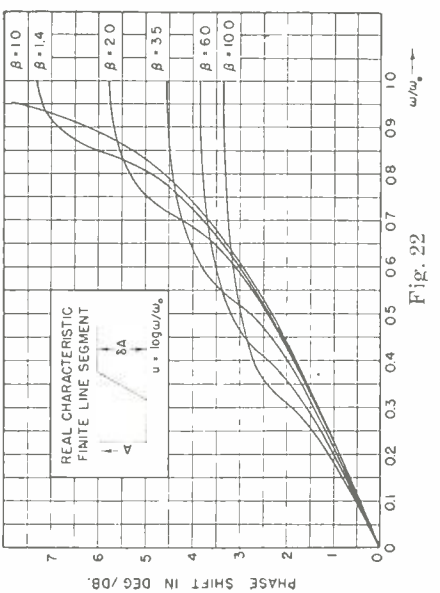

Fig. 22

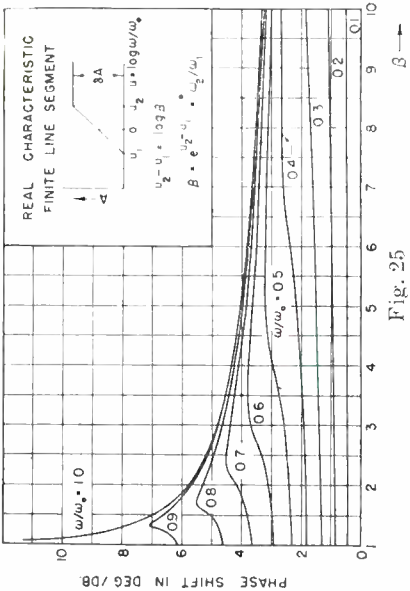

Fig. 25

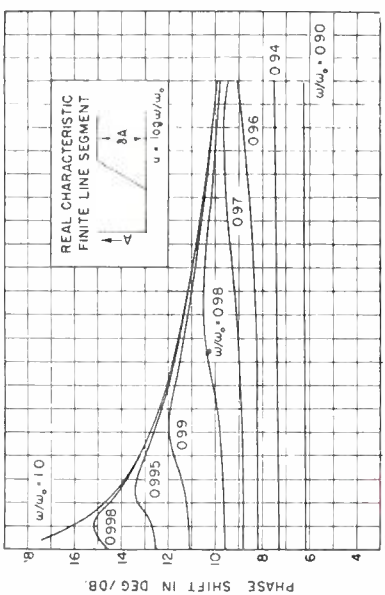

Fig. 27

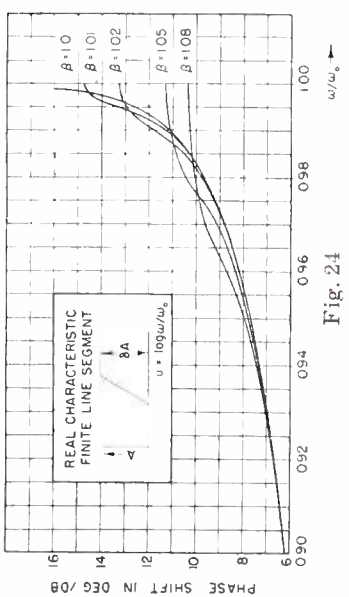

Fig. 24

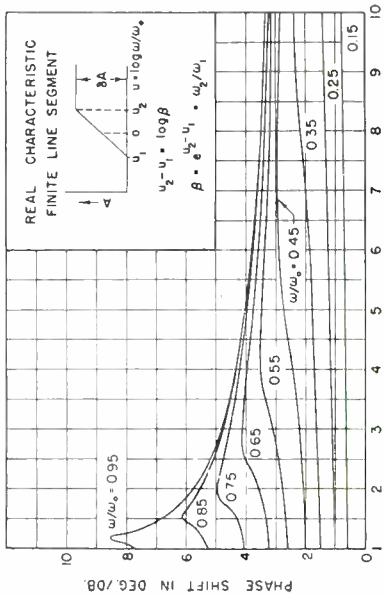

Fig. 26

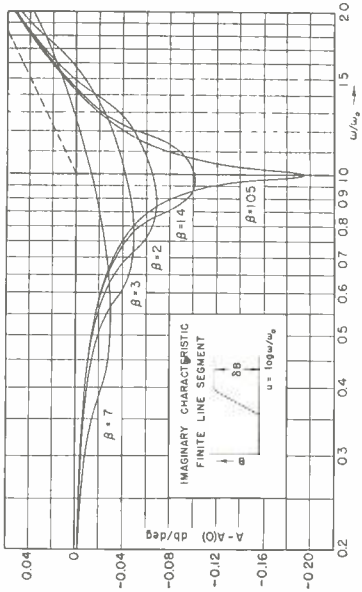

Fig. 29

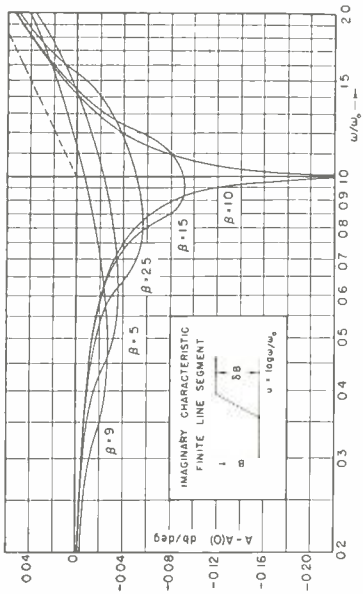

Fig. 28

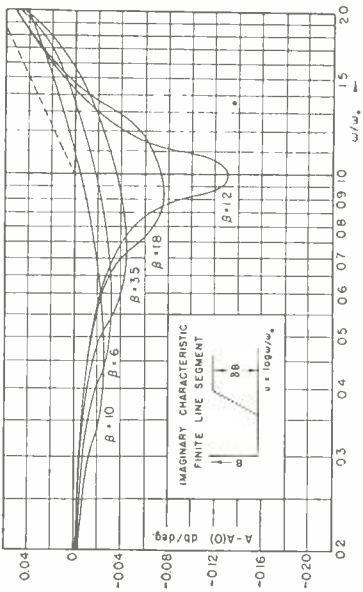

Fig. 31

Fig. 30

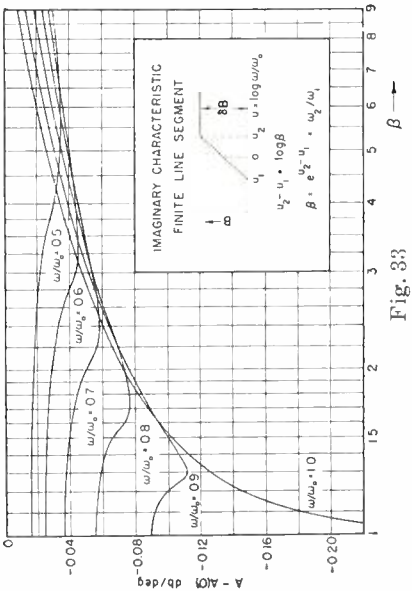

Fig. 33

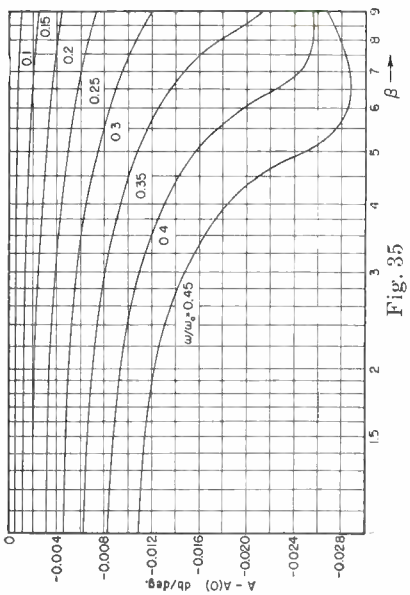

Fig. 35

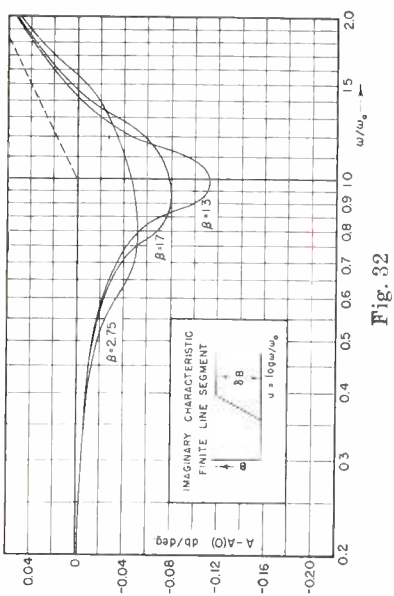

Fig. 32

Fig. 34

PERFORMANCE OF 931-A TYPE MULTIPLIER IN A SCINTILLATION COUNTER*†

By

G. A. Morton and J. A. Mitchell

Research Department, RCA Laboratories Division, Princeton, N. J.

Summary—The scintillation type nuclear radiation detector represents an extremely important advance and holds promise of displacing the older types of detectors for many applications. It depends for its operation on the conversion into an electrical pulse of the light flash produced by a suitable phosphor crystal when the latter absorbs a nuclear particle such as an alpha, beta or gamma ray, or neutron. The conversion of the light flash is effected by means of a secondary emission multiplier.

The present paper gives the results of the examination of a number of RCA 931A type multipliers for their suitability for this application. The properties of interest are (1) the pulse performance of the multiplier under conditions such that individual, or at most only a few, photoelectrons from the photocathode contribute to the pulse, and (2) the number and distribution of spurious pulses generated by the multiplier in darkness.

It was found that the pulse height distribution at the output of a multiplier, due to pulses from individual photoelectrons, is considerably broader than would be expected from a Poisson's distribution of secondary electrons at each stage. Distribution curves are given.

In complete darkness a good multiplier at room temperature is found to produce 300 to 600 pulses per second with a height equal to or greater than the charge on an electron times the average gain of the tube. Curves are given of dark current pulse distributions, the effect of temperature, shield potentials, etc.

Introduction

THE scintillation counter[1] represents one of the most important advances in devices for the detection of nuclear radiations since the invention of the Geiger-Mueller counter. Although this new detector is still in its infancy, it is for many purposes superior to the older types of detectors, and it holds promise of displacing the Geiger counter for a great many applications. At the present the scintillation counter is rather complicated and requires more elaborate circuitry

---

* Decimal Classification: (R800) 535.38.

† Work was done in part under U. S. Navy, Bureau of Ships Contract NObsr 42460.

[1] M. Blau and B. Dreyfus, "The Photo-Tube in Radio Active Measurements", *Rev. Sci. Instr.*, Vol. 16, No. 9, p. 245, Sept., 1945; H. Kallman, *Natur und Technik*, July, 1947; J. W. Coltman and F. H. Marshall, "Some Characteristics of the Photo-Multiplier Radiation Detector", *Phys. Rev.*, Vol. 72, No. 6, p. 528, Sept. 15, 1947; J. W. Coltman and F. H. Marshall, "Photomultiplier Radiation Detector", *Nucleonics*, Vol. 1, No. 3, p. 58, Nov., 1947.

than does the Geiger counter. However, it is already apparent that simplifications can be made along many lines. Probably the end device will be no more involved than present conventional counters.

The principle of the scintillation counter in its simplest form is illustrated in Figure 1. In this figure, *A* is a transparent phosphor crystal. When a nuclear particle is absorbed by this crystal, it emits a flash of light. Many crystals have this property. For example, zinc sulphide, calcium tungstate, anthracine, and thalium activated sodium iodide have been found useful in scintillation counters.[2] The flash of light falls on the multiplier *B* producing photoemission from its photocathode and consequently a current pulse in the output. This pulse is amplified by amplifier *C*. The output from amplifier *C* passes through a pulse height discriminator *D*, which allows only pulses with amplitudes exceeding some preassigned value to be supplied to the count rate indicator.

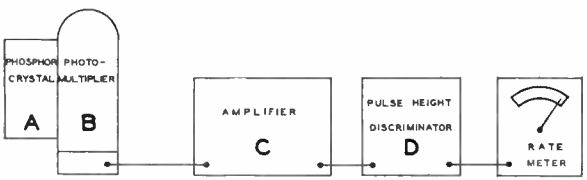

Fig. 1—Scintillation counter.

The phosphor crystal is chosen for its efficiency in converting nuclear radiation into visible light and for its ability to produce a flash of light of extremely short duration when excited by the nuclear particle. Crystals can be found with flash duration times of 10^{-8} or even 10^{-9} seconds. Since these times are long compared to the processes involved in the multiplier, the resolving time of a scintillation counter can be made to be a small fraction of a microsecond. This is to be compared with the 50 to 100 microseconds resolving time for conventional Geiger counters. This very short resolving time, as compared to many of the older type of detectors, is one of its important advantages. Furthermore, crystals can be found which can convert the nuclear radiation with several orders of magnitude greater efficiency than is possible with a Geiger counter. This is particularly true in the case of gamma rays for which the efficiency of a Geiger counter is very

[2] P. R. Bell, "The Use of Anthracene as a Scintillation Counter", *Phys. Rev.*, Vol. 73, No. 11, page 1405, June 1, 1948; R. J. Moon, "Inorganic Crystals for the Detection of High Energy Particles and Quanta", *Phys. Rev.*, Vol. 73, No. 10, p. 1210, May 15, 1948; M. Deutsch, "Naphthalene Counters for Beta and Gamma Rays", *Nucleonics*, Vol. 2, No. 3, p. 58, March, 1948; R. Hofstadter, "Alkali Halide Scintillation Counters", *Phys. Rev.*, Vol. 74, No. 1, p. 100, July 1, 1948.

low. The high efficiency of this scintillation counter is another important advantage of the device.

The pulse height discriminator is necessary because a secondary emission multiplier, even in darkness, exhibits a relatively copious pulse output, and it is necessary to exclude as many as possible of these pulses from the pulse rate indicator. By choosing a suitable phosphor and using the largest practical optical coupling between the phosphor and the photocathode, it is possible to make the pulses due to the scintillation larger than the majority of the dark current pulses.

Obviously, to design a scintillation counter which takes full advantage of the capability of the device, it is necessary to know something about the nature of the dark pulses as well as the pulses produced by the scintillations. The investigation described below was undertaken in order to obtain information about the pulse performance of the 931A and 1P28 type of photo multipliers.

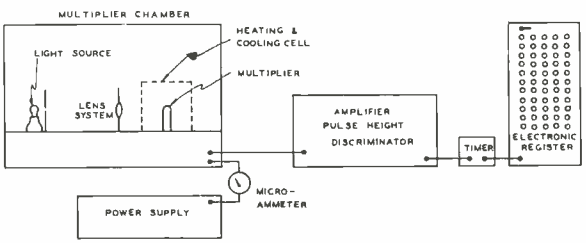

Fig. 2—Experimental Measuring Equipment.

Experimental Equipment

The pulse performance of the multipliers being investigated was measured by means of the amplifier, pulse height selector and register shown in Figure 2.

The multiplier was contained in a chamber, which was so constructed that it could be operated at room temperature or cooled to dry-ice temperature. A small light source was provided in the chamber so that the multiplier could be tested under various conditions of illumination as well as in darkness. The light source was so arranged that it could be used to illuminate the entire photocathode, or its light could be concentrated into a small spot which could be focused on any point of the photocathode. The circuits in the measuring chamber permitted the measurement of the current flowing to or from the electrodes of the multiplier under test.

The output of the multiplier was supplied to a Bell-Jordan amplifier[3]

[3] W. H. Jordan and P. R. Bell, "General Purpose Linear Amplifier", *Rev. Sci. Instr.*, Vol. 18, No. 10, p. 703, October, 1947.

through a suitable coupling resistor. The amplifier consisted of a four-stage preamplifier followed by a seven-stage linear amplifier. The latter is equipped with a pulse height selector which rejected all pulses below any predetermined pulse height. The output of the amplifier was fed to an RCA Decade Timer so modified that it could be used as an electronic register. An electronic timer was used to control the counting time.

The coupling resistor between the multiplier and amplifier was 10,000 ohms and the total capacity of the coupling circuit, including the capacity of the collector in the multiplier and the grid of the first tube of the preamplifier, was measured as about 30 micromicrofarads. The overall gain of the amplifier used for the multiplier measurements described below was about 10,000.

The amplifier was operated in such a way that the rise time was of the order of 0.15 microseconds and the response time 0.3 to 0.4 microseconds. The scaler would record periodic pulses at a rate somewhat greater than one hundred thousand per second. A determination of the resolving time of the entire system, by means of the self coincidences of random pulses, indicated a resolving time of about 6 microseconds. With this resolving time, pulses from individual electrons leaving the photocathode could be measured on the register.

Dark Current Pulses

The first phase of the investigation to be discussed concerns itself with the pulses due to dark current in the multiplier. The dark current is, of course, that current which appears at the output when no light falls on the photocathode. This dark current is the sum of several contributing causes. First, and most fundamental, the photocathode emits thermionic electrons which are multiplied by the succeeding dynodes and appears at the collector as part of the dark current. Second, any small amount of residual gas may become ionized giving rise to a current. Finally, cold discharge from points or irregularities on the electrodes and ohmic leakage also contribute to the dark current. The dark current from an exceptional multiplier at room temperature, operating at a voltage of 100 volts per stage, will be of the order of 0.05 microampere or less. It is more usual for a multiplier under these same conditions to have as much as a microampere or more dark current.

If the dark current were entirely due to emission from the photocathode, and each electron released was multiplied by the average gain of the multiplier, the output current would be in the form of pulses, each representing a charge of $e \cdot G$. However, in a real multiplier,

although a stage may have an average gain of R, each electron striking this stage does not produce exactly R secondary electrons. The actual number will be greater or smaller than R with a probability given by some distribution law. Since this occurs at every stage of the multiplier, the pulse height of pulses due to the thermionically emitted electrons must also be spread over a distribution. Similarly, pulses due to gas ion effects are not of uniform height but also follow a distribution law. The pulses due to ohmic leakage are very small, and can, without serious error, be neglected in considering a multiplier for use in a counter-type scintillation detector.

Figure 3 gives a typical pulse height distribution curve for a good multiplier at room temperature. The ordinates of this curve are in pulses per second and the abscissa pulse heights in units of the charge, equal to the charge of an electron times the average gain of the multiplier. It will be noted that there are approximately 600 pulses per second with a height equal to one unit of charge $e \cdot G$ or greater. If the curve is extrapolated to zero pulse height, the value would be about 1000 pulses per second (this extrapolation is not valid, due to the fact that it omits the many small pulses caused by ohmic leakage currents, etc.). Although considerable quantitative differences were found in the pulse distribution from various multipliers, the curve shown is fairly representative of those found for good multipliers. A less suitable tube used under the same conditions may show 10 to 100 times the number of pulses per second of unit height shown in the figure. It is interesting to note that if one integrates the curve shown in Figure 3 to obtain the current represented by these pulses one finds that this portion of the current represents less than 1 per cent of the total dark current. The remainder of the dark current is in the form of very small pulses which are below the amplifier noise level of the system used in the present measurements.

The dark current pulse rate is markedly dependent upon the temperature of the tube. Figure 4 illustrates the variation in number of pulses per second for two tubes over the temperature range from 27 to 50 degrees centigrade. Curve A is for a good tube (type 1P28); curve B is for a considerably poorer tube (type 931A). It will be noted that the pulse rate changes by a factor of 4 to 10 over this relatively small temperature range. If the tube is cooled to a low temperature, the pulse rate decreases very considerably. For example, the tube shown in curve A with 500 pulses per second at room temperature has a pulse rate less than 5 per second at dry ice temperature. In general, the pulse height distribution does not change much with temperature. However, it will be found that the larger pulses do not decrease quite

as rapidly as small pulses when the tube is cooled. This effect is emphasized if the shield around the tube is positive, with respect to the photocathode (the effect of the electrostatic shield around the tube will be discussed in some detail later).

The number of pulses per second of a given height increase as the overall voltage on the multiplier is increased. This is due to the fact that the gain of the multiplier increases. If the distribution is plotted in terms of a unit equal to $e \cdot G$, it is found to remain relatively unchanged with change of voltage over a considerable range, e.g. from 60 volts per stage and 100 volts or more per stage. However, even over this voltage range some change can be noted as will be discussed later. If the overall voltage exceeds a certain amount, a considerable number of large pulses appear in the output, due to cold discharge phenomena in the multiplier.

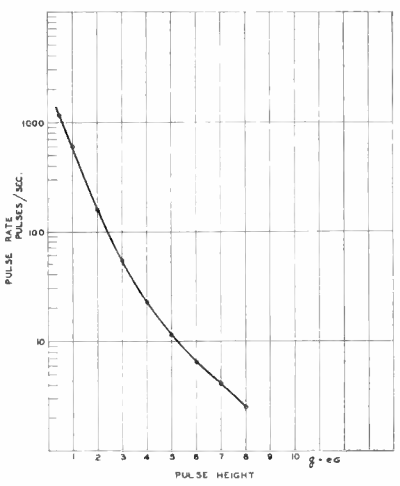

Fig. 3—Dark current pulse height distribution.

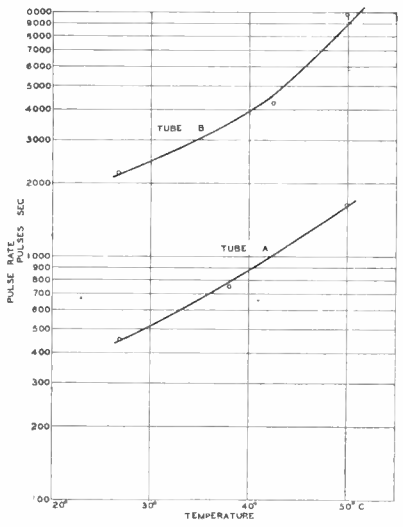

Fig. 4—Dark current pulses and temperature.

An external electrostatic shield around the glass envelope of a multiplier may have a marked effect on its noise output.* It is found that a good multiplier having a low pulse output is relatively unaffected by the dc potential of a shield surrounding the envelope. However, the number of pulses in the output of many multipliers may be greatly changed by varying the potential of the external shield. Figure 5 illustrates the performance of such a multiplier as the shield potential is varied. The collector of this multiplier was grounded and the

* This effect was first pointed out to the authors by Dr. A. M. Glover, RCA Victor Division, Lancaster, Pennsylvania.

cathodes operated at 1,000 volts. It will be seen that as the shield is made negative to about —800 volts the count rate decreases. In the range from 200 volts positive to 50 or 100 volts negative with respect to the photocathode, the counting rate remains relatively constant. Making the shield more negative again increases the dark current pulse rate. It should be pointed out that while the general effect of shield potential on multiplier performance will be as indicated, there are very large quantitative differences between different multipliers. Although the exact cause of this effect is not known, it is probably due to the effect of the potential of the inner surface of the glass near the photocathode on ions in the tube. The potential of the inner surface of the glass is altered by the leakage through the glass to the external shield. Where the multiplier envelope is of a high resistance glass, as in the case of the 1P28, the potential of the external shield makes little difference on the pulse performance.

Performance Under Light Stimulation

The nature of the pulse output from a multiplier stimulated by light is of equal importance with the dark current pulse performance in determining its suitability for scintillation counters. Therefore, a series of multipliers were measured under conditions of light stimulation, such that the pulses due to individual photoelectrons could be measured. For these measurements, the multiplier in the measuring chamber was cooled to the temperature of dry ice in order to reduce the dark pulses to a low value. Under these conditions, as has already been pointed out, a good multiplier will produce less than 5 pulses per second of amplitude corresponding to one electron times the average gain of the multiplier.

The effective gain of the multiplier being known, a measurement of the output current change when the multiplier is illuminated gives a measure of the photocurrent leaving the photocathode. From this photocurrent the number of photoelectrons leaving the cathode each second can be determined directly. Using a known number of photoelectrons per second from the photocathode, the number of output pulses per second as a function of pulse height were measured. Figure 6 illustrates a typical distribution curve obtained in this way. The ordinate of this figure is the number of pulses observed divided by the number of photoelectrons from the photocathode, while the abscissa, as before, is measured in units equal to the charge on an electron times the effective gain of the multiplier. One of the first things that will be noticed is that the curve does not approach unity for zero pulse

height, but rather intersects the axis at 0.7. This means that 30 per cent of the photoelectrons from the photocathode do not reach the output of the multiplier. If the voltage between the photocathode and first dynode is raised, the fraction of photoelectrons which eventually appears in the output is increased. This is illustrated by the family of curves in Figure 7. The distribution curves obtained under the different conditions of voltage between the first dynode and photocathode are essentially the same. However, when examined in detail, it will be found that the distribution is slightly sharper at higher voltages. In general, the distribution of pulse heights obtained from the light stimulated multiplier shows noticeably fewer large pulses than it does for the dark current.

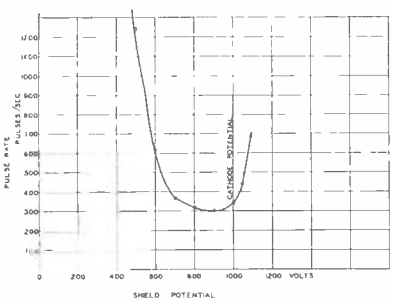

Fig. 5—Effect of shield potential on dark current pulses.

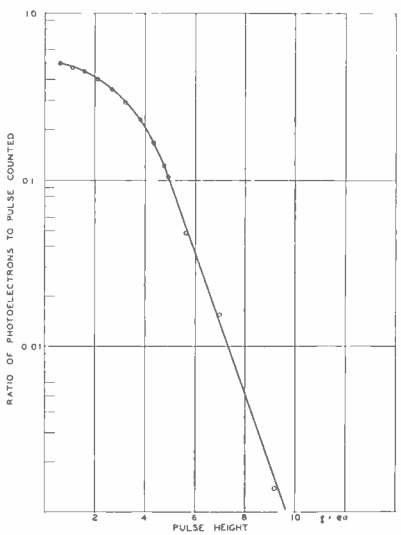

Fig. 6—Pulse height of photoelectric pulses.

The distributions obtained are not those that would be expected under the assumption that the secondary emission from each stage followed a Poisson distribution. Under this assumption, the nature of the distribution curve can be deduced as follows: if the secondary emission ratio for a stage is R, then the probability of Z electrons being emitted when an electron strikes, the stage is by Poisson's Law

$$p(Z) = \frac{e^{-R}R^{Z}}{Z!}.$$

With this as a basis, a generating function[4] $F(x)$ can be set up for the n stages in cascade, where

$$F(x) = f_1(f_2(f_3(\text{- - - - }(f_n(x))))))$$

and

$$f_k(x) = \sum_{Z=0}^{\infty} P(Z)\, x^Z = \sum_{Z=0}^{\infty} \frac{e^{-R}R^Z}{Z!}\, x^Z = e^{-R}e^{Rx}$$

hence

$$F(x) = e^{-R}e^{Re^{-R}e^{Re^{-R}e^{R}}}$$

repeated n times.

It is a property of this function that the yield expectation is given by:

$$\bar{Z} = F'(1)$$

and the second moment by:

$$\overline{\Delta Z^2} = F''(1) + F'(1) - [F'(1)]^2.$$

Performing the indicated operations, the yield expectation is of course:

$$Z = R^n$$

and the second moment

$$\overline{\Delta Z^2} = R^n(R^n + R^{n-1} + \text{- - - - - - } R + 1)$$

$$= \frac{R^n(R^{n+1} - 1)}{(R - 1)}.$$

If n is a large number, as is the case in practice, the second moment per electron reduces to:

$$\frac{\overline{\Delta Z^2}}{Z^2} = \frac{R}{R - 1}.$$

The actual measured distribution, however, is found to have a second

[4] T. Jorgensen, Jr., "On Probability Generating Functions", *Amer. Jour. Phys.*, Vol. 16, No. 5, p. 285, May, 1948.

moment of more nearly twice the value predicted by the relation given above. This difference may be because the secondary electrons from each dynode do not follow a Poisson distribution or alternatively, it may be because of the loss of electrons between one stage and the next. The second explanation probably accounts for most of the increase in the spread of the distribution of pulses at the output.

Returning again to the matter of the efficiency of collection of electrons by the first dynode, a series of measurements were made where the light was focused on a small spot of the photocathode. Figure

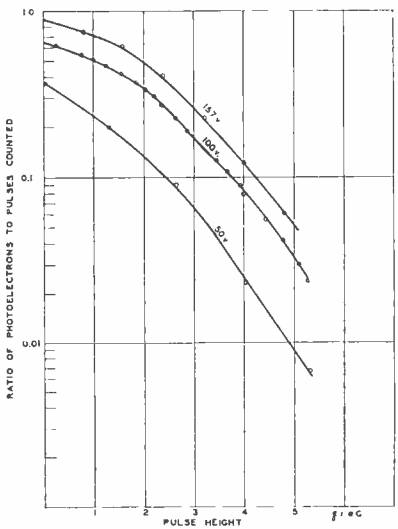

Fig. 7—Distribution with different photocathode to dynode voltages.

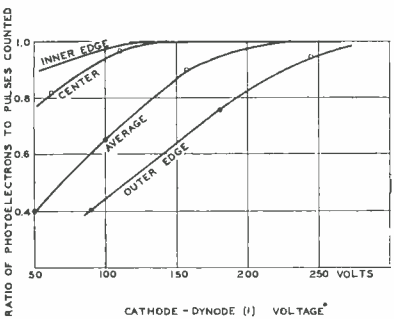

Fig. 8—Fraction of photoelectrons reaching dynode.

8 shows a family of curves taken in this way. It is apparent that the photoelectrons from a spot near the inner edge of the photocathode and near the center of the photocathode are totally collected at a relatively low voltage. However, electrons originating from the outer edge of the photocathode require a very high voltage for efficient collection. Again, the pulse height distribution curves obtained from the emitting spot in different positions on the photocathode are almost identical.

Conclusion

The curve given in Figure 3 permits the determination of the number of dark current pulses per second from a good multiplier for any pulse height setting. This, for example, would give the background output of a detector. Selecting the maximum allowable background

count for a given application of the scintillation detector, the number of photoelectrons required from each scintillation to ensure its detection can readily be determined with the aid of the curve in Figure 6. Also from curves 8 and 9 it is evident that some improvement in efficiency can be obtained by using a somewhat higher voltage between the photocathode and first dynode. For example, where a multiplier is operated with a 100 volts per stage, 150 volts between the photocathode and first dynode ensures a higher percentage utilization of the primary photoelectrons. Finally, a very real advantage can be obtained with some multipliers by operating the tube with a conducting shield around it which is maintained at cathode potential. The 931-A type of multiplier (i.e. RCA 931-A, 1P21, and 1P28) was, of course, not designed for a scintillation counter. Nevertheless this type of multiplier makes it possible, with proper care, to design a satisfactory scintillation detector.

DEVELOPMENTAL TELEVISION TRANSMITTER FOR 500-900 MEGACYCLES*

By

R. R. Law, W. B. Whalley, R. P. Stone

Research Department, RCA Laboratories Division,
Princeton, N. J.

Summary—*Tubes and circuits have been developed which make possible a one-kilowatt-peak-power wide-band television transmitter for the 500-900-Mc band. A detailed account of these developments is presented.*

The ultra-high-frequency tube employed in this transmitter is a modified form of the 600-Mc oxide-coated-cathode pulse-triode developed during the war[1]. In a push-pull amplifier a pair of these tubes gives a continuous-wave output of more than one Kw at 800 Mc, and in wide-band service such as would accommodate a color television picture of the highest quality, a peak power of more than one Kw is readily obtained. A novel feature of the new tube is the tungsten-wire grid which leads to an unusually rugged tube. Because of excellent grid cooling there is no trace of grid emission; this fact undoubtedly contributes to the stability of the system.

Wide-band operation imposes severe requirements on circuit design. In the rf amplifier, precaution is taken to keep the stored energy low. In the video amplifier, operation at high power level is accomplished by employing the above mentioned pulse triode to cathode-modulate the rf amplifier. This combination of a large-area-cathode "Class-A" modulator tube and an intermediate-area-cathode "Class-B" rf tube is advantageous for wide-band service.

Introduction

DURING the course of the development of a 600-Mc oxide-coated-cathode pulse triode during the war[1], it became apparent that a modified version of this tube would be advantageous for continuous-wave applications. Consideration of the fundamental electronics of ultra-high-frequency transmitting tubes[2-7] indicated that

---

* Decimal Classification: R583.4 × R583.6

[1] R. R. Law, D. G. Burnside, R. P. Stone, W. B. Whalley, "Development of Pulse Triodes and Circuit to Give One Megawatt at 600 Megacycles", *RCA Review*, Vol. VII, No. 2, pp. 253-264, June, 1946.

[2] D. C. Prince, "Vacuum Tubes as Power Oscillators", *Proc. I.R.E.*, Vol. II, p. 275, June; p. 405, August; and p. 527, October, 1923.

[3] W. G. Wagener, "The Developmental Problems and Operating Characteristics of Two New Ultra-High-Frequency Triodes", *Proc. I.R.E.*, Vol. 26, pp. 401-414, April, 1938.

[4] A. V. Haeff, "Effect of Electron Transit Time on Efficiency of a Power Amplifier", *RCA Review*, Vol. IV, No. 1, pp. 114-122, July, 1939.

[5] C. C. Wang, "Large-Signal High-Frequency Electronics of Thermionic Vacuum Tubes", *Proc. I.R.E.*, Vol. 29, pp. 200-214, April, 1941.

[6,7] See following page.

such a tube might perform satisfactorily in the 500- to 900-Mc band, particularly if the interelectrode spacing could be kept small.

On the basis of this theory and as a result of preliminary tests it appeared that a push-pull rf power amplifier employing a pair of these tubes should give one-Kw continuous-wave at 800 Mc. Furthermore, from an estimate of the ratio of stored-to-active energy, it seemed that such an amplifier should have a bandwidth of between 15 and 20 Mc. In the light of the thinking at that time, development of wide-band transmitters to explore the possibilities of television at higher frequencies was very desirable. Also, there were a number of basic questions to be answered. Are oxide-coated-cathodes suitable for use in moderate power ultra-high-frequency transmitting tubes? What is the best way to modulate the triode? And finally, is neutralization necessary in grounded-grid circuits? This paper outlines the results of a study to answer these and other questions.

Tube Development

The essential features of the tube developed for these tests may be seen in Figure 1. Starting at the lower left and proceeding clockwise around the photograph may be seen: 1) the stem assembly; 2) the cathode-support assembly; 3) the heater; 4) the cathode; 5) the cathode-heater assembly; 6) the cathode-stem assembly; 7) the grid assembly; 8) the grid-stem assembly; 9) the final assembly; and in conclusion, in the center of the photograph, the complete tube including air-cooled radiator.

The cathode is approximately one and one-half inches in diameter and has a coated area of about 7.5 square centimeters. The heater, a single helical coil of 0.010 inch diameter insulated tungsten wire, requires about 3 amperes at 18 volts to bring the cathode to operating temperature in the absence of back bombardment.

The grid consists of 180 pieces of 0.007 inch diameter tungsten wire silver-soldered to the oxygen-free-high-conductivity copper cap and support cone. The ends of the tungsten wires are lightly nickel-plated to facilitate "wetting" by the solder. In order that none of the wires shall inadvertently bow inward, they are sprung outward by a stainless-steel jig which holds them as they are soldered in a hydrogen-atmosphere furnace. The slots in the base of the grid cone provide flexibility to mitigate ill effects from differential expansion between

[6] G. J. Lehmann and A. R. Vallarino, "Study of Ultra-High-Frequency Tubes by Dimensional Analysis", *Proc. I.R.E.*, Vol. 33, No. 10, p. 663, October, 1945.

[7] R. R. Law, "Electronics of Ultra-High-Frequency Triodes", accepted for publication in *Proc. I.R.E.*

Fig. 1—Details of ultra-high-frequency continuous-wave triode.

the grid cone and the Kovar grid flange. The grid cone is spot welded directly to the grid flange. An electroplated layer of nickel on the base of the cone facilitates making this weld. Because of the excellent grid cooling there is no trace of grid emission. This construction makes possible an unusually rugged tube, and the wires are so refractory that the grid is almost indestructible.

One of the perennial problems in making vacuum tubes is how to seal in the mount or assembled tube without damaging critical parts. Although use of a nitrogen atmosphere to prevent oxidation[8] will suffice for thoriated-tungsten filament tubes, oxide-coated-cathode tubes are more susceptible to damage by overheating and contamination. "Cold-sealing" has been accomplished by radio-frequency-heating tech-

[8] S. Frankel, J. J. Glauber, J. P. Wallenstein, "Medium-Power Triode for 600-Megacycles", *Proc. I.R.E.*, Vol. 34, pp. 986-991, December, 1946.

niques[9], but for experimental tubes the equipment required for this process cannot be justified. In view of the attractiveness of the gold-diffusion seal[10], development of a technique for joining Kovar-to-Kovar by this method was undertaken. It was found that such a seal could be made by the following procedure: 1) copper-plate the Kovar parts, approximately 0.001 inch thick; 2) fire in hydrogen atmosphere for 20 minutes at 1030°C to bond the copper to the Kovar; 3) perform glassing operation in the conventional manner; 4) remove oxide and again copper-plate, the copper layer so applied adheres firmly to the Kovar and provides a vacuum-tight copper-Kovar bond; and finally, 5) a gold ring compressed between the two copper-plated Kovar parts serves to unite the parts during baking by the familiar gold-diffusion process.

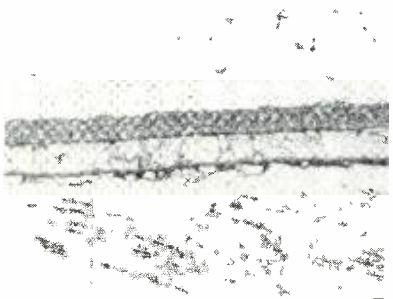

Fig. 2—Diffusion seal for bonding Kovar-to-Kovar.

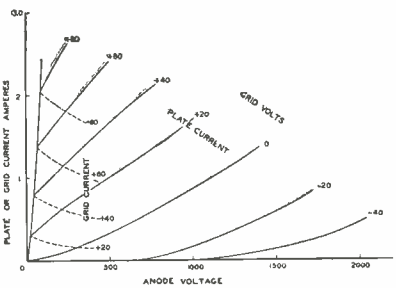

Fig. 3—Static characteristics of ultra-high-frequency continuous-wave triode.

Figure 2 is a photomicrograph of one side of such a composite seal. The Kovar is below, the gold above. The lighter layer between the gold and Kovar is the copper-plate that was fired at 1030°C. The dark layer is unfired copper. There is no visible evidence that the gold has penetrated the copper during the 450°C bake, but when the parts are forcibly pulled apart a layer of gold adheres to the copper. This sealing technique permits assembly of the tube parts without contamination and in the present case does away with the all too familiar problem of poisoning of the oxide-coated-cathodes. Furthermore, the better vacuum obtainable with cleaner parts undoubtedly improves life.

The static characteristics of this tube are shown in Figure 3. For purposes of comparison, its continuous-wave performance as an oscil-

[9] W. P. Bennett, E. A. Eshbach, C. E. Haller, W. R. Keye, "A New 100-Watt Triode for 1000 Megacycles", *Proc. I.R.E.*, Vol. 36, No. 10, pp. 1296-1302, October, 1948.

[10] J. B. Fiske, H. D. Hagstrum, L. P. Hartman, "The Magnetron as a Generator of Centimeter Waves", *The Bell System Technical Journal*, Vol. XXV, No. 2, April, 1946.

lator at 800 Mc is shown in Figure 4. On the basis of this performance the empirical relation for efficiency[7] indicates that its equivalent cathode-grid spacing is 0.015 inch. This checks with the dimensions of the parts when allowance is made for the fact that the hot spacing is approximately 60 per cent of the cold spacing.

Preliminary life tests were made at power levels corresponding to 300, 400, and 500 watts continuous-wave output in rf amplifier service. With the limited data available there is no correlation between life and power level. Inasmuch as the 300-watt-continuous-wave level with a single tube corresponds to transmitting one-kw-peak-power with a "black" picture in the two-tube television transmitter, the remainder of the tests were run at the 300-watt-continuous-wave level.

The primary factor affecting life is cathode temperature. Because of back bombardment resulting from transit-time effects, the heater input must be materially reduced. In practice, it is found that after the tube is up to normal power, the heater power should be reduced about 50 per cent. An additional point of interest came out of the life test data in view of the fact that early samples employed a cathode coating of less than 3 milligrams per square centimeter, whereas 7 to 12 milligrams per square centimeter is recommended. This compromise was introduced in the early tests to minimize cathode peeling during manufacture which frequently occurs during humid weather. These samples gave 400 to 600 hours life. Later samples employing the recommended coating gave more than 1,000 hours life. Evidently life is proportional to cathode thickness.

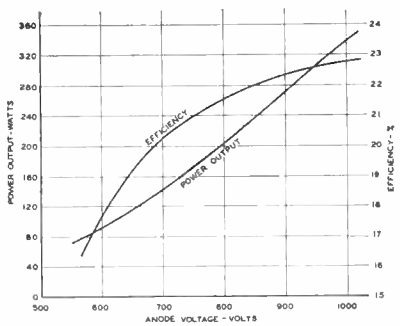

Fig. 4—Performance of continuous-wave triode as oscillator at 800 Mc.

Circuit Development

From the static characteristics of Figure 3 and the experimentally determined optimum operating point it may be deduced that the rf anode voltage swing is about 1,000 volts peak-to-peak under conditions corresponding to one kilowatt power output from the two-tube transmitter. In view of the 0.080 inch grid-anode spacing, the energy stored at the tube electrodes is about 1.0 micro-joule or less than 0.06 micro-joule per square centimeter. The active energy, or energy supplied by the tubes on the other hand is 1.2 micro-joules or approximately 0.08 micro-joule per cycle per square centimeter at 800 Mc. Inasmuch as

$$Q = (2\pi)\ (\text{Stored Energy})/(\text{Active Energy per Cycle})$$

and bandwidth or frequency separation between half-power points Δf is[11]

$$\Delta f = (\text{Operating Frequency})/(Q \text{ of System}),$$

the bandwidth resulting from the capacitance of the tube elements themselves would be greater than 180 Mc. This bandwidth is so large as to be of little practical significance other than to emphasize the fact that the circuit will be the determining factor.

In the case of the cathode-modulated rf amplifier the energy stored in the cathode-grid circuit has no adverse effect on bandwidth. In fact, it may be desirable to store energy in this circuit to stabilize the driver during peak power pulses. In contrast, energy stored in the anode circuit is very detrimental. Unfortunately the present tube cannot be operated in fundamental-mode circuits at these frequencies, and harmonic-mode operation materially increases the stored energy. For push-pull operation the anode line must be three-halves wavelength long. Connections for dc are made at the midpoint. Furthermore, if the circuit is to be tunable over an appreciable frequency range, the electrical position of the discontinuity between tube and circuit will shift. In view of this, it is desirable to keep the characteristic impedance of the circuit so low that special means of transformation will not be required. This is possible in the present case. The four-inch-diameter-internal-conductor one-quarter-inch-radial-separation line even with the most unfavorable match gives rise to a maximum voltage of less than 600 volts peak-to-peak. On this basis the maximum energy stored in the circuit at 800 Mc would be about 5 micro-joules.

To complete the estimate of bandwidth, allowance must be made for the energy stored in the unmatched portion of the output system. Because it is difficult to adjust the load coupling loop size, matching stubs are desirable. With a voltage-standing-wave ratio of $\sqrt{2}$, the energy stored in the stubs and unmatched portion of the output system is about 3.0 micro-joules. To sum up, at 800 Mc the energy distribution would be:

Energy stored in tubes	1.0 micro-joules
Energy stored in circuit	5.0 micro-joules
Energy stored in matching stubs	3.0 micro-joules
Total energy stored	9.0 micro-joules
Active energy per cycle	1.2 micro-joules

[11] F. E. Terman, RADIO ENGINEERING HANDBOOK, McGraw-Hill Book Co., Inc., New York, N. Y., 1943, pp. 429-430.

whereupon the estimated bandwidth is

$$f = \frac{(800)\,(1.2 \times 10^{-6})}{2\pi\,(9.0 \times 10^{-6})} = 17 \text{ megacycles.}$$

In practice the bandwidth may be somewhat greater than this if the load-coupling-loop match or the tube-to-circuit match are more favorable.

The physical layout of the circuits developed for this transmitter may be seen in Figures 5 and 6. In Figure 5, the unit on the left is the driver and the unit on the right is the cathode-modulated rf amplifier. The coaxial line serving to transmit power from the anode cavity of the driver to the cathode cavity of the amplifier with its

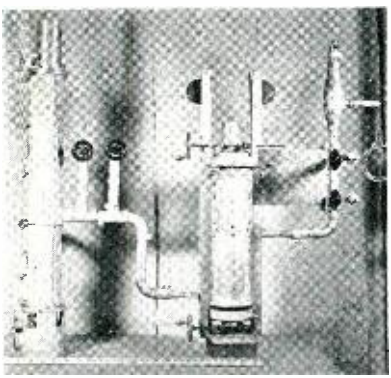

Fig. 5—500-900 Mc driver and rf power amplifier.

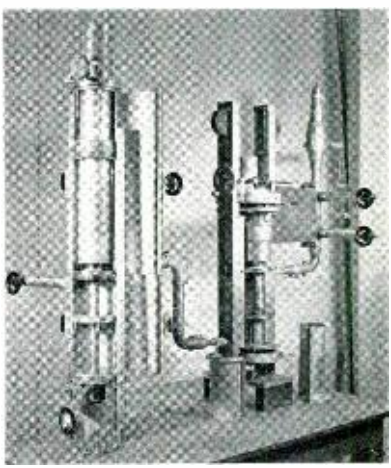

Fig. 6—Rf circuit details.

matching stubs may be seen in the center of the picture. The coaxial line serving to transmit power from the amplifier to the water-cooled resistance load with its matching stubs may be seen in the right of the picture. In Figure 6, the covers of the units have been swung open or partially removed to reveal circuit details.

To take advantage of the bandwidth capabilities of this amplifier, the wide-band modulator shown in Figure 7 was developed. This modulator employs a pair of the aforementioned pulse triodes[1] to cathode-modulate the rf amplifier. These modulator tubes make possible a current change of more than two amperes at an equivalent transconductance of 0.15 amperes per volt. Such a combination of a large-area-cathode "Class-A" modulator tube and an intermediate-area-cathode "Class-B" radio frequency tube is advantageous in wide-band service. The cathode-coupled stage ahead of the pulse triodes serves

to lower the effective input capacitance presented to the video amplifier.

Bias to the cathodes of the amplifier and final modulator stage is supplied through the special choke "L" which is split into sections of progressively increasing size to provide relatively high impedance over the video band. So long as this impedance is large compared to $R_p/(1+\mu)$, the gain is substantially constant and equal[11] to $\mu/(1+\mu)$. In operation, the dc current to the anodes of the amplifier and modulator is substantially constant; modulation at video frequencies serves to switch the current from the amplifier to the modulator and vice versa.

Performance of System

The overall performance of the rf power amplifier and composite system is indicated in Figures 8, 9, and 10.

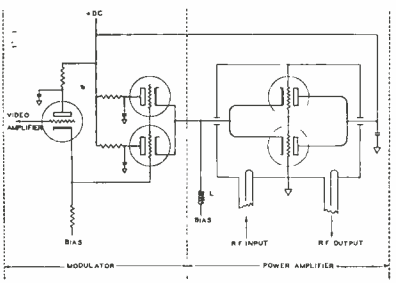

Fig. 7—Wide-band modulator circuit.

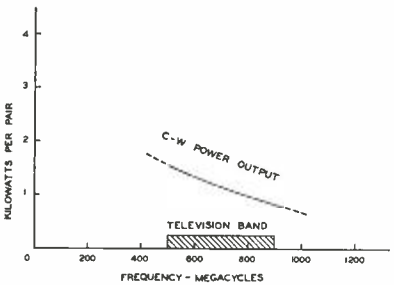

Fig. 8 — Variation of rf power amplifier output with frequency.

Figure 8 shows the variation of continuous-wave power output with frequency at a fixed anode voltage of 900 volts. It will be observed that the anode efficiency of the amplifier is appreciably higher than that shown for the oscillator in Figure 4. The difference arises from the fact that the oscillator must supply its own exciting power whereas the amplifier does not. Inasmuch as the power gain of this tube as an amplifier under typical operating conditions is approximately three, the amplifier output and efficiency may be expected to be about 50 per cent greater than that of the oscillator.

Figure 9 indicates the broadband potentialities of the amplifier. Here is plotted the relative voltage in the sidebands as a function of sideband frequency relative to the 800 Mc carrier. The circled points joined by the solid line were taken by direct measurement of sideband voltage in a calibrated spectrum analyzer. Conjugate points were measured with the same circuit adjustment; in each case adjustments were made so that both sidebands would have equal amplitude. The ease with which these adjustments could be accomplished suggests that

the response is nearly symmetrical. Due to the finite bandwidth of the spectrum analyzer it was not possible to measure the response immediately adjacent to the carrier. The intermediate region was checked by direct observation of percentage modulation on the oscilloscope[12]. To increase the accuracy of readings the data were taken at high percentage modulation. Thus, the amplitude of the modulating voltage was adjusted to give 90 per cent modulation at low frequency, whereupon its amplitude was held constant as its frequency was varied. Because of this choice, the ordinate scale of Figure 9 corresponds to percentage modulation as well as relative sideband voltage.

As may be seen from this response curve, the —3-db points are approximately 19 Mc apart. If vestigial sideband operation were employed, such an amplifier would accommodate a color television picture of the highest quality.

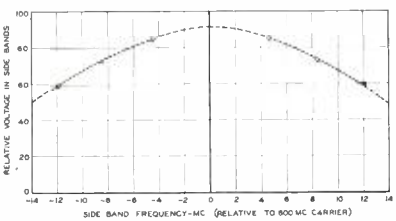

Fig. 9—Wide-band response of rf power amplifier.

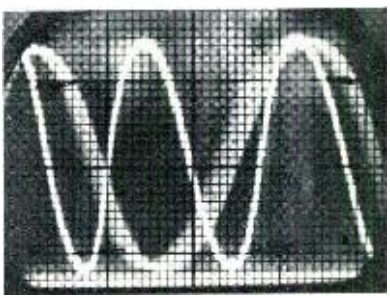

Fig. 10—Rectified rf output with sine wave modulation.

The linearity of modulation is indicated in Figure 10. This photograph shows the rf load-diode-voltage as a function of time with 1.6 Mc sine wave modulation. Zero power level as established by the vibroswitch[12] is indicated by the horizontal line at the bottom of the picture. Under the conditions portrayed the peaks correspond to 1.4 Kw and the modulation is very nearly 100 per cent.

Contrary to the experience of previous workers[8,13,14] there has been no indication of a need for neutralization. This difference arises from the low impedance of the present tubes as compared to those previously available. Although it is possible to adjust the present amplifier so that it will oscillate, this adjustment is far from the normal operating

[12] T. J. Buzalski, "A Method of Measuring the Degree of Modulation of a Television Signal", *RCA Review*, Vol. VII, No. 2, pp. 265-271, June, 1946.

[13] E. Labin, "Design of the Output Stage of a High Power Television Transmitter", *Electrical Communications*, Vol. 20, No. 3, p. 193, 1942.

[14] C. E. Strong, "The Inverted Amplifier", *Electronics*, Vol. 13, pp. 14-16, July, 1940.

point. Because of the relatively high mu, the cathode-anode capacitance is low and the undesired cathode excitation is small in comparison to the driver excitation required for the low impedance system throughout the 500-900 Mc frequency range. Oscillation is possible only when the amplifier is unloaded and when the anode and cathode cavities are detuned to give the appropriate grid-anode-voltage phase relationship[15].

Conclusions

Tests in a developmental 500-900 Mc television transmitter indicate that oxide-coated cathode triodes may be used for moderate power ultra-high-frequency transmitter applications. Although modulation of the triode presents a serious problem, for wide-band service this difficulty is in part overcome by employing a large-area-cathode "Class-A" modulator tube to cathode-modulate an intermediate-area-cathode "Class-B" rf tube. With tubes and circuits of proper design operating under wide-band conditions there is no need for neutralization in this frequency range.

Acknowledgments

The writers wish to express their appreciation for the stimulating discussions and practical assistance given by many members of the RCA Laboratories Technical Staff and Service Groups.

[15] E. E. Spitzer, "Grounded-Grid Power Amplifiers", *Electronics*, Vol. 19, pp. 136-141, April, 1946.

ELECTRO-OPTICAL CHARACTERISTICS OF TELEVISION SYSTEMS*

By

Otto H. Schade

Tube Department, RCA Victor Division,
Harrison, N. J.

NOTE: This paper consists of an Introduction and four parts: Part I—Characteristics of Vision and Visual Systems; Part II—Electro-Optical Specifications for Television Systems; Part III—Electro-Optical Characteristics of Camera Systems; Part IV—Correlation and Evaluation of Electro-Optical Characteristics of Imaging Systems. The Introduction and Part I appeared in the March 1948 issue of RCA Review, Part II in the June 1948 issue, and Part III in the September 1948 issue. Part IV, the concluding part, follows.

PART IV — CORRELATION AND EVALUATION OF ELECTRO-OPTICAL CHARACTERISTICS OF IMAGING SYSTEMS

Summary—*Principal characteristics of the motion picture process are evaluated and co-ordinated with the television process by determining the transfer characteristics, signal-to-fluctuation ratios, and the aperture flux response of photographic film. A quantitative analysis and comparison of the performance of specific imaging systems such as the standard television and motion picture system is undertaken. The transfer characteristics of the image orthicon and the gradation scale of television images are treated in greater detail, and the critical brightness for threshold grain visibility (noise) is determined from the optical signal-to-fluctuation ratio in the reproduced image.*

Methods for increasing the image sharpness are shown to be processes adding a negative "aperture" characteristic to the system. A general curve for a subjective rating of image sharpness is established by combining the "aperture"-response characteristics of the eye and the external imaging process.

A. Characteristics of the Motion Picture Process

Photographic film is used extensively in television systems as a source of picture signals, particularly in the form of motion picture film. A brief analysis is made to co-ordinate the characteristics of the photographic process and the silver image on positive film with the television process.

1. *Signal-to-Fluctuation Ratios and Transfer Characteristics*

The principles of the photoelectric and energy-storing processes in

* Decimal Classification: R138.3 × R583.12

photographic and television cameras have been discussed in Part IIIA. It is known that, when photographic film is exposed to light, photoelectric action produces a certain number of submicroscopic silver "specks" which are subsequently developed into much larger silver grains. The number of grains per unit area is proportional to the photographic density D and increases with exposure E according to a law of diminishing returns. Because the grain distribution is substantially random and grain sizes are controlled to remain within certain limits for a particular film type, signal and fluctuations in the primary process (light to grain number) are determined fundamentally by the number n' of "equivalent" grains in a given picture element area a as outlined in Part IIIA, Equation (40).*

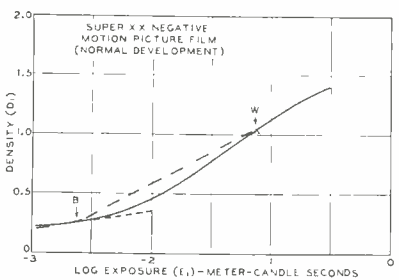

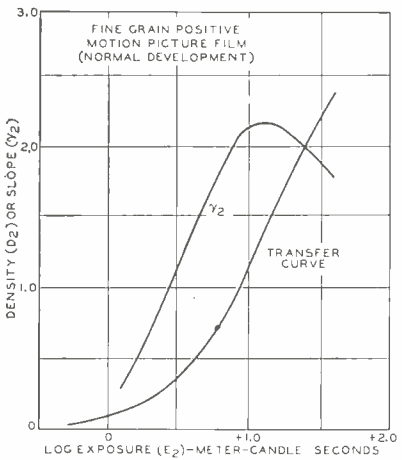

Fig. 73 — Transfer characteristics of motion picture film.

The normal sensitometric curves of film $D = f(\log E)$

shown in Figure 73 may, therefore, be regarded also as a graph of the relative silver grain density n'/a as a function of exposure E in semi-logarithmic coordinates and may thus be compared directly with the transfer characteristics of the camera tube shown in Part III, Figures 66 and 67. The signal-to-rms fluctuation ratio $|R|_D$ of the primary process can, therefore, be computed with Equation (40) and may be written

$$|R|_D = D/(D/n')^{\frac{1}{2}} \tag{83}$$

where n' is the number of equivalent grains at the density D of 1 in a selected elemental area a. In the secondary (copying) process of light modulation by the film, the new transfer characteristic $\tau = f(D)$ is introduced and the fluctuation ratio is altered because of the

* Deviations from the theory occur near the ends of the transfer range as in most practical processes.

reciprocal logarithmic relation between density and transmission τ, $D = 1/\log \tau$. The modified ratio $|R|_1$ in the light-signal transmitted by the negative film is inverted and increases with the transmission τ as computed from the rms density fluctuation or deviation

$$\Delta D_1 = (D_1/n')^{\frac{1}{2}} = \log \Delta\tau_1/\tau_1 \quad (84a) \qquad \text{and} \qquad |R|_1 = \tau_1/\Delta\tau_1. \quad (84b)$$

The ratios $|R|_D$ and $|R|_1$ are shown in Figure 74 as a function of negative film transmission τ_1 for a grain number n' of 100 per element at unit density D of 1. To represent a particular film type, the picture element a must be specified, or, for a specified elemental area (channel width), $|R|_1$ is to be determined by a grain count or by measurement (See page 657).

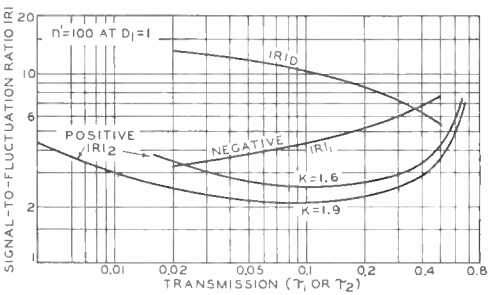

Fig. 74—Signal-to-fluctuation ratios in the motion picture process:
For $\overline{N}_{ca} = 410$ and Super XX negative film, multiply $|R|$ by 5.25
For $\overline{N}_{ca} = 410$ and Panatomic X negative film multiply $|R|$ by 7.8

The theoretical change of $|R|_1$ from $\tau = 0.06$ to $\tau = 0.44$ is confirmed by the oscillograms, Figure 75, taken with the television microphotometer on Super XX film. The ratio of signal (pulse at right hand side) to peak-to-peak fluctuation agrees in relative magnitude with the computed values in Figure 74.

Signal and fluctuations undergo further changes in the copying process from the low-gamma negative to a higher-gamma positive film which causes, in general, an expansion of the light signal. The ratio $|R|_1$ is, therefore, reduced to a lower value $|R|_2$ (See Part III, A5). Because of logarithmic transfer relations, the exposure E_2 of the positive film is given by

$$\log E_2 = K - D_1 \quad (85)$$

where K is a constant specifying the exposure level. Typical overall transfer characteristics, $\tau_2 = f(E_1)$, for a motion picture film process computed with the values $K = 1.6$ and 1.9 and the film characteristics, Figure 73, are shown in Figure 76. The modified fluctuation ratio $|R|_2 = \tau_2/\Delta\tau_2$ (See Figure 74) is computed with Equation (84) by multiplying the deviation ΔD_1 by the associated positive film gamma:

$$\Delta D_2 = \Delta D_1 \gamma_2 = \log \Delta\tau_2/\tau_2 \qquad \text{and} \qquad |R|_2 = \tau_2/\Delta\tau_2. \tag{86}$$

This value $|R|_2$ does not contain fluctuations introduced by the positive film grain which add in quadrature, but these can be neglected when the positive film has a finer grain than the negative film.

2. Equivalent Optical and Electrical Channels for Random Fluctuations

The picture element a defined by a physical aperture of uniform transmission (square or round) for the purpose of a grain count or a scanning operation is not equivalent in size to the picture element defined by a sharply terminated electrical channel with uniform frequency response (See Part III, A1). The electrical channel Δf of the television system cuts off the uniformly distributed frequency components of random fluctuations at a frequency corresponding to the balanced line number $\overline{N}_{co}$ (See Part I, B2).

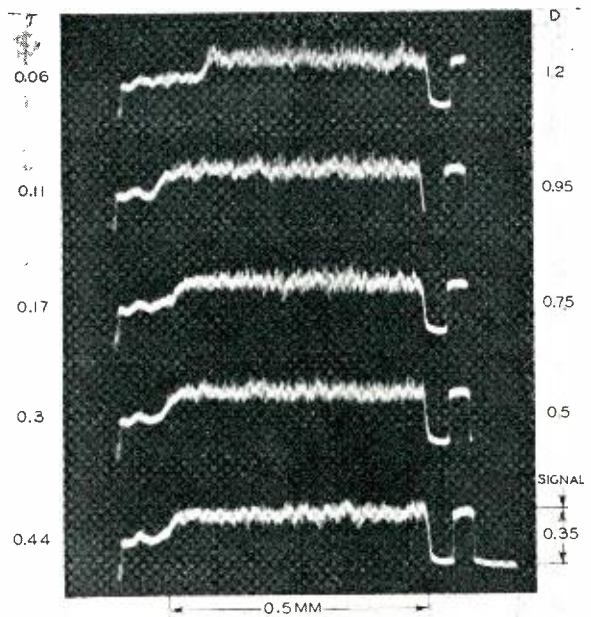

Fig. 75—Oscillogram of film-grain fluctuations at five different densities.

The size of the physical "aperture" duplicating the effect of a square-cutting electrical filter on the rms value of fluctuations can be established from the response characteristic of the scanning aperture to *sine-wave* flux patterns of constant amplitude. The "filter factor" m for random fluctuations is then determined as outlined in Part I, B2, pp29.* The sine-wave response of a square aperture is

* The filter factors given in Part I for the eye and kinescope were computed from the equivalent square-wave response ($r\Delta\bar{\psi}$), because the sine-wave response was not known. The values m are, therefore, somewhat too low for channels near and beyond eye resolution. The filter factor computed from the equivalent square-wave response in the total pass band of the square aperture is $m' = 0.58$ as compared to the correct sine-wave value $m = 0.66$.

given by the $(\sin x)/x$ function (Figure 77). The filter factor computed from this "frequency response" curve has the value m of 0.66 for a channel extending to the first zero N_c. The equivalent electrical channel of constant frequency response ($m = 1$) extends, therefore, to the line number

$$\overline{N}_{eo} = m\,N_c = 0.66\,N_c \qquad (87)$$

As the size of the square aperture is $\delta = V/(N_\delta) = 2V/N_c$ (See Part IIA) we obtain

$$\delta = V/(N_\delta) = 1.32\,V/\overline{N}_{eo} \text{ (square aperture).} \qquad (88)$$

The diameter of a round aperture of equal area is larger by $\sqrt{4/\pi}$. The equivalent round aperture is, hence, approximated by

$$\delta = 1.49\,V/\overline{N}_{eo} \text{ (round aperture).} \qquad (89)$$

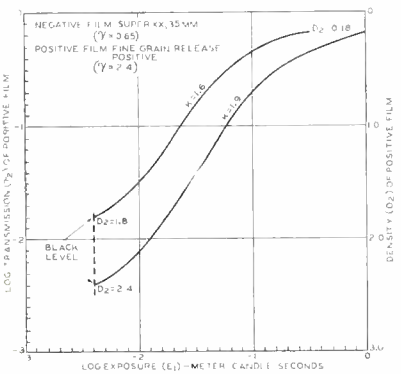

Fig. 76—Over-all transfer characteristic of motion picture film process.

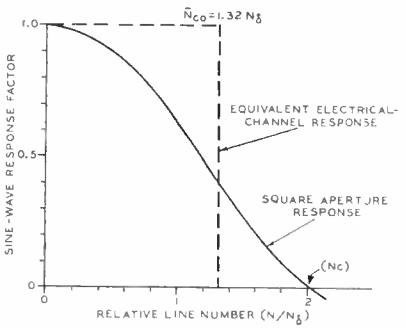

Fig. 77—Sine-wave response characteristics with equal filter effect on the RMS value of random fluctuations.

The filtering effect of a (standard) television channel ($\Delta f = 4.25$ megacycles) with the balanced line number $\overline{N}_{eo}$ of 410 can, therefore, be duplicated on film by a grain count or a scanning operation with the equivalent round aperture given by equation (89). For 35-millimeter film with the vertical frame size of 15.7 millimeters, the aperture diameter is $\delta = 57$ microns.

Jones and Higgins[31] have measured rms fluctuation values by scanning with a round aperture $\delta' = 39$ microns. Their values (See Table VIII) multiplied by the aperture ratio $\delta/\delta' = 57/39$ furnish the rms

[31] L. A. Jones and G. C. Higgins, "Photographic Granularity and Graininess", *Jour. Opt. Soc. Amer.*, Vol. 36, No. 4, pp. 203-207, April, 1946.

value $|R|_1$ of negative film as modified by the filter effect of a standard television channel. The corresponding fluctuation ratios $|R|_1$ and $|R|_2$ of motion picture film processes using Super XX or Panatomic X negative film are established by multiplying the $|R|$-scale in Figure 74 by the respective ratios $34.1/6.5 = 5.25$ or $52.1/6.7 = 7.8$. The relative "graininess" of motion picture and television images as seen by the eye will be discussed later.

Table VIII—Signal-to-Fluctuation Ratios of Photographic Film.

Film Type	Density	τ_1	$\|R\|_1$* ($\delta = 39\mu$)	$\|R\|_1$ ($\delta = 57\mu$)
Super XX	0.43	0.37	23.3	34.1
Panatomic X	0.4	0.396	35.7	52.1

* Values from reference (31).

The equivalent grain number n'_{57} for a 57-micron circle on Super XX film can be computed by multiplying the number $n' = 100$ assumed for Figure 74 by 5.25^2. This furnishes $n'_{57} \simeq 2750$ for $D = 1$. A 10-micron *square* contains $n'_{10} \simeq 100$ average grains. The side of this elemental area is equal to one line width at the limiting resolution of this film ($N_c = 100$ lines per millimeter) and indicates five grain layers, each layer containing approximately 4.5×4.5 spaced grains, with an average grain diameter in the order of 1 micron.

Microphotometer measurements of grain structures confirm that finer grains and fewer layers result, in general, in a higher limiting resolution; while high signal-to-fluctuation ratios require a large number of preferably similar grains within the considered element size to form a more continuous layer of closely packed grains side by side or staggered in depth.

3. Resolving Power, Contrast, and Aperture Response Characteristics

The resolving power N_c and the aperture flux response characteristic $r\Delta\bar{\psi} = f(N)$ of film, depend on the size of its silver grains and the number of grain layers (thickness of emulsion). Observations on a number of film types indicate a line width $1/N_c$ at the limiting resolution in the order of 6 to 10 average grain diameters. When the test signals are large, the response characteristic $r\Delta\bar{\psi}$ of a single film process is distorted by the exponential light transfer characteristic. To establish a reference to *the rated resolving power* of film which is determined with large signals, i.e., a test pattern contrast $C = 20$ to 30, measurements with this contrast have been made on several film types with the television microphotometer (See Part III). Typical

oscillograms are shown in Figure 78. A correction for lens response errors according to Equation (30), Part II, is necessary when measuring film with a resolution $N_c > 100$ television lines per millimeter. The response curve for a test object contrast $C \simeq 25$ is approximated quite well in the range $N/N_c < 0.8$ by $r\Delta\overline{\psi} = e^{-3.5\,N/N_c}$ (90)

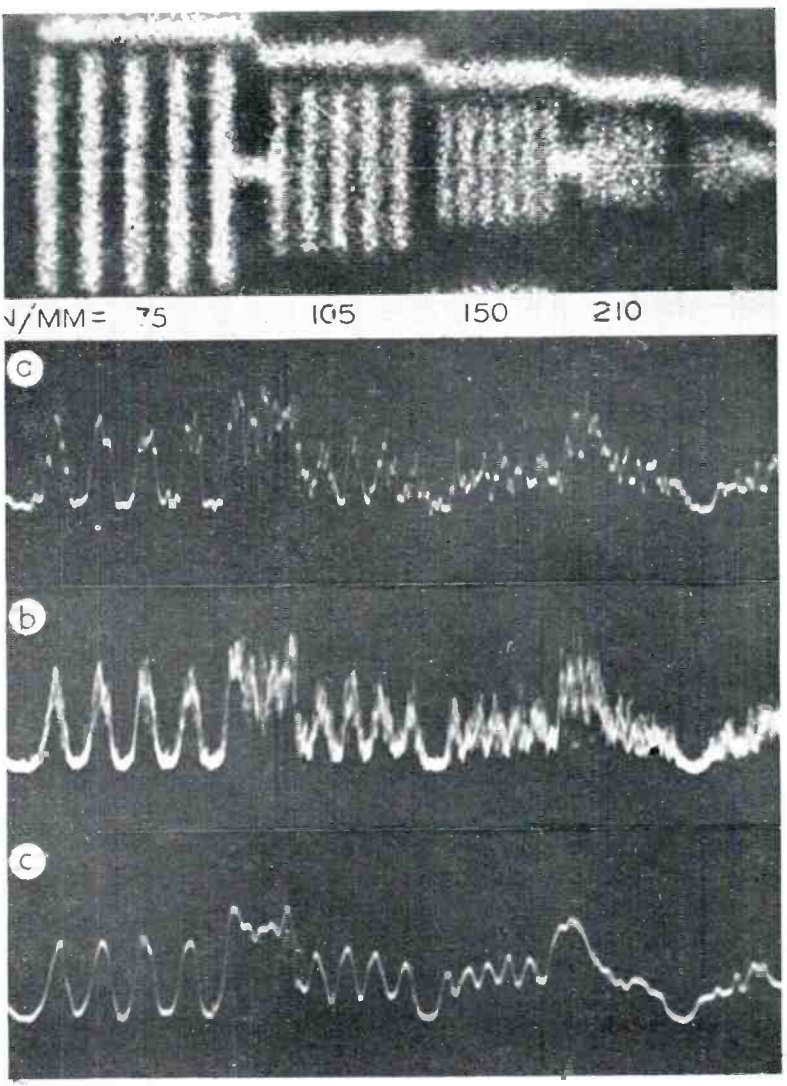

Fig. 78—Kinescope image and microphotometer traces showing limiting resolution of microfile film. a. Single line cross section. b. Six line cross sections superimposed. c. Single line cross section traced with larger scanning beam not resolving individual grains.

(Figure 79) where N_c is the rated resolving power* of the film type.

Response factors obtained with smaller signals, i.e., with a test object contrast $C = 2$, are more significant because the transfer characteristic is fairly linear for these increments. A series of measurements made with $C = 2$ on Super XX 35-millimeter film gave substantially the same values $r\Delta\bar{\psi}$ for exposures E_1 varied over a range of 20 to 1. The response curve, Figure 80, is a typical aperture response characteristic with a limiting resolution N_c equal to approximately 80 per cent of the rated value. Transfer of the negative test pattern into a positive causes further decrease of resolution due to the cascaded aperture effect of the second film. According to Equation (30), Part II, a positive film with double resolving power decreases the resolution by 10 per cent. This value is in substantial agreement with measured values (Figure 80). The signal distortion of the negative film is largely eliminated by the positive process. The response

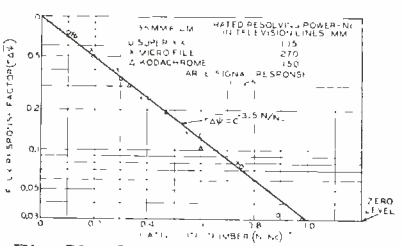

Fig. 79—General aperture response characteristics of photographic film for large signals.

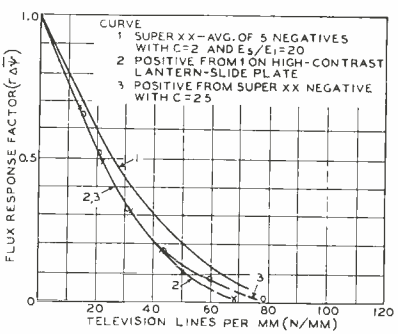

Fig. 80 — Aperture response of Super XX film before and after transfer on fine-grain positive film.

curves for $C = 25$ and $C = 2$ coincide in the positives except near cutoff which depends in visibility on the signal-to-fluctuation ratio. The flux response curves $r\Delta\bar{\psi}$ for positives made from negatives taken on Super XX film are representative of the performance of 35-millimeter motion picture film. The measurements furnish the values $N_c \simeq 75$ lines per millimeter and the value at 50-per cent response $N_{0.5} = 21$ lines per millimeter. For the 35-millimeter frame size $V = 15.7$ millimeters, the corresponding values are $N_c \cong 1175$ and $N_{0.5} = 330$ television lines.

It is possible to obtain higher aperture-response factors with large signals because non-linear film characteristics can act as peak limiters, and, by properly adjusted exposures, can suppress grain and square up sinusoidal waveforms. A resolution test made in this manner is obviously not indicating a normal aperture response because such exposures

* This value N_c corresponds to $r\Delta\bar{\psi} \approx 0.03$: higher values correspond to lower response factors.

destroy normal gradation. The "clipping" action, however, can be used to advantage when making test patterns.

B. The Over-All Characteristics of Television and Motion Picture Systems

1. *Sensitivity and Scene Luminance*

The scene luminance B_o required for a normal "exposure" in a photographic or television camera is determined basically by the photosensitivity and storage capacity of the particular film type or photo surface of the camera tube (See Part III). The sensitivity of the imaging system (for a given photosensitivity or "quantum" efficiency) decreases inversely with the storage capacity, but the image quality increases because larger energies result in higher signal-to-fluctuation ratios $|R|$, better resolution $\overline{N}_{co}$, or both, depending on the particular system. The scene luminance must be increased as the square of $|R|$ or $\overline{N}_{co}$. (See Equation (44), Part III). The criterion for a normal photographic exposure is the rendition of tone values near the "black" level. The *exposure index* of film (Weston, G. E., or ASA Exposure Index) is based on a light range of 30 to 1 on the film curve (See B to W in Figure 73) so positioned that the slope of the curve at point B is $\frac{1}{3}$ the slope of the straight line connecting points B and W. The "Kodak" speed $1/E$ is determined from the exposure E (meter candles $\times$ seconds) required for the black-level point B. Because Super XX film requires $E = 0.0025$, its Kodak speed is $1/E = 400$. Weston and G.E. speed ratings are obtained by multiplication with the factors 0.25 and 0.4, respectively, and have the values 100 and 160.

The speed index of camera tubes may be computed for comparison. The illumination E_i for point B on the characteristic of a high-capacitance image orthicon (Figure 67b, Part III) is $E_i = 0.008$ foot-candles for normal picture content. Because the exposure time T_f is 1/30 second, the exposure index (meter-candle seconds) is $1/E = 30/0.085 = 350$, corresponding to a Weston speed of 88. The close match with Super XX film in this example is incidental and misleading as high-capacitance tubes are not limited to the photosensitivity of the tube used for the example and have been built with higher photosensitivity. (See S for type 2P23 in Table VII, Part III). A more adequate basis for a comparison is the light flux required for equal performance, i.e., equal depth of focus, signal-to-fluctuation ratio, transfer range, and resolution. If this comparison is carried out, an image orthicon with seven times the intrinsic photosensitivity of the tube used for the example will be found to require approximately the same light flux as Super XX 35-millimeter motion picture film. (Com-

parisons of the over-all transfer characteristic, signal-to-fluctuation ratio, and resolution of the two systems are made in subsequent sections). Experimental tubes with even higher photosensitivity have been made.

A sensitivity rating of an image pickup device is frequently based on the light flux required for obtaining an image of reduced quality (lower $|R|$). When the scene luminance is reduced, the television system becomes increasingly more sensitive and surpasses the film camera, which ceases to function at light flux values considerably higher than the threshold value of the television camera.[26] The loss of sensitivity in high-quality operation of the image orthicon is caused partially by a loss of charge storage due to electron redistribution which is instrumental in obtaining a longer tone range.

A specification of the scene luminance required for a given fluctuation ratio $|R|$ and depth of focus is more informative than a "speed" rating. The high-light luminance $\hat{B}_o$ for the television camera may be computed in four steps:

1) Determine the lens diameter δ for the required depth of focus. (Equation (73), Part III)
2) Compute $|R|_{max}$ for the storage capacitance C of the camera tube. (For electron multiplier types, Equation (52), Part III)
3) Compute the image flux $\psi_{i(R)}$ (Equation (78) or (82) and Table VII, Part III)
4) The high-light luminance is then given by $\hat{B}_o = \psi_{i(R)}/g_o$ (Equation (61), Part III)

The light flux values plotted in Figure 68, Part III have been corrected for the decreasing transfer efficiency at higher light levels. Lens diameters and optical transfer factors g_o are given in Table VI, Part III for a depth of focus equal to the vertical scene dimension. The high-light luminance $\hat{B}_o$ (white card reading in foot-lamberts) for this depth of focus has been computed for various values $|R|$ and several camera tube types and is given in Table IX.

Table IX

$\|R\|_{max}$	Iconoscope $\hat{B}_o$ foot-lamberts for $\rho =$				Image Orthicon 5655 $\hat{B}_o$ foot-lamberts for $\rho =$				Image Orthicon 2P23 $\hat{B}_o$ foot-lamberts for $\rho =$			
	ψ_i	2.5	4.	8	ψ_i	2.5	4	8	ψ_i	2.5	4	8
150	0.3	720	190	7750	0.03	72	190.	775.				
100	0.15	360	950	3870	0.009	21.6	57	232				
50	0.05	120	317	1290	0.0018	4.3	11	464	0.0008	1.9	5.2	20.6
25									0.00015	0.36	0.95	3.9

The values $\hat{B}_0$ required for "close-ups" ($\rho = 8$) are prohibitive for the iconoscope, which has to be operated with a larger lens opening at a sacrifice of depth of field. (The lens stops for the conditions in Table IX can be found in Table VI, Part III for various camera plate sizes.) The high sensitivity of the image orthicon has permitted a considerable increase in the depth of the sharply imaged field at normal illumination levels.

2. Over-all Transfer Characteristics

The light transfer characteristics of modern television camera tubes cover a dynamic light range in the order of 100 to 1. This range increases somewhat for scenes with low average brightness but may decrease substantially due to electron redistribution effects and over-exposure when scenes with large high-light areas are transmitted (Compare Part III). Television camera tubes have a smaller latitude than photographic film and are perhaps more sensitive to errors in exposure when optimum performance is desired. This is particularly true of the type 2P23 image orthicon because of its relatively low storage capacitance and high photosensitivity. To illustrate the performance of image orthicons, a series of oscillograms, Figures 81 to 86, have been taken which show a signal cross-section from a photographic step tablet covering a light range of 100 to 1 (20 db) in 2 db steps. The linear time base corresponds, therefore, to a logarithmic step-exposure scale. Because the current scale is linear, the oscillogram is a transfer characteristic in semi-log coordinates. The step tablet is a film strip 8 millimeters wide and 85 millimeters long in an 8×10 inch viewing field. The end steps are opaque to produce black level pulses on the oscilloscope. The strip is placed vertically in front of an illuminator and the electrical response is observed with a vertical cross-section selector. Figures 81 and 82 show a composite photographic print of three transfer characteristics of the 2P23 and 5655 image orthicons obtained from the step tablet when surrounded by a high-light field.

The oscillograms illustrate clearly the black compression caused by redistributed electrons and secondaries from the collector screen when the "target bias" is too small (1 volt). In a dark background, the discharge of potentials is considerably reduced and confined to the step edges as shown by the sawtooth step shape in Figures 83 and 84. Shadow detail is found, in many cases, in darker sections of the scene and high-light detail in light sections. This condition is shown in Figure 85a, where the dark section of the step tablet was placed in a black field and the light section in a white field as indicated by the black and white level lines under and over the oscillogram trace. Figure

85b shows the reverse case. A comparison with Figures 82 and 84 indicates that the discharge by mesh secondaries (1-volt potential) from adjacent high-light regions does not extend over large distances. The effect of varying the exposure is illustrated by Figure 86 for a 2.7-volt potential limit and a two-level background. (The *f:* numbers of the camera lens indicate the relative exposure.) It should be noted that edge effects maintain visibility of the step contours even in over-exposures (sawtooth shape of steps) but do not reproduce the differences of actual tone values.

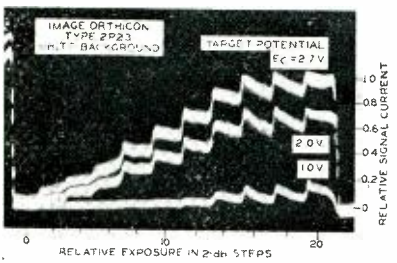

Fig. 81

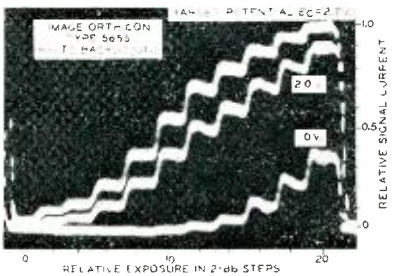

Fig. 82

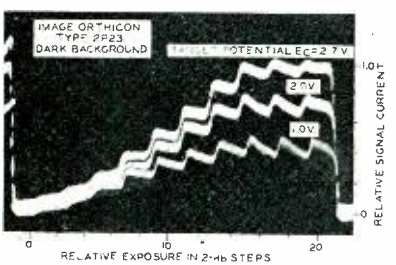

Fig. 83

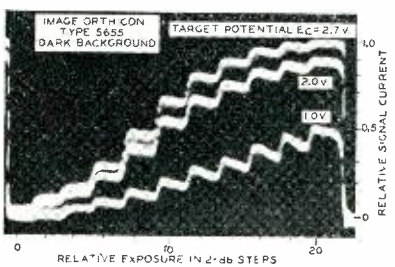

Fig. 84

Oscillograms of dynamic transfer characteristics of image orthicons (20 db = 100:1 range)

The oscillograms of the dynamic transfer characteristics give proof that the major difference between the 2P23 and 5655 camera tubes is their storage capacitance and photosensitivity, the 5655 giving a higher signal-to-fluctuation ratio but requiring a higher scene luminance (See Table IX). To prevent overexposure and undesirable relief effects and to obtain good shadow detail it is good practice in the studio to avoid too large a contrast range, (i.e., heavy shadows) by the use of soft "basic" lighting and by employing modeling lights of moderate intensity. In order to compute the over-all light transfer characteristic of the television system it is necessary to take into account optical effects modifying the static transfer characteristic of the kinescope, which otherwise follows essentially a 3rd power law.

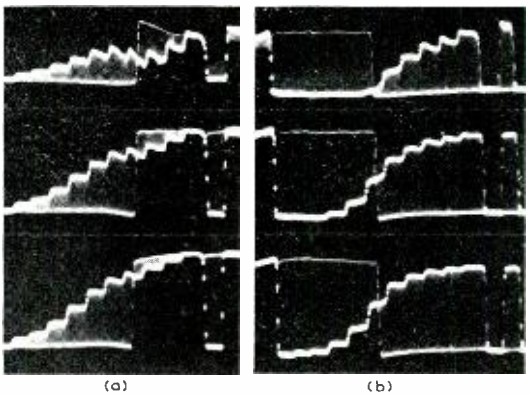

Fig. 85 — Oscillograms of dynamic transfer characteristics of a 5655 image orthicon with two-level background.

(a) Low light range in dark background, high light range in white background.

(b) Low light range in white background, high light range in dark background.

The range of the dynamic kinescope operating characteristic is reduced by a light bias of 1 or 2 per cent as shown in Figure 87. A light bias of this order can occur in a dark room because of light diffusion in the screen material and reflection on the glass surfaces. This "flare" light bias is actually not uniform and decreases in a manner similar to "lens flare" with distance from a high-light area (See B1*b*, Part III).

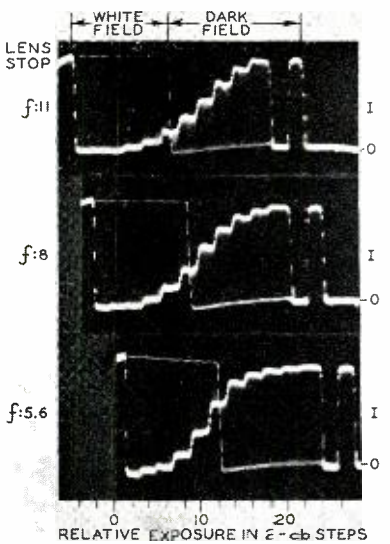

Fig. 86—Oscillograms of dynamic transfer characteristics of a 5655 image orthicon at target potential $E_c = 2.7$ volts with two-level background for three different exposures.

The over-all transfer characteristics in Figure 88 have been computed in the usual manner for the image orthicon operation shown in Figure 82, a *linear* amplifier characteristic, and the kinescope characteristic Figure 87. A simple

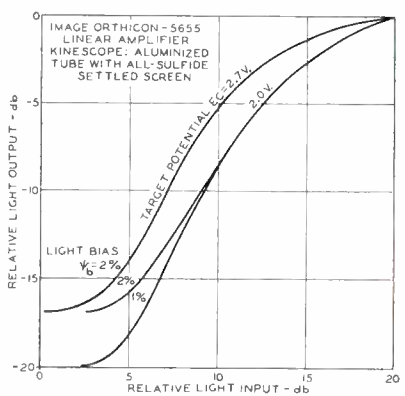

Fig. 88—Light-transfer characteristics of television process (ψ_b = combined ambient and flare light flux).

visual test for linearity of the over-all transfer characteristic can be made by reproducing a logarithmic step tablet and comparing it with an identical step tablet placed over a white background of the kinescope field parallel to the reproduced tablet. A direct measurement of the over-all characteristic can be made by covering the kinescope field with a black mask having a slit over the vertically positioned step tablet image and observing the oscilloscope trace (60-cycle sweep) of the modulated light output by means of a 931-A multiplier phototube. Both tests are in good agreement with the computed transfer characteristic.

The over-all transfer curve of a 35-millimeter motion picture system, Figure 89, has been constructed from Figure 76 by adding the effects of lens flare and ambient light. A light bias of 2 per cent is probably near the minimum value obtainable for the brightness levels in motion picture theaters. A comparison with the television transfer curve, Figure 88, reveals off-hand only minor differences. A slightly increased range in light input can be covered by the television system by introducing an amplifier transfer characteristic with moderate logarithmic compression, provided the camera tube is correctly adjusted and exposed. The corresponding reduction in contrast difference (lower slope), however, is not necessarily an advantage, and particularly not in the presence of ambient room light.

Camera tubes with constant transfer efficiency such as the

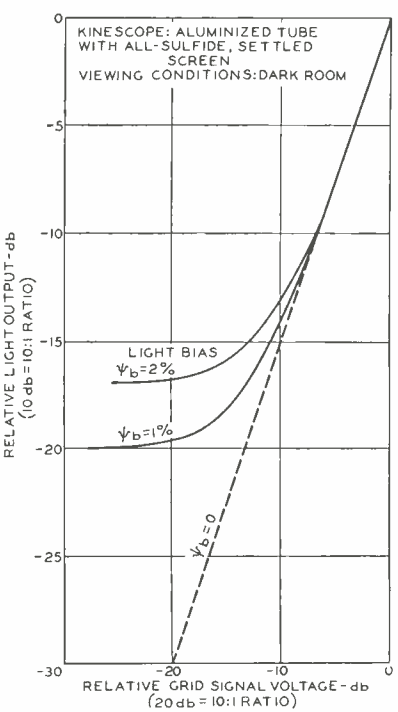

Fig. 87—Dynamic transfer characteristics of kinescope.

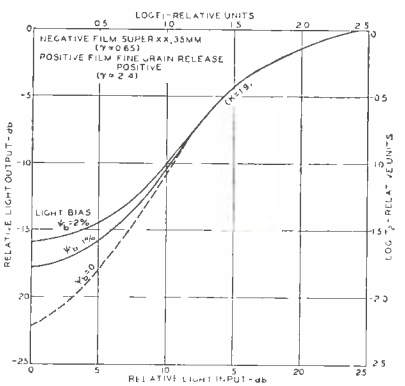

Fig. 89—Light-transfer characteristics of motion picture process (ψ_b = combined ambient and lens flare light flux).

orthicon, or a system generating video signals by a light-spot scanner (flying-spot systems), require a considerable compression of signals in the amplifier to obtain linearity in the over-all transfer curve. The amplifier is given a characteristic which is the inverse of the kinescope transfer curve inclusive of flare light bias (Figure 87) because the signal from these pickup devices is linearly related to the light input.

The contrast scale of normal television and motion picture systems falls somewhat short of a 100 to 1 range which has been considered a desirable standard (See Part I). Halation and light scattering in the kinescope or ambient light and lens flare are largely responsible for the reduction of image contrast. A gradual compression of signal values (low-"gamma" negative) is expedient in the film process to preserve a long tone scale when the object light range is large; but it does not produce similar effects in a television camera chain, because present storage-type camera tubes cannot reproduce a dynamic light range exceeding at best a ratio of 100 to 1. Upon further examination it is observed that the mechanism for obtaining a longer signal range in storage-type camera tubes (gradual saturation) causes redistribution effects, which are responsible for "shading" over larger areas or cause more localized deviations from normal signal levels (sawtooth shape of steps in oscillograms).

These "spurious signals" affect the smoothness or texture of the image. In image orthicons the redistribution and spurious effects decrease when the exposure is reduced, the shortened range resulting in a better tone quality. This limitation is, of course, not an inherent characteristic of a television system, but at present, the shorter latitude of the camera tube can be accommodated by advantageous and skillful lighting in the television studio.

3. *"Grain" Visibility, Brightness, and Optical Signal-to-Fluctuation Ratios*

The visibility of random brightness fluctuations as a function of the optical channel width $\overline{N}_{co}$ provided by a television system and taking into account the filtering action of the eye and kinescope has been discussed in Part I. The relatively high maximum values $|R|_{max} =$ 300 to 500 for the electrical signal given in Part II, page 283, are not obtainable with present camera tubes, nor are they realized by the motion picture process. These values were based on a peak brightness of 32 foot-lamberts. Because the visibility of "grain" fluctuations decreases with brightness, a comparison of the television image with motion pictures should be made at the brightness level of a 35-millimeter film projection which is less than 10 foot-lamberts. The threshold visibility of grain fluctuations in a 4.25-megacycle channel at a viewing

ratio $\rho = 4$ was, therefore, determined by measurements. The optical ratio $|R|_o$ for threshold grain visibility is plotted in Figure 90 as a function of brightness for an unmodulated viewing field (curve 0) and for fields containing a normal picture modulation (curves A and B). Curve 0 was obtained as follows: known electrical fluctuation ratios were generated with a light-spot scanner followed by a linear amplifier. The optical ratio from the kinescope screen is computed as one-third of the electrical values because of the 3rd-power expansion by the kinescope transfer characteristic (See Part III, A5). The amplifier gain was then adjusted to a screen brightness (with respect to the correct black level) for which threshold visibility occurs at $\rho = 4$. This

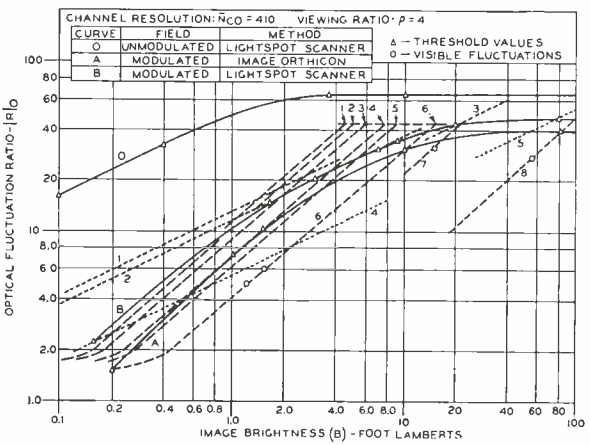

Fig. 90 — Development of characteristic curves of the optical signal-to-fluctuation ratio $|R|_o$ for threshold grain visibility at various brightness levels.

brightness was measured with an illuminometer. Curve 0 is in agreement with the value for $\overline{N}_{co} = 410$ and $B > 2$ foot-lamberts shown on Table I, Part I, for the eye alone, because the kinescope used in the earlier computations (Figure 13, Part I, page 35) has been replaced by a tube with very high response ($r\Delta\overline{\psi} = 0.8$ at $N = 500$; curve 1 in Figure 42, Part I, page 282).

The visibility of random fluctuations is reduced considerably when the field is modulated by image signals and was measured as follows. Curve A was determined with a 5655 image orthicon giving the measured *electrical* fluctuation ratio $|R|_{max} = 130$. Four 8×10-inch Kodachrome transparencies were used as a source of picture signals, one being a high-key image, one a low-key image, the third one contained a large white area, and the fourth one contained well-distributed tone values in small areas. The optical signal-to-fluctuation ratio on the kinescope was computed for a linear amplifier from the transfer characteristic shown in Figure 88 and varies with signal as shown by the dashed lines (1 to 8) in Figure 90. The maximum *optical* fluctuation

ratio of the system was, therefore, one third of the electrical ratio, i.e., $|R|_{max}$ (optical) $\simeq 43$. By varying the signal strength (gain of the linear amplifier), the $|R|$ curve is displaced horizontally in Figure 90. Curves 1 to 3 yielded "noise"-free pictures; and curve 4 gave threshold visibility of fluctuations in the middle tone range, curve 6 gave visible fluctuation in the middle tone range and threshold visibility at a high and a low brightness value. The threshold ratio curve is thus determined by measurement of the brightness values giving threshold grain visibility. Variation of the image content disclosed no noticeable change in the observed threshold values. The low-key image was found to be reproducible without fluctuations at a higher peak brightness (See curve 5) because it contained middle tone values only in small detail areas.

Curve *B* was determined in a similar manner by slide pickup with a light-spot scanner. Because the amplifier was linear, the $|R|$-curves for this signal source retain substantially a ½-power slope over nearly the entire image-brightness range and the optical grain-fluctuation ratio is again reduced to ⅓ by the kinescope expansion. In view of the normal spread of data which is to be expected in observations of this type, the agreement of the two methods (A and B) is quite satisfactory.

The mean curve *M* shown in Figure 91 represents, in good approximation, the critical optical ratio $|R|_o$ for threshold visibility of grain fluctuations in a television channel or an equivalent optical channel with $\bar{N}_{co} = 410$. (The kinescope filter factor can be neglected.)

Fluctuation-free images are obtained at brightness values placing the $|R|$ curve of the imaging system to the left or tangent to the threshold curve. The tangent curve *A* represents a television system using a storage-type tube such as the image orthicon or iconoscope. Because the optical fluctuation ratio is very close to ⅓ of the electrical ratio produced by the camera tube, an electrical ratio of $|R|_{max} = 150$ permits a maximum image brightness $\hat{B} = 7$ foot-lamberts for a fluctuation-free kinescope image at $\rho = 4$. The brightness $\hat{B}$ may be increased by perhaps a factor of two without objectionable fluctuations (curve 1) which are visible in practically all tone values of the image.

Curve *B* of Figure 91 represents the condition for grain-free images from a linear signal source such as a light-spot scanner (no auxiliary currents causing fluctuations). When the over-all transfer characteristic is linearized by electrical compensation of the kinescope characteristic, the electrical and optical ratios $|R|$ coincide. A ratio $|R|_{max} = 75$ is easily obtainable with normal slide or motion picture densities and yields grain-free images with a peak brightness $\hat{B}$ near 50 foot-lamberts. An increase of $\hat{B}$ to 100 foot-lamberts (curve 2) causes

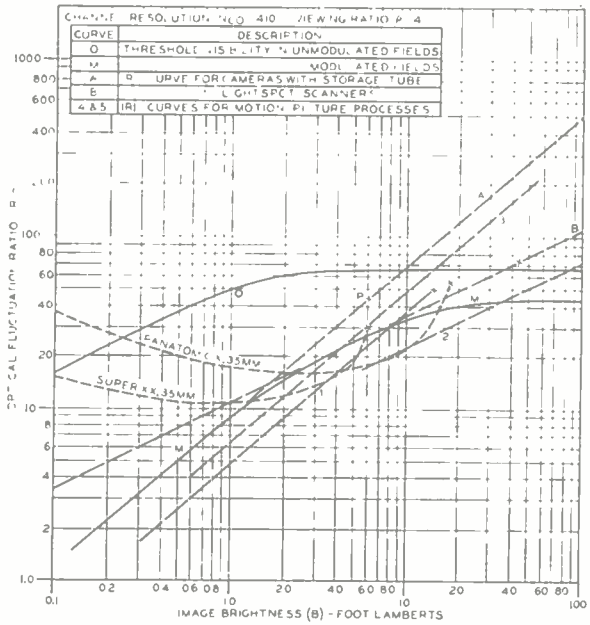

Fig. 91—Location of $|R|$-characteristics for various imaging processes with respect to threshold visibility curve of grain fluctuations.

visible fluctuations in the middle tone values. Substantially grain-free images at $\hat{B} = 50$ foot-lamberts from an image orthicon chain (curve 3) require high electrical ratios in the order $|R|_{max} = 600$ as indicated in Part I.

Reproduction of a 35-millimeter motion picture film at normal theater brightness over an ideal television channel with $\overline{N}_{ro} = 410$ places the grain fluctuation characteristic $|R|_2$ (See Figure 74) in the position shown by the Super XX curve in Figure 91. A direct optical projection of the film results in practically the same positioning, because the increased bandwidth and the better storage factor ($s' = 1.5$, See Part III, page 494 et seq.) cancel each other. The characteristic computed for Super XX negative film appears to be in good agreement with visual observations in motion picture houses, because it indicates a grain-free reproduction of shadows and some graininess in the lighter middle tones and high lights. In comparison with an image orthicon camera chain ($\hat{B} =$ point P, curve A), the 35-millimeter motion picture Super XX offers no advantage at equal brightness values. At television brightness levels, the middle and lower tone values of the film move into the fluctuation region. A slower negative material with fine grain, such as Panatomic X film, permits a brightness increase to $\hat{B} \cong 17$ foot-lamberts as shown in Figure 91. The fluctuation curves for 16-millimeter motion pictures are lower by a factor of two on the $|R|$-scale unless the film is a reduction print made from 35-millimeter negative film.

It is quite apparent that the grain of motion picture film can be "seen" over a good standard television system and that it is nearly always controlling the fluctuation level in television reproductions of normal 16-millimeter film. In kinescope photography on 16-millimeter film[32], a relatively slow fine-grain negative or reversal film can be used because of the high brightness levels available. The fluctuation level can then be reduced and is not necessarily limiting the quality of the recording.

4. The Aperture Response Characteristics of Imaging Systems

a. An experimental proof of the theory for cascaded aperture processes

The theoretical analysis of aperture processes in cascade (Part II) has provided the rule that the over-all resolution number at a given response factor in a multi-stage process can be found by a quadrature addition of the individual resolution line numbers as expressed by the equation

$$1/N_p = \sqrt{(1/N_1)^2 + (1/N_2)^2 + \cdots + (1/N_n)^2} \qquad (30)$$

It was pointed out that this rule does not apply accurately to response factors near zero, i.e., to line numbers near the limiting resolution, but that it is a good approximation for values $r\Delta\bar{\psi} > 0.3$. A quantitative proof by measurement of the response characteristics of two cascaded imaging processes is illustrated by Figure 92. A line-group test pattern is projected in sharp focus by lens 1 onto a diffuse reflecting screen. This image is picked up by the camera lens 2 of a television camera which is adjusted to an out-of-focus position causing a first zero at a relatively low line number N_c as observed on the kinescope viewing screen. The first image is now defocussed by lens 1 to the same cutoff N_c on the diffuse reflecting screen 1. The cascaded response of the two out-of-focus imaging systems is then measured by the methods described in Part III, and is shown by curve 1 + 2 in Figure 92.

The component characteristics (curves 1 and 2) of the system are measured similarly with one image in sharp focus and the other image defocussed to the previous value N_c. The measured characteristics 1 and 2 permit calculation of the cascaded response curve 3. The agreement between the measured and computed response characteristics 1 + 2 and 3 in Figure 92 is a quantitative proof that Equation (30) furnishes the cascaded aperture response of practical complex apertures in good approximation in the range $r\Delta\bar{\psi} > 0.2$.

---

[32] R. M. Fraser, "Motion Picture Photography of Television Images", *RCA Review*, Vol. IX, No. 2, pp. 202-217, June, 1948.

b. *The correction of aperture response characteristics and image sharpness by negative aperture processes*

The analysis and synthesis of complex apertures and aperture response characteristics as a sum of component apertures or characteristics has been discussed and verified by experiment in Part III. It is logical that subtraction of an undesired component (such as curve 2 in Figure 93) from a complex response characteristic, (curve 1) produces a simpler characteristic with higher (relative) response factors which result in a sharper image. Subtraction of a characteristic is equivalent to an addition of a "negative" response characteristic. The correction process, (photographic or electrical) may, hence, be considered as a "negative" aperture process. The apertures used in these processes are positive as well as the flux values which are positive quantities of light, silver grains or electrons. If phase-reversing or attenuating elements are inserted, however, flux changes or "signal" components can be generated which are negative with respect to the original signal. The amplitude range and shape of the negative-signal response curve is controlled by the "apertures" of the correcting process to provide the desired correction. These concepts are useful and necessary in coordinating optical and electrical processes. Negative aperture-processes are not used in cascade with the normal process but the correction "signals" are superimposed on the normal process. In overall response calculations made by applying Equation (30), the effect of an aperture correction stage is, therefore, not included as a negative cascaded aperture, but must be evaluated separately. It is important in a synthesis to include the spurious response of the correction aperture in the addition (See curve 2, Figure 93) and to select response characteristics which will add up to a smooth curve. Errors in this

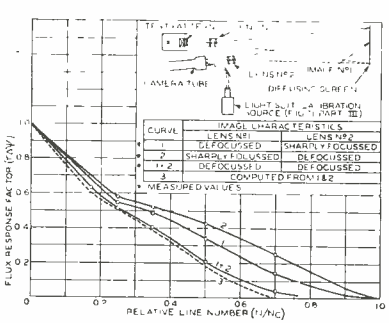

Fig. 92—Flux response characteristics of two cascaded imaging systems.

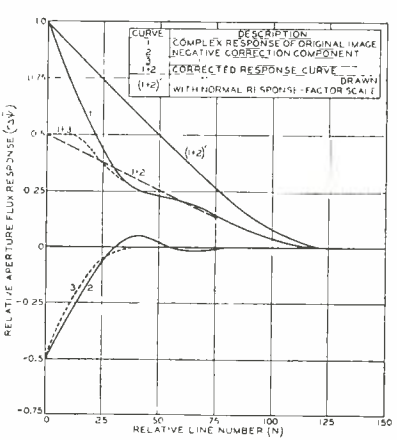

Fig. 93—Aperture response correction by "negative" response characteristics.

respect cause spurious signals or transients in both photographic and electrical processes.

The correction decreases the signal output or "gain" which would normally be obtained from the process (See curve $1 + 2$) and requires, therefore, a stage with increased amplication to restore normal signal amplitudes (curve $(1 + 2)'$ in Figure 93). In a photographic process the increased amplification is furnished by a film characteristic with higher slope (γ).

The correction process illustrated by response characteristics in Figure 93 can be duplicated by a photographic process employing optical two-dimensional apertures. The characteristic 1 is synthesized by two round apertures with equal flux and first zeros at $N_c = 30$ and $N_c = 120$. A test pattern is copied by out-of-focus projection (See Part II) on a photographic plate in a double exposure with two corresponding lens stops and the relative exposure times 1 to 16. A print from plate 1 is reproduced in Figure 94 and illustrates the poor aperture response of curve 1, Figure 93, which is to be corrected. An auxiliary plate 2a is made at the same enlarger setting by an exposure with the larger aperture only ($N_c = 30$). A positive plate 2b of proper density is then made by contact printing (phase reversal process) from 2a to obtain the "negative" response characteristic 2 in Figure 93, illustrated by the print Figure 95. The aperture correction of the image Figure 94 from plate 1 is made by printing plates 1 and 2b in contact and in register. The result is the considerably sharper image, Figure 96, representing curve $(1 + 2)'$ in Figure 93. Although giving a perfect correction, the described process requires an auxiliary image (plate

Fig. 94—Photograph of test pattern obtained by an optical aperture with characteristics given by curve 1, Figure 93.

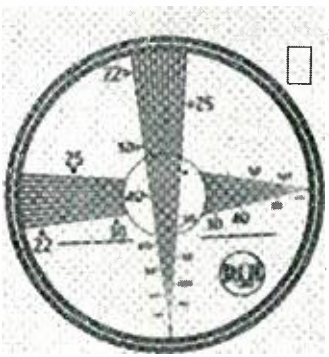

Fig. 95—Photograph of test pattern obtained from the correcting positive plate having the "negative" response characteristic given by curve 2, Figure 93.

2a) made from the original test pattern. If only the poor "signal" from plate 1 is available the correction signal must be derived from this plate by making the low-resolution correction positive directly from plate 1 by out-of-focus projection or diffuse copying with unity magnification. Because the copying process is a cascading operation, the copying aperture will always cause a widening of contours and produce an aperture response which contains a component having a cutoff N_c lower than any component ($N_c = 40$) of the original. A negative response curve obtained from a cascading operation (from 1) such as curve 3 in Figure 93 will, therefore, always cause a negative overshoot or "transient" in the corrected image. When the correction is not too large, the overshoot which appears as a relief effect is not disturbing. In the case of the example, an over-correction was made

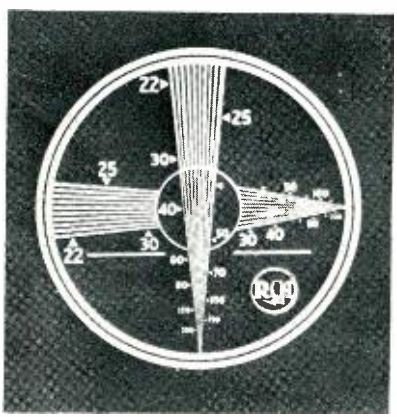

Fig. 96—Photograph of test pattern obtained with the photographically corrected aperture response given by curve 1 + 2, Figure 93.

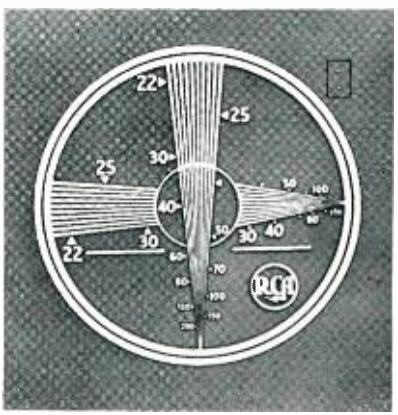

Fig. 97—Photograph of test pattern illustrating strong "transient" due to over-correction with a positive plate.

with a slightly larger correcting aperture than necessary to bring out the strong transient illustrated by Figure 97, as the normal effect was small and would probably be lost in the reproduction. It is evident that the two images must be accurately registered in the correction process because any error introducing a "phase shift" of the components causes strong transients as in electrical processes.

A television system is well suited for insertion of aperture correction processes. Its electrical characteristics, in particular, can easily be modified to subtract or add signal components in the range of the frequency response characteristic which determines the "horizontal" aperture response of the electrical channel. The aperture response signals from the television camera are corrected by inserting electrical

networks which cause a reduced amplification of low-frequency signals, i.e., a "negative" signal component with respect to low-frequency signals. If adequate phase correction is included, the *horizontal* aperture response of the television system may be raised to its maximum value (See Part II) provided the cutoff point of the over-all response of the uncorrected system occurs at a higher line number than the electrical channel cutoff.

The oscillograms in Figure 98 illustrate the electrical aperture correction of signals from a line-group test pattern. The uncorrected signal response in a 20-megacycle channel (trace 1) has decreased to a sine wave shape at $N = 100$. With aperture and phase correction the transition curve is considerably steepened and the response has become normal at $N = 350$ (trace 2). Insertion of a 3-section lowpass filter

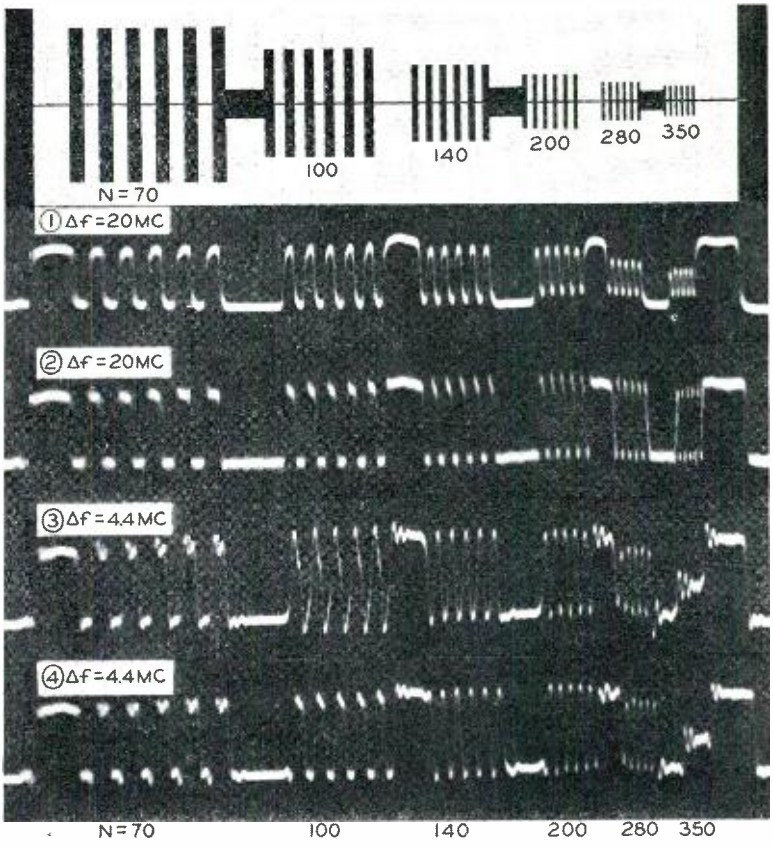

Fig. 98—Oscillograms of test pattern illustrating electrical aperture correction in the horizontal dimension and effects of limiting the frequency channel by a filter.

with sharp cutoff at $N_c = 350$ lines ($\Delta f = 4.4$ megacycles) resulted in trace 3 which demonstrates the incomplete phase correction of the filter by the one-sided transients from a unit function signal. Addition of a simple phase correcting circuit results in the trace 4, which approaches closely the theoretical response shown in Part II by Figure 36 and Figure 37, curve 5. The substantial increase of detail contrast obtained by electrical aperture correction in a 1000-line channel is demonstrated by the photographs Figures 99a and 99b which show the expanded center of a wedge test pattern before and after correction. (The pattern numbers are to be multiplied by ten. The horizontal expansion is obtained by a 4 to 1 expansion of the horizontal kinescope deflection.)

The electrical correction decreases the effective aperture width of the system but does not affect its height, forming a slit aperture with higher response in the horizontal direction. In over-all response calcu-

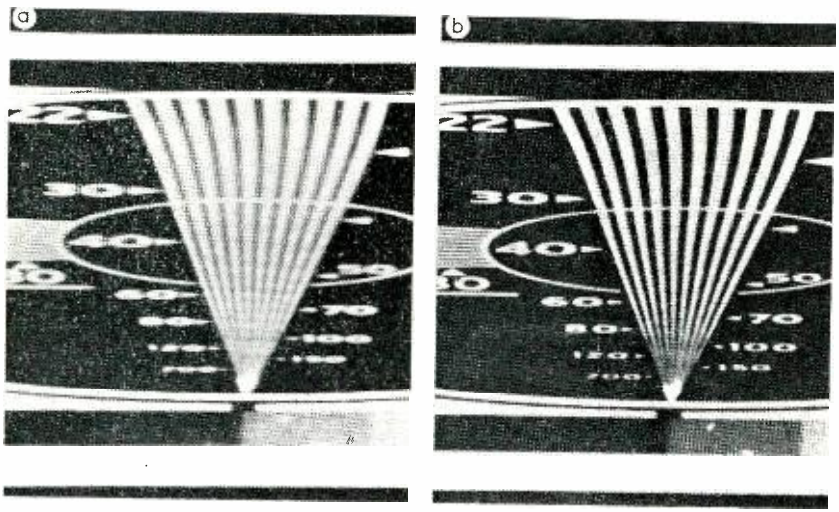

Fig. 99—Photographs of expanded wedge test-pattern image
a. without aperture correction
b. with electrical aperture correction in horizontal dimension.

lations, an asymmetric two-dimensional aperture can be treated as two one-dimensional apertures in cascade, with the horizontal and vertical resolution values multiplied by $\sqrt{2}$. For example, an aperture having the vertical resolution $N_v = 300$ lines and the horizontal resolution $N_H = 600$ lines at a given response factor is equivalent to an aperture with the cascaded values $N_v = 425$ and $N_H = 850$ which, according to Equation (30), is a symmetric aperture with the balanced resolution $\overline{N} = 380$.

According to this method the maximum increase in resolution obtainable by the one-dimensional horizontal aperture correction is limited to $\overline{N} = N_V \sqrt{2}$. The balanced resolution $\overline{N}$ is frequently evaluated by assuming that an asymmetric aperture may be replaced by a symmetric aperture of equal area as expressed by the geometric mean value $\overline{N} = \sqrt{N_H \times N_V}$. For a moderate unbalance of resolution values, both methods give similar values, but for larger differences of N_V and N_H, the geometric mean value $\overline{N}$ increases steadily indicating no limit to the maximum resolution obtainable by a one-dimensional aperture correction. It is obvious that the apparent sharpness of images with asymmetric resolution depends on the distribution of vertical and horizontal components in the subject material. For normal subjects and large unbalances of resolution the geometric mean value appears much too high while the cascading method furnishes more reasonable values which are perhaps somewhat conservative when compared with subjective observations (see ref. (5)).

Aperture correction processes increase the high-frequency components of random fluctuations by the same ratio as the detail signals.* The degree of correction is, therefore, limited in practical processes by the decrease in the signal-to-fluctuation ratio. Moderate "high peaking" (2 to 3 times at $N = 400$) increases the fluctuation visibility only slightly when the normal fluctuation energy is uniformly distributed in the frequency channel (See Part I).

c. *The aperture response of practical television and motion picture systems*

The aperture response of the various transducing processes in motion picture and television systems has been established in preceding parts of this paper. The component characteristics (1 to 3) of a typical 35-millimeter motion picture process are shown in Figure 100. The cascaded aperture response characteristics 4a and 4b, computed with Equation (30), show the relatively small difference in over-all response caused by decreasing the camera lens stop from f:2.8 to f:2.3 because the projection lens and film response are the main factors controlling the over-all response characteristic.

The response characteristics of a television system with standard channel are shown in Figure 101. The theoretical response of the system has been broken down into its vertical and horizontal components 3a and 3b (See Part II, B2, page 267 et seq.) which, in cascade, result in the theoretical curve 7 of the system. The response characteristics of the experimental camera tube (2) and kinescope (4) represent the best values obtainable in the laboratory.

* The fluctuation filter factor has values $m > 1$.

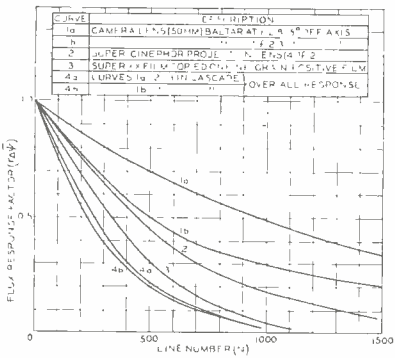

Fig. 100—Aperture response characteristics of 35-millimeter motion picture process.

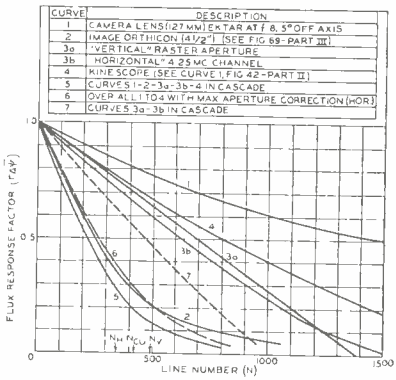

Fig. 101—Aperture response characteristics of television process with 4.25-megacycle channel width.

It is evident that the camera tube is the characteristic controlling the over-all response (5) of the system which is the cascaded value of curves 1, 2, 3a, 3b, and 4. The insertion of "horizontal" aperture correction circuits can eliminate the deterioration caused by the components 1, 2, and 4 in one dimension, resulting in the theoretical horizontal response component shown by curve 3b. The response of the system in the vertical dimension is given by the system curve 3a in cascade with the equivalent *vertical components* of the elements 1, 2, and 4, which are obtained by multiplying the resolution scales N of these characteristics by the cascading factor $\sqrt{2}$. The over-all response of the system with optimum aperture correction is then obtained by cascading the system curves 3b, 3a with the "stretched" curves $N_1\sqrt{2}$, $N_2\sqrt{2}$ and $N_4\sqrt{2}$. This process furnishes the corrected response curve 6.

The over-all aperture response characteristics of the television process (curves 5 and 6 of Figure 101) are *equivalent* characteristics because the real characteristics of the television raster and the electrical channel which have a higher response at $N < \overline{N}_{c0}$ but no response beyond $N \geqq \overline{N}_{c0}$, have been expressed by the optical equivalents (3a and 3b) derived in Part II. Because the equivalence is based on a varying picture content at a viewing ratio $\rho = 4$, the over-all characteristics are representative for a comparison with motion picture processes. *The equivalence for still pictures is expected to vary with picture content as repetitive detail beyond the value* $\overline{N}_{c0}$ *is actually not reproduced, although fine single lines and contours may have a sharpness represented by the equivalent response curve.* It is interesting that the present 525-line television system ($N_V = 490$, and $N_H = 340$) results in a balanced contour sharpness even though the limiting

resolution values are unbalanced. However, it does not necessarily follow that this resolution ratio will produce balanced contour sharpness with other systems employing different line numbers. Such factors as viewing distance, scanning line number, and kind of subject material must be considered because they affect the visibility of the scanning lines and cutoff transients (See Part II).

A point-by-point comparison of the over-all response characteristics 4 in Figure 100 and 6 in Figure 101 reveals an almost perfect match for response factors $r\Delta\overline{\psi}$ greater than 0.1. This does not mean that a television system can *reproduce* a motion picture film without loss of quality because only a theoretically perfect imaging system can accomplish this feat. The equivalence applies rather to images obtained by a direct pickup of the same subject. In case of a motion picture reproduction over a television system, a comparison should, therefore, be made with a retake and reprojection of the original projected motion picture by means of a second motion picture process. It is quite apparent that the mechanical position and focus errors caused by film motion in cameras and projectors result in an additional degradation of sharpness which has been neglected and which does not occur in a television process where single stationary image surfaces are used.

A practical television system with sharp cutoff at $\overline{N}_{co} = 410$ *lines can, therefore, produce an image sharpness approaching in effect the sharpness of a commercial 35-millimeter motion picture.* This result appears optimistic by comparison with the best television transmissions made at this time. It must be remembered, however, that commercially available tubes have lower aperture response values than the experimental tubes of the example and that additional aperture effects may occur in modulating systems, radio links and receivers. Furthermore, when judging the sharpness of an image it is difficult to mentally exclude the distracting effects of fluctuations, contrast errors, and particularly defects due to spurious signals. Good detail response in a long contrast scale places severe requirements on the mechanical and electrical uniformity of image and multiplier surfaces and the fineness of the collector screens in the camera tube. It is, therefore, often preferable to operate present camera tubes somewhat out-of-focus until these problems have been solved. A long tone range in combination with good aperture response at all levels and freedom from blemishes are requirements for producing the smoothness, fine drawing, and "texture" of a good photograph.

5. An evaluation of "sharpness" by including the process of vision.

The eye is the final judge in an evaluation of image sharpness. It is, however, an instrument which can be influenced by a number of

image properties other than resolution (See above). The eye does not analyze the exact cause and magnitude of a difference in the apparent sharpness of two images, but merely judges one image to be sharper, less sharp, or equally sharp than the other image or the original scene. If the eye judges these differences on a logarithmic basis the "minimum perceptible sharpness difference" should represent a constant increment on a scale plotted in decibels. The eye is an imaging system having a certain aperture response; it can, therefore, judge a sharpness difference only by the difference in retinal images which is technically the change in resolution caused by cascading an external imaging process with the process of vision. According to this reasoning, the relative sharpness of an image (or process) *as seen by the eye* can be expressed by the ratio of the decreased retinal resolution (N_{e+p}) obtained by cascading the visual process with an external process N_p, to the normal (retinal) resolution N_e, at a given response factor. The relative sharpness N_{e+p}/N_e is computed with Equation (30) and expressed by the relation

$$N_{e+p}/N_e = (N_e N_p)/\sqrt{N_e^2 + N_p^2}. \qquad (91)$$

A plot of Equation (91) as a function of the resolution ratio N_p/N_e in logarithmic coordinates (Figure 102) may be regarded as a basic function relating aperture response and line number of an external process to subjective sharpness impressions. Direct reading scales (such as scale A for $r\Delta\bar{\psi} = 0.5$) for the line number N_p of the external process can be located by the index number $N_p/N_e = 1$, which, for the desired response factor is given by the eye characteristic (Figure 20, Part II, page 253) for a viewing ratio $\rho = 4$.

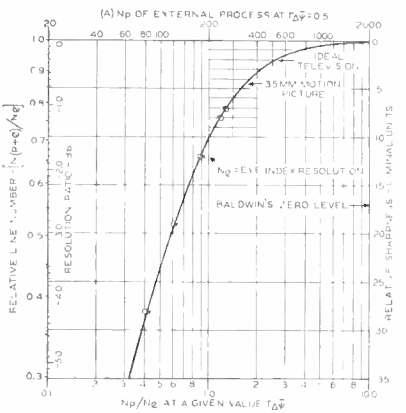

Fig. 102—Curve for evaluating the subjective sharpness of an imaging process.

The sharpness curve indicates that an increase in resolution from 150 to 200 lines (at $r\Delta\bar{\psi} = 0.5$) in an external imaging process causes a sharpness increase of 0.8 db; an equal increase of sharpness requiring progressively larger resolution differences at higher line numbers, such as a change from 260 to 600 lines. It is of considerable interest to determine the minimum perceptible sharpness difference, i.e., the "liminal" unit of the sharpness scale, to permit a quantitative interpretation of the sharpness of images.

This liminal unit has been determined by Baldwin[5] in a series of carefully made subjective observations on images with known resolution. Baldwin plotted sharpness in liminal units against the number n of square figures of confusion in out-of-focus motion picture projections. The balanced line number computed from n (Equation (38) Part III) furnishes the 50 per cent response value for the projector. The true value in the projected motion picture is obtained by cascading the value N (projector) with the film value for $r\Delta\bar{\psi} = 0.5$ (compare Figure 100). One set of corrected values is given in Table X.

Table X

Liminal units of sharpness	Number of figures of confusion n	Line number at $r\Delta\bar{\psi} = 0.5$ for $N_{film} = 350$
−11	10,000	84.2
−2	25,000	123.6
+5	61,000	182.
+9	130,000	223.
+10	160,000	246.

By adjusting the size of the liminal unit and varying the resolution index for the eye and the film, Baldwin's zero level had to be placed 17 liminal units below maximum sharpness (which is close to his estimate) to obtain the best fit of his values with the computed curve shape. (See Figure 102.) The graphic operation gives a simultaneous solution for the eye and film resolution at $r\Delta\bar{\psi} = 0.5$, which are in excellent agreement with the measured value.

The graphic experiment may be regarded as a proof that the visual process can be treated as an aperture process and that the sensory response to changes in sharpness follows substantially a logarithmic law. The liminal unit of sharpness represents a change of 0.15 db, i.e., a constant percentage (approximately 3 per cent) in the relative retinal resolution $N_{(p+e)}/N_e$ at a given response factor and viewing ratio.

The curve of sharpness shown in Figure 102 supplies an answer to many problems. It furnishes the difference in resolution N_p which can just be seen in a comparison of response characteristics; the effect of an improvement in the aperture response of a system; the number of sharpness units lost in the process of recording a television performance on motion picture film; the difference in sharpness between two imaging processes and many others.

According to Baldwin, one liminal unit is a barely perceptible difference, two units being required to make a definitely noticeable

change in the sharpness of an image. An imaging process reproducing a line number $N \geqq 700$ with a response of 50 per cent and $N \geqq 1050$ with a response of 30 per cent can thus be rated as absolutely "sharp" at a 4 to 1 viewing ratio. The limiting resolution of photographic processes having this sharpness is at least 3000 lines and in most cases over twice this value. The sharpness rating of a few processes of interest expressed in liminal units below the "zero level" of maximum subjective sharpness is listed in Table XI* for a viewing ratio $\rho = 4$. The motion picture process #1 rates —6.5 liminal units and is equalled by the television process #6 with aperture correction. The aperture correction causes a sharpness increase of 2.5 units which is a noticeable improvement. A light-spot slide scanning system #7 can produce

Table XI—Subjective Sharpness of Imaging Processes at $\rho = 4$.

#	Process	Camera Lens	Film	Sharpness Level liminal units
1	Commercial Motion Picture Process 35 mm (Figure 100)	f:2.5	Super XX or Plus X	—6.5
2	Commercial Motion Picture Process 16 mm	f:2.5	Super XX or Plus X	—15 (approx.)
3	Miniature Camera (High-quality Projector)	f:5 to f:11	Kodachrome	—3
4	Miniature Camera (High-quality Enlarger)	f:5 to f:11	Panatomic X	—2.6
5	2¼" x 3¼" Camera (High-quality Enlarger)	f:5 to f:11	Super XX or Plus X	—0.5
6	Standard Television Process (Image Orthicon)		best tubes	
	Figure 101, curve 5	f:8		—9
	Aperture corrected, curve 6	f:8		—6.5
7	Standard Television Process Light-Spot Slide Scanner	f:4.5	Miniature Slide	—5.
	Aperture corrected		Kodachrome	
8	Reproduction of Commercial 35-mm film by Standard Television Process with Light-Spot Film Scanner		35-mm positive from Super XX or Plus X	—9.5
9	Reproduction of Commercial 35-mm Film by an Identical Motion Picture Process	(repetition of process #1 with a second camera, film process and projector)		—11.5

a slightly sharper image (by 1.5 units). When a 35-millimeter motion picture is scanned, the light-spot scanner decreases the sharpness of process #1 by only 3 units (See #8) which is an excellent performance, because a repetition of the photographic 35-millimeter process (#9) would decrease the image sharpness to —11.5, i.e., by 5 units.

A 2¼ × 3¼-inch photographic camera can just produce a perfectly sharp picture with normal film types (for $\rho = 4$), while images from a good miniature camera rate approximately 2 units lower and do not attain "needle sharpness" with film types of normal speed and range.

* The over-all aperture response calculations are based on lens and film data obtained by measurement as described in this paper.

It will be of interest to briefly describe a series of tests made nearly two years ago to obtain information on the comparative sharpness of television and photographic processes. The tests were based on a visual comparison of photographs made over a television system, with direct photographs in which the limiting resolution ($\overline{N}_{e0}$ or N_e) had been adjusted to various values. The purpose of the tests was to determine the relative cutoff ratio $\overline{N}_{e0}/N_e$ of the two processes which gave images of equal sharpness. Television images of two of the three test objects selected as originals are reproduced in Figures 103 and 104. The objects were photographed on 3¼ × 4¼-inch negatives and enlarged by out-of-focus projection to 8 × 10-inch prints with varying degrees of sharpness. The cutoff N_e (indicated by the first "zero" on a resolution wedge) was adjusted to the values 200, 300, 450, 650, and 870 lines. Because a sharp enlargement had a limiting resolution $N_e = 4500$ lines, this print series (A) yielded grain-free images with the relatively sharp optical cutoff caused by a round aperture with substantially uniform flux distribution.

A second series (B) of 8 × 10-inch prints was made by "sharp" enlargements from selected miniature film negatives taken with a Contax Camera and Zeiss Sonnar Lens at its optimum stop, f:6.3, on Super XX film and Panatomic X film and developed in fine-grain developer. The vertical dimension of the image was adjusted to 4.5, 6, 8, 10, 12, 15, and 15.2 millimeters to obtain a series of cutoff values N_e caused predominantly by the aperture response of the film.

Finally, the test objects were reproduced over a high-quality television system containing a band-limiting filter which permitted sharp electrical cutoff at various bandwidths up to 20 megacycles. The scanning line numbers used were 525 and 637. The kinescope pictures obtained with this television chain were photographed on 3¼ × 4¼-inch film. A time exposure (½ second) eliminated fluctuations in the 8 × 10-inch enlargements. All prints were made as nearly alike in contrast as possible.

The test was conducted by arranging the prints of the photographic processes according to sharpness and asking ten observers to match the television prints with prints of equivalent sharpness.* The grain-free television prints with sharp cutoff at $\overline{N}_{e0} = 420$ lines, for example, were found equivalent in sharpness to the substantially grain-limited photographs of series B having a limiting resolution $N_e = 850$ lines, and equivalent to grain-free defocussed photographs of series A having a (first zero) cutoff at $N_e = 600$ lines. The results of the tests are

* No reference numbers indicating N_e could be seen by the observer.

Fig. 103—Photograph of test object over a television system ($N_{co} = 420$).

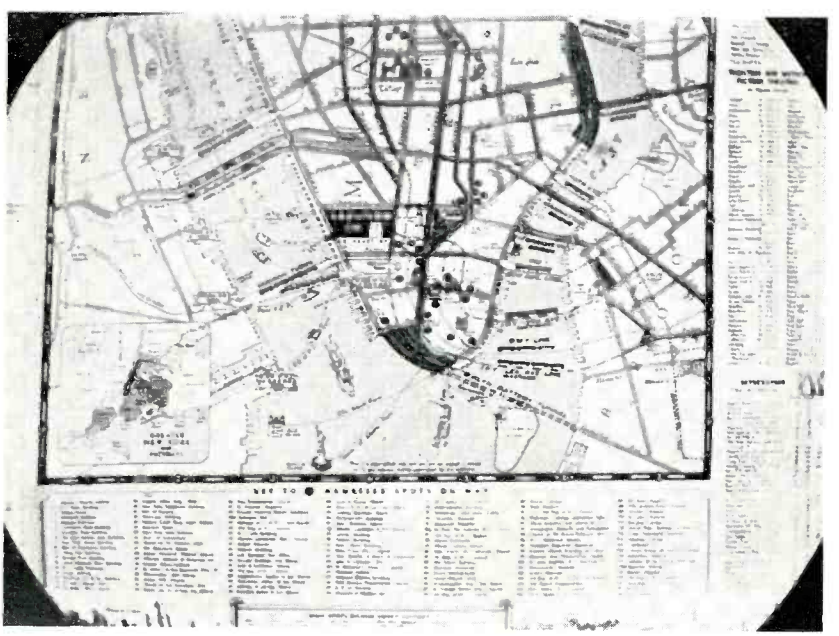

Fig. 104—Photograph of test object over a television system ($N_{co} = 420$).

expressed by the cutoff ratios

$$\frac{\overline{N}_{c0}\ (\text{grain-free television})}{N_c\ (\text{grain-free film})} \simeq 0.7 \quad (\text{Series A})$$

$$\frac{\overline{N}_{c0}\ (\text{grain-free television})}{N_c\ (\text{grain-limited film})} \simeq 0.5 \quad (\text{Series B})$$

The aperture response characteristics of the television system and the photographic images, series A and B, were not known at the time of the tests, but can be established with fairly good accuracy from the characteristics of the system components. The television system characteristics were essentially those shown by Figure 101, except for a kinescope with somewhat lower response and a less complete phase correction. These differences are estimated to account for a decrease of not more than one liminal unit in the sharpness of the system, which is, therefore, —7.5, i.e., one unit less than given for the corrected system in Table IX.

The line number $N_{0.5}$ at $r\Delta\overline{\psi} = 0.5$ for the series A photographs obtained by out-of-focus projection can be established from the characteristics of the projection "aperture". The spurious response observed beyond the first zero point N_c indicated a round aperture with sharper cutoff than given by a cosine-square density, but not sharper than that obtained with uniform density. The ratio $N_{0.5}/N_c$ lies, therefore, between the values 0.40 and 0.48.* With the average value $N_{0.5} = 0.44\,N_c$ and the observed cutoff ratio $\overline{N}_{c0}\,N_c = 0.7$, the line number giving 50 per cent response in series A photographs is found to be $N_{0.5} = 0.63\ \overline{N}_{c0}$, i.e., 63 per cent of the balanced line number of the equivalent television system. For $\overline{N}_{c0} = 410$, we obtain $N_{0.5}$ (series A) $= 258$; and from Figure 102 the sharpness rating of —7 liminal units. The computed sharpness difference of only ½ unit agrees well with the observed equality of matched television and series A prints.

The series B prints were substantially grain limited in resolution as proven later by aperture response measurements of the particular camera lens which was used also in the enlarging process. The shape of the aperture response characteristic of series B images is, therefore, given with good approximation by the film curve 2 in Figure 80, which has the ratio $\overline{N}_{0.5}/N_c = 0.3$. With the ratio $\overline{N}_{c0}/N_c = 0.5$ for series B images, we obtain for $\overline{N}_{c0} = 410$ the value $N_{0.5}$ (series B) $=$ 246, and from Figure 102 a sharpness rating of —7.2 liminal units.

The close agreement and correlation of subjective sharpness ratings with the liminal number obtained by aperture response calculations

* See part II Appendix, Table III.

may be regarded as additional proof that resolution, detail contrast, and image sharpness are adequately and quantitatively interpreted by applying the "aperture" theory developed in this paper.

Conclusions

The quality of television and photographic images depends in a large measure on three basic characteristics of the imaging process: the ratio of signals to random fluctuations, the transfer characteristic, and the detail contrast response. These characteristics are measured and determined by objective methods which apply equally well to all components of photographic and electro-optical imaging systems. A unified system of specifying and measuring definition and detail contrast by the flux response of defining "apertures" has been demonstrated, permitting for the first time a practical analysis and rating of lenses, photographic film, television camera tubes, kinescopes, and other image-forming devices on an objective numerical basis. An interpretation of the numerical values obtained by calculation or measurement of the three characteristics which determine image quality requires correlation with the corresponding subjective impressions: graininess, tone scale, and sharpness. This correlation has been established by analyzing the characteristics of vision and by including these characteristics in an evaluation of the over-all process of seeing through an image-reproducing system.

Calculation and measurement have shown that, provided defects and non-uniformities in both processes are of comparable magnitude, a standard practical television system with a balanced resolution of 410 lines is technically capable of attaining an image equivalent in quality to commercial 35-millimeter motion pictures.

Acknowledgments

In the course of the several years through which these investigations have extended, the author has profited from the experience and helpful criticism of his associates, particularly Dr. Albert Rose of RCA Laboratories on the general subject of photosensitive devices and W. A. Harris of this company on the theory of random fluctuations.

The author also wishes to express his appreciation to the Bausch and Lomb Optical Company and the Eastman Kodak Company for their courtesy in supplying high-quality lenses for test purposes and special photographic material. Various discussions with Drs. T. G. Veal, R. Kingslake, C. D. Reid and other members of the Eastman Kodak Company have been stimulating and helpful in connection with lenses and the photographic process.

THE TRANSITROL, AN EXPERIMENTAL AUTOMATIC-FREQUENCY-CONTROL TUBE*

By

JEROME KURSHAN

Research Department, RCA Laboratories Division,
Princeton, New Jersey

Summary—*A tetrode may be operated with its #2 grid as the anode of an oscillator and its plate as an electron reflector. The reflector potential controls the electron transit time and hence the oscillation frequency. This and other forms of transit time control are investigated theoretically and experimentally. An approximate expression for the control sensitivity is*

$$s = df/V = -kY_m\theta(\cos\ \theta)/4\pi C\ (V_a - V)$$

where k is the feedback fraction which is of the order of 0.2, Y_m the magnitude of the transadmittance, C the circuit capacitance, V_a the anode voltage, V the reflector voltage and θ the total transit angle. This predicts a maximum in s near $\theta = \pi/4$ and a second and greater maximum near $\theta = 2\pi$.

In a circuit suitable for local oscillator use in the frequency-modulation (FM) broadcast band (88-108 megacycles), s = 100 kilocycles/volt was readily obtained with a special tube. In a particular application to an FM receiver, warm-up frequency drift at the high-frequency end of the band was reduced by a factor of 4.5. A receiver with the automatic-frequency-control (AFC) circuit requires 2 resistors and 1 condenser more than a conventional receiver, but saves a radio-frequency choke. Another successful application has been as a one-tube FM transmitter with the reflector electrode modulated directly by a microphone output.

Standard pentodes also allow transit time control, but do not have optimum spacing. Optimizing the design for one frequency will result in less control sensitivity at lower frequencies, but there will still be a residual improvement over an uncontrolled oscillator.

I. INTRODUCTION

COMMERCIAL utilization of the VHF region (30-300 megacycles) of the radio spectrum would be aided by more effective automatic-frequency-control (AFC) devices for these frequencies. The need for AFC is greater here than in the AM broadcast band (0.55-1.6 megacycles). For example, in the FM broadcast band centered at 98 megacycles, a detuning of 10 kilocycles is caused by a local oscillator drift of only 0.01 per cent. Unfortunately, oscillator drift is hardest to control at the higher frequencies because a greater fraction of the tuned circuit is located inside the tube. Even at the somewhat

* Decimal Classification: R355.91 × R361.215

lower frequencies of the first six television channels, AFC can be used advantageously to eliminate the need for fine tuning of pre-set positions on a multichannel tuner.

The idea of electronic AFC is not a new one when effected by means of a separate reactance tube.[1] A typical arrangement is to put the plate-cathode impedance of a tube across the oscillator tuned circuit. A phase splitter supplies quadrature voltage to the grid and the tube output impedance then has a reactive component whose magnitude is determined by the grid bias. This bias is supplied by a suitable discriminator circuit to correct for any frequency deviations. This works quite well, but is rarely used in the lower frequency home broadcast receivers because the required stability is readily achieved without it and the discriminator, which has to be added, increases the cost. For FM reception, however, the discriminator is already present as the second detector. Unfortunately, at 100 megacycles, the simple reactance tube does not function as intended. Inter-electrode capacitance and transit time effects are sufficiently large to interfere with the operation of the quadrature circuits. In addition, the plate resistance of the reactance tube may seriously load the tuned circuit.

Even if the reactance tube worked better, it would still represent an extra tube added to the receiver complement. Recently a double triode tube (6J6) has been used with apparent success as a combination oscillator and reactance tube at VHF in an 8-channel television receiver,* and in an AM-FM communications receiver.[2] This arrangement in effect also uses an extra tube since the second triode unit would otherwise have been available, e.g., for use as a mixer.

This paper describes a new AFC tube which combines the functions of local oscillator and reactance device into a single unit. It works on the principle of controlling the transit time of the electrons and is particularly suited to the VHF region. The name "Transitrol" has been given to this device for ease in reference.

II. Transit-Time Frequency Control

An effect frequently observed in converter operation is the pulling of the oscillator frequency by changing bias on the radio-frequency signal grid.[3] This is caused by electrons reflected from the vicinity

[1] F. E. Terman, RADIO ENGINEERS HANDBOOK, McGraw-Hill Book Co., New York, N. Y., 1943 (pp. 654-656).

* Philco, model 48-1000.

[2] N. W. Aram, L. M. Hershey and M. Hobbs, "FM Reception Problems and their Solution," *Electronics*, Vol. 20, pp. 108-113, September, 1947.

[3] E. W. Herold, "The Operation of Frequency Converters and Mixers for Superheterodyne Reception," *Proc. I.R.E.*, Vol. 30, No. 2 p. 89, February, 1942.

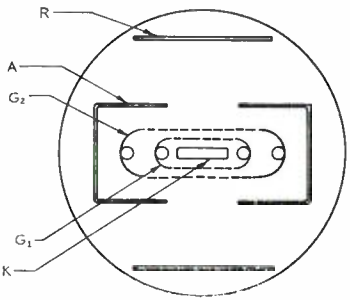

Fig. 1—Transit-time controlled oscillator tube.

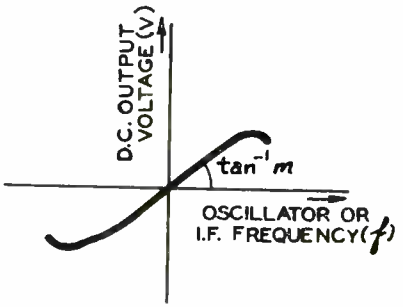

Fig. 2—Typical discriminator characteristic.

of this grid back to the oscillator section where they interact with the electrodes and space charge. These electrons have variable transit times depending on the signal grid bias and so introduce a variable susceptance across the oscillator circuit. Such effects have been largely overcome in the 6SA7 (or 6BE6) type of tube# but are still sometimes troublesome at the higher frequencies.

It occurred to E. W. Herold of these laboratories that this action might be turned to advantage in a device designed to utilize this transit time effect to control the frequency of an oscillator. He suggested a tube somewhat like that shown in Figure 1. Electrons leave the cathode K, pass through the control grid G_1, are accelerated by the screen G_2 and reach the anode A after reflection ahead of the reflector R. By changing the potential on R, the transit time of electrons between grid and anode can be altered. It was with this basic idea as a starting point that the work described in this report was undertaken.

III. Analysis of Operation

A. *Automatic Frequency Control*

The discriminator converts frequency changes into amplitude variations. In FM reception, it is used to detect the modulation and provide the audio frequency signal. With the aid of a simple filter, the same discriminator can usually be arranged to provide in a dc voltage which varies with the average frequency of the radio-frequency signal. Figure 2 shows a typical discriminator characteristic. A representative value for the slope of the central part of the curve is 0.1 volts/kilocycle for a 10.7-megacycle intermediate frequency and a strong signal.

See Reference 1, pp. 570-571.

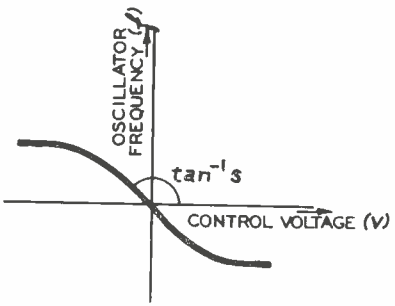

Fig. 3—Desirable controlled oscillator characteristic.

A desirable characteristic for the controlled oscillator is one which is of flat-topped S-shape, as shown in Figure 3. It is apparent that maximum AFC is exercised when the slopes are of opposite sign (for a local-oscillator frequency greater than the signal frequency) and large in magnitude. It is necessary, however, that the frequency excursion over which the oscillator is controlled be restricted to prevent lock-in over too wide a range, which would interfere with the desired manual tuning and cause channel-skipping. The exact expressions are derived in Appendix I. It is shown there that the drift is reduced by a factor $1/(1-sm)$ where m and s are the slopes of the oscillator and discriminator characteristics. It may be noted that if $m = 0.1$ volt/kilocycle and if an improvement of 5 times is desired, s must be 40 kilocycles/volt. We will call the quantity $s = df/dV$ the "control sensitivity" of the oscillator.

B. The Oscillator Circuit

The exact analysis of the mechanism of the oscillator will depend on the particular circuit used. Certain generalizations can, however, be made which apply to all cases. The circuit may usually be simplified to that shown in Figure 4. Both the inductance L and the capacitance C will include distributed and stray components as well as the intentional lumped values. The conductance g represents the losses, both internal and external to the tube, i represents a current generator and is related to the voltage e_o by

$$i = k\, y_m\, e_o$$

where y_m is the tube transadmittance. The factor k depends on the phase and magnitude of the feedback from plate to grid and the various voltage dividers in the circuit such as those formed by blocking capacitors. For convenience, the direction of i in Figure 4 has been chosen so that a real and positive k implies feedback to the grid 180 degrees out of phase with the plate voltage, the normal connection of an oscillator. Although k may be complex,

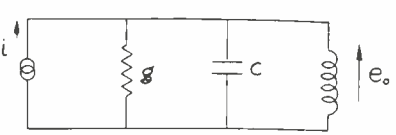

Fig. 4—Equivalent circuit for vacuum tube oscillator.

its phase angle will be small in typical circuits and k will be treated as real. On the other hand, control of the oscillator frequency will now be seen to depend on y_m being complex.

$$\text{Let} \quad y_m = g_m + j\, b_m. \tag{1}$$

The condition that oscillations of angular frequency ω exist is

$$k\,(g_m + j\, b_m) = g + j\omega C + (1/j\omega L). \tag{2}$$

Equating reals and imaginaries gives

$$k\, g_m = g \tag{3}$$

$$k\, b_m = \omega C - (1/\omega L). \tag{4}$$

Oscillations will be sustained if g_m is equal to, or greater than, the value required by Equation (3). An approximate solution of Equation (4) will be most informative. If the term in b_m is small compared to the others,

$$\omega = \sqrt{1/LC}\,|\,1 + 1/(2\sqrt{L/C}\,k\, b_m)\,|. \tag{5}$$

Using the definition of section A above, the control sensitivity of the oscillator is

$$s = \frac{df}{dV} = \frac{1}{2\pi}\frac{d\omega}{dV}$$

where V is the controlling voltage, here the reflector voltage.

$$s = \frac{1}{2\pi}\frac{d\omega}{db_m}\frac{db_m}{dV} = \frac{1}{4\pi}\frac{k}{C}\frac{db_m}{dV}. \tag{6}$$

We thus see that a small C will favor large control sensitivity (although, unfortunately, it will cause the warm-up change in interelectrode capacitance to be more important) and are led to an investigation of db_m/dV.

C. Electronics and Transit Angle

There is a wide variety of possible electrode configurations for the AFC tube, but for a first approximation let us consider the arrangement shown in Figure 1 and assume small interaction between electrons and anode until the former finally hit the latter. The susceptance component of the transadmittance arises from the time τ that it takes

an electron to travel between G_1 and A. We may define the transit angle as usual by $\theta = \omega\tau$. Under the conditions assumed, this transit angle is seen to be the negative of the phase angle of the transadmittance which may be written $y_m = Y_m e^{-j\theta}$.

Consequently $\qquad g_m = Y_m \cos\theta, \qquad b_m = -Y_m \sin\theta. \qquad (7)$

It is shown in Appendix II that this leads to the following approximate equation for the oscillator control sensitivity:

$$s = -\frac{k\, Y_m\, \theta \cos\theta}{4\pi C\,(V_a - V)} \qquad (8)$$

where V_a is the anode potential and V the control potential. It should be remembered that in this last expression, θ is a function of both V_a and V in addition to the spacing d. We desire s to be a maximum, and it is easy to see what must be done to achieve this by adjustment of d. This is a reasonable approach since in practice V_a and V will have a limited range of suitable values. Indeed, one may say that V_a and V should be as near zero as practical, since s will then be greater for a given θ. If this adjustment of V_a and V affects θ adversely, d may then be changed to give the optimum value of θ.

Setting $\partial s/\partial\theta = 0$ gives $\qquad \theta = \cot\theta.$

This equation has an infinite number of solutions which may be found graphically or from tables. The first few are tabulated below:

No.	θ *Radians*	θ *Degrees*	$\theta \cos\theta$ *Radians*
1	.86	49	0.56
2	$\pi + .285$	$180 + 16.3$	-3.3
3	$2\pi + .155$	$360 + 9$	-6.2
↓	↓	↓	↓
n	$(n-1)\pi$	$(n-1)\ 180$	$(-1)^{n-1}(n-1)\pi$

It would appear that a factor of 6 is gained by going to the second maximum of $\theta\cos\theta$ (by increasing D). Unfortunately, this corresponds to a transit angle near π and severe loading would result. At the third maximum, however, $\theta\cos\theta$ will be almost doubled again and operation will occur with a transit angle near 2π. It should be noted, however, that the second maximum might be used to advantage if the

oscillator were designed with in-phase feedback from anode to grid.[4]

An estimate of the expected optimum control sensitivity can be made by using Equation (8) with $k = 0.2$, $Y_m = 2 \times 10^{-3}$ mhos, $\theta \cos \theta = 0.5$, $C = 10^{-11}$ farads, $V_a = 50$ volts, $V = 0$. This gives $s = df/dV = -30$ kilocycles/volt. This estimate does not take space charge effects into account. It is interesting to note that the *absolute* sensitivity s (which is not the fractional frequency change) should be independent of frequency, provided (1) the transit angle θ can be maintained at the optimum value, and (2) C can be kept low.

Throughout this analysis, it has been tacitly assumed that control is effected by varying the reflector potential V. It is conceivable that varying the anode potential V_a might be more effective, even though this will take more control power. It is shown in Appendix III that unless $-V > 3V_a$, reflector potential control is the more sensitive. In general, $-V < V_a$ and so anode potential control will not be considered further.

The general behavior of this type of oscillator can now be summarized qualitatively. Some of the emitted electrons go directly to the anode and have small transit angles. They contribute only to the g_m of the tube and are important in maintaining oscillations. The electrons which pass the anode on the way out from the cathode are reflected and eventually reach the anode with large transit angles. In general, these contribute both to the g_m and b_m of the tube. Varying the reflector potential alters the transit angle and hence the transsusceptance and so changes the oscillator frequency. The amplitude of oscillation will also be affected if the transconductance changes. However, for transit angles near $n\pi$, where n is large, maximum control will occur near a zero in dg_m/dV.

IV. Suitability of Commercial Tubes

It is convenient to use a simple tetrode for the controlled oscillator. Most of the electrons then pass through the #1 and #2 grids on their way out from the cathode, are turned back near the plate used as a reflector and finally impinge on the #2 grid which is the anode of the oscillator.[5] This behavior may be contrasted with that of the tube

[4] McArthur has described a related device which, however, operates with the grid at cathode potential: E. D. McArthur, "The Dyotron—a New Microwave Oscillator," *Proc. I.R.E.*, Vol. 36, No. 3, p. 378, March, 1948 (abstract).

[5] A device bearing superficial resemblance to the one herein described has been reported by C. J. Bakker and G. deVries, "Amplification of Small Alternating Tensions by an Inductive Action of the Electrons in a Radio Valve," *Physica*, Vol. 1, pp. 1045-1054, October, 1934. (Philips Reprint No.

shown in Figure 1; the outstanding difference is the continuous interaction between electrons and anode (#2 grid) which now must exist once an electron has passed the control grid. Of course, a part of this interaction would also have been present in the earlier discussion except for the idealization of conditions.

Although tetrode receiving tubes are no longer common, a pentode might do almost as well. The suppressor might be at either ground or plate potential, depending on available external connections and the performance. A survey was made of available commercial tubes to determine their performance in the FM broadcast band, 88-108 megacycles. With the standard intermediate-frequency of 10.7 megacycles, the local oscillator will normally range from 99 to 119 megacycles. Tests were limited to miniature-type tubes as being most suitable for commercial application at these frequencies.

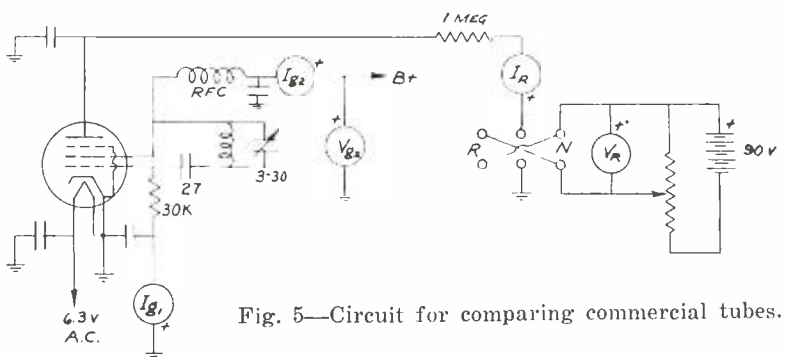

Fig. 5—Circuit for comparing commercial tubes.

The circuit used is shown in Figure 5. It is a Colpitts oscillator using the interelectrode capacities for feedback. Such an arrangement, employing a grounded cathode, is the simplest to use at these frequencies and works quite well. It avoids heater chokes or bifilar windings, but has the disadvantage that neither end of the tuned circuit is at ground potential, for it is important that the cathode be at ground potential when using transit-time control. Restrictions on the grounding of electrodes arise as follows: It is necessary that there be a radio-frequency field between #2 grid and reflector; otherwise the transit of the electrons would effectively terminate when they first passed the #2 grid since they could induce no voltage on the tank circuit thenceforth. The most practical arrangement is to have the reflector at radio-frequency ground and the #2 grid high, as shown. This, in turn, requires that the cathode be at ground potential to avoid

930); they also use a tetrode with a negative voltage on the plate. This, however, is the output electrode of an amplifier and has currents induced in it by the electron stream reflected in front of it.

reflector current due to electrons which would be emitted at the negative peaks of cathode voltage. Although the resulting circuit shown in Figure 5 does not have the tuning capacitor grounded, this should not be a serious drawback since inductance tuning is generally preferred at these frequencies, especially in wide band applications. The advantages are more convenient circuits and constant bandwidth for the radio-frequency stages. As a result, the trend in recent FM receiver design has been toward numerous novel inductance tuner.

It was hoped that the results of these tests could be summarized in simple tabular form. Ideally, such data would show the effect of the different G_2-plate spacings employed in the various tube types; one could see the influence of spacing on control sensitivity and pick the tube coming nearest to the optimum. Unfortunately, the tubes are not comparable on this basis because other aspects vary which strongly influence the performance. These include G_1-G_2 spacings, electrode shapes, transconductance and interelectrode capacitances.

Both analysis and experiment showed that low voltage on grid #2 and the reflector were desirable to get maximum control sensitivity with a given tube. The best tubes operated with 50 volts on G_2 as a suitable compromise between sensitivity and oscillation amplitude. In most cases, 75 volts gave the maximum allowable dissipation in grid #2 since no plate current is drawn, but some tubes would not oscillate with 50 or even 75 volts on G_2. At least 1 or 2 volts negative reflector potential was always needed to prevent current to the reflector. This may have been due to contact potentials and initial speeds, but in some cases, the electrons were obviously getting substantial "excess" energies, as is possible when traversing an alternating field with a large transit angle.[6]

The 9001 gave the greatest control sensitivity ($s = df/dV$) but oscillations were very weak. The 6AK5 performed most reliably, but the control sensitivity was not so high as that readily obtainable in some special tubes to be described. It is possible that the transit distance was *greater* than optimum for operation near the first maximum in control sensitivity. The 6AG5 did not oscillate except with very large values of reflector potential (90 volts) because of the large spacing between screen and plate. The 6AU6 with grounded suppressor behaved like the 6AG5. The 6AU6, however, had a separate connection to the suppressor. Experiments showed that when suppressor and plate were tied together, the suppressor acted as the reflector. Oscil-

[6] K. S. Knol, M. J. O. Strutt, A. van der Ziel, "On the Motion of Electrons in an Alternating Electric Field," *Physica*, Vol. 5, p. 326, May, 1938.

lations were still poor, however, requiring some 5-15 volts (negative) on the reflector even with $V_{g2} = 100$ V.

With the 6BE6 converter tube the #3 grid was used as a reflector. Although the spacing was apparently too large and oscillations occurred only with 15-20 volts (negative) on the reflector, oscillation amplitude and frequency shifts were relatively large so that this was made the prototype for the special tubes described later. The 12AW6 is similar to the 6AG5 except for higher heater and voltage and a separate suppressor connection. The latter feature enabled it to be operated in the fashion of Figure 1 where the suppressor beam plates (there is no actual wire grid) are the oscillator anode and the screen is used merely as an accelerator at radio-frequency ground potential. Static measurements showed that with suppressor and #2 grid at the same d-c potential, there was a good focussing action of reflected electrons on to the suppressor. Although the spacings were relatively large, good frequency shifts were obtained, even at the high voltages needed for satisfactory operation. However, the electrons seemed to pick up considerable energy from the radio-frequency field and reflector potentials of 15 volts or more were needed to prevent electron current to the reflector.

V. Design and Performance of a Special Tube

One of the strongest oscillators found among the commercial tubes tested was a 6BE6 with its #3 or radio-frequency signal grid used as a reflector. Since the reflector bias had to be at least 20 volts negative, it was apparent that the reflector spacing was too large. Accordingly, a tube was built which used 6BE6 parts out to the #3 grid which in turn was replaced by a simple reflector-plate of a diameter calculated to give optimum performance with zero reflector potential. Of course, the elements normally outside this electrode were omitted. Figure 6 is a cross-sectional scale drawing of this tube.

The tube performed about as expected. Some other tubes, constructed with slightly different diameter reflectors, showed it to be optimum for this type of construction. Figure 7 gives typical frequency control data for this tube when used in the circuit of Figure 5.

VI. Receiver With Transitrol AFC

A test of the Transitrol in an FM receiver was made using a commercial FM receiver. The ratio detector was modified to give a balanced d-c output with respect to ground; this served as the control voltage and was applied through a 10-megohm filter and isolation resistor. A

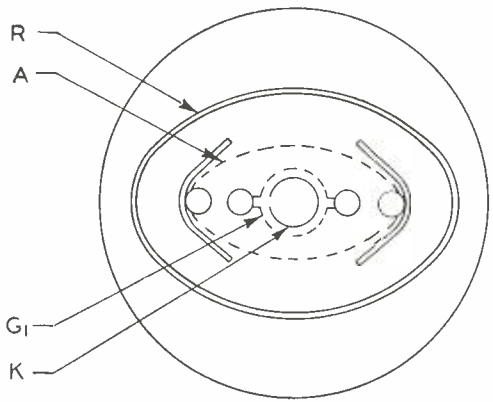

Fig. 6—Special AFC tube.

switch was provided, by which the Transitrol reflector could be connected to the AFC voltage or to ground.

Considerable trouble was encountered because the receiver was capacitor tuned. The Transitrol circuit requires the cathode to be at radio-frequency ground potential to eliminate electron currents to a negative reflector. The best oscillator circuit to use at these frequencies is that of Figure 5. This requires both sides of the tank capacitor to be at high radio-frequency potential and is only suitable for inductively tuned receivers. A Hartley oscillator suffers the same trouble.

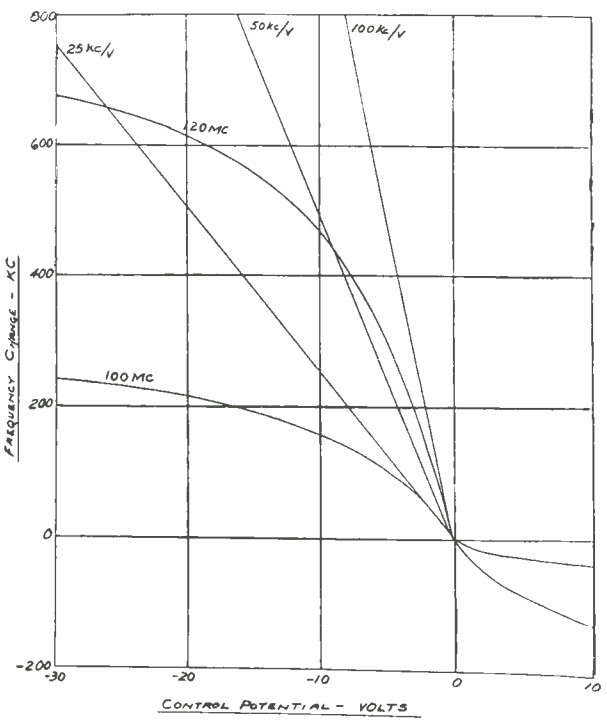

Fig. 7 — Frequency control of special AFC tube in circuit of Figure 5. ($V_{g2} = 50$ volts.)

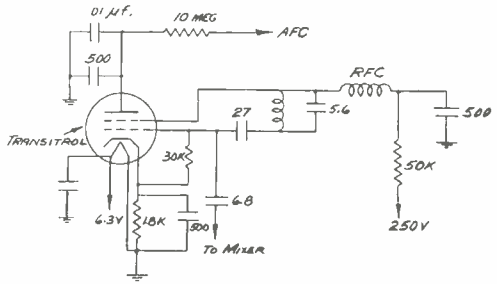

Fig. 8 — AFC oscillator circuit used on FM receiver.

Experiments showed that a Colpitts circuit with the variable capacitor between either control grid and cathode or #2 grid and cathode would not operate satisfactorily over the whole tuning range. A "tuned plate" oscillator with a feedback coil to the control grid was then set up. While this seemed to perform fairly well by itself the mixer stage loaded it excessively. It was apparent that special coupling means would be necessary to get adequate feedback with this type of circuit, and so it was abandoned and the receiver performance was determined with a permeability-tuned Colpitts oscillator constructed on a sub-chassis. The circuit is shown in Figure 8. Cathode bias is provided so that the AFC voltage may be centered at ground potential. Performance of the Transitrol in this circuit is shown in Figure 9. This is an improvement over the earlier data (Figure 7) which can be attributed to the smaller tuning capacitance.

The warm-up drift of the receiver oscillator, as manufactured, is given in Figure 10(a) and at the high-frequency end of the band it is 230 kilocycles in the first 9 minutes. Drifts are measured as the difference from the frequency existing 30 seconds after the set is turned on until a plateau is reached. It should be remembered that the local oscillator frequency is 10.7 megacycles above the signal frequency, making the os-

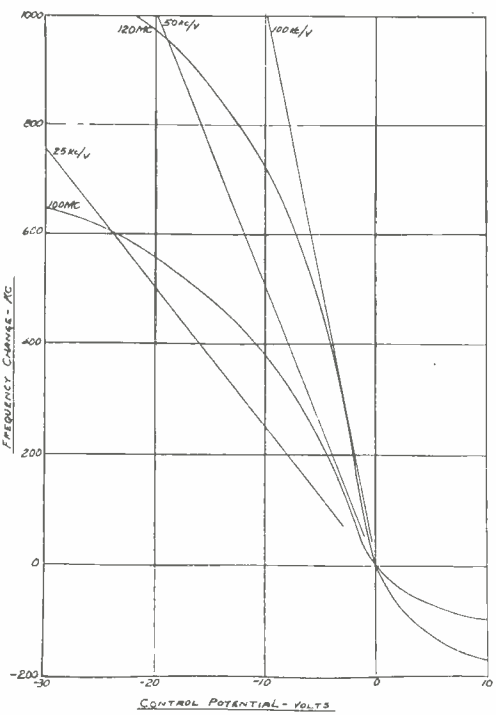

Fig. 9—Frequency control of special AFC tube in circuit of Fig. 8. ($V_{g2} = 50$ volts.)

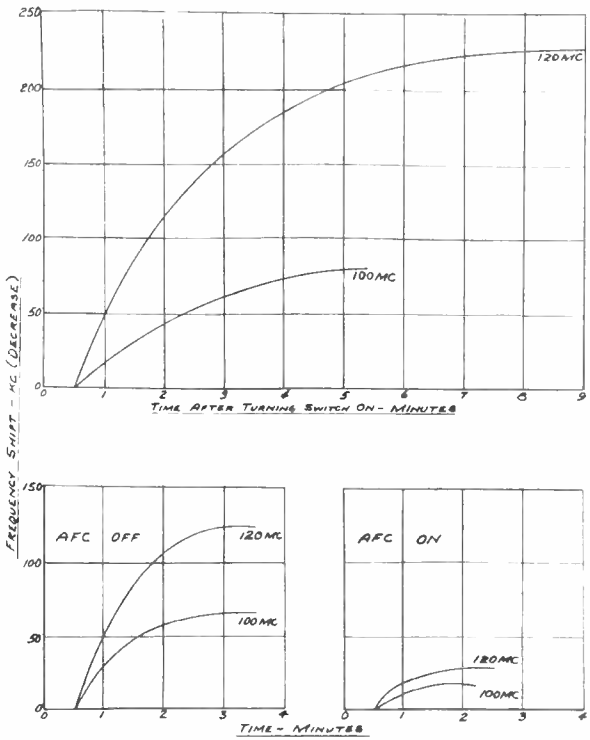

Fig. 10—(a) Upper figure: Original local oscillator drift of receiver. (b) Lower figures: Drift of receiver with AFC.

cillator range approximately 99 to 119 megacycles to cover the FM broadcast band. Receiver drift with the Transitrol in place is given in Figure 10(b). Even with the AFC off, the drift at 120 megacycles is reduced to 125 kilocycles in 3 minutes, an improvement probably due in part to the substitution of a ceramic socket for the phenolic type employed in manufacture. With the AFC on, the drift was reduced to 28 kilocycles, a further improvement by a factor of 4.5 times.

Since the Transitrol is inherently sensitive to $B+$ supply voltage, the improvement in frequency stability with regard to line voltage changes is not so striking. However, since the original receiver was satisfactory in this respect, the residual frequency variations are not important. The data for these conclusions are plotted in Figure 11.

VII. One-Tube FM Transmitter

It is apparent that by applying amplitude modulation to the reflector electrode, the Transitrol can be used to generate a frequency modulated signal directly. Although the modulation characteristic is not inherently linear, this device has the advantages of high sensitivity and high

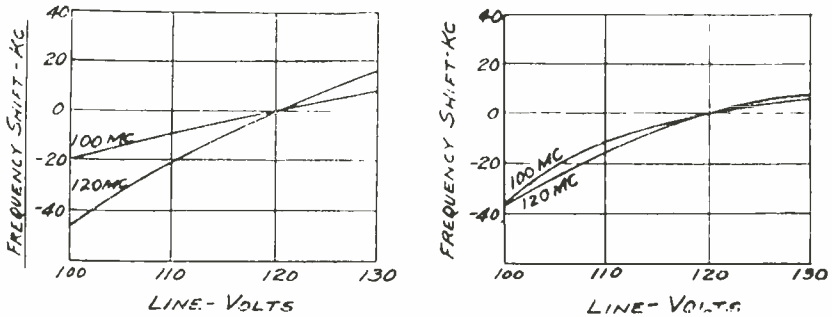

Fig. 11—(a) Left figure: Effect of line voltage on original receiver. (b) Right figure: Effect of line voltage on receiver with AFC.

impedance. To test this application, a tube was connected as in Figure 8 except for the reflector which was by-passed for radio-frequency and connected directly (no amplifier) to a microphone which gave about .02 volt root-mean-square for ordinary speech. The radiated signal at 105 megacycles was picked up on the FM receiver previously mentioned and sounded natural. Based on the static characteristic, the frequency deviation was estimated to be 28 kilocycles. Visual (oscilloscopic) check using a 400-cycle sine-wave oscillator for modulation showed no apparent audio distortion.

VIII. Acknowledgment

Grateful acknowledgment is made to E. W. Herold who supplied valuable suggestions throughout the course of the work.

Appendix I

Automatic Frequency Control

Suppose that in the absence of AFC some variable parameter x affects the oscillator frequency as shown in Figure 12, x may represent temperature or tuning control position, etc. Let the curves of Figures 2, 3, and 12 have slopes of m, s, and d, respectively. d is then a measure of the "drift" of the oscillator in the absence of AFC.

We may consider x as the only independent variable. The control voltage (V) and the frequency (f) are functions of x ultimately, although x does not appear in the explicit relation between V and f It is convenient to consider the functional relationship

$$f = F(x, V). \tag{A-1}$$

Then the partial derivatives are given by

$$F_1 = \partial f/\partial x]_V = d, F_2 = \partial f/\partial V]_x = s.$$

Also, if $V = g(f)$, $g' = dV/df = m$.

Differentiating (A-1) $df/dx = F_1 + F_2 (dV/dx)$,

but $dV/dx = g' (df/dx) = m (df/dx)$.

Therefore, $df/dx = d + s \cdot m (df/dx)$ or $df/dx = d/(1 - s \cdot m)$.

Thus, the drift is reduced by the factor $1/(1 - s \cdot m)$.

The case in which the signal frequency shifts is not of interest here, although it is even simpler to treat and gives the same expression for the reduction in "drift".

Appendix II

Control Sensitivity

Substituting from Equation (7) into Equation (6) gives

$$s = -\frac{1}{4\pi}\frac{k}{C} Y_m \cos\theta \frac{d\theta}{dV}. \qquad \text{(A-2)}$$

Now,
$$d\theta/dV = \tau(d\omega/dV) + \omega(d\tau/dV) \qquad \text{(A-3)}$$
$$= 2\pi\tau' s + \omega(d\tau/dV).$$

Substituting for $d\theta/dV$ in (A-2) gives

$$s = -\frac{k Y_m \theta \cos\theta}{4\pi\tau C\,|1 + (d Y_m 2\omega C)\,\theta\cos\theta|}\frac{d\tau}{dV}. \qquad \text{(A-4)}$$

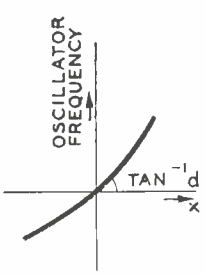

Fig. 12—External influence on oscillator.

It will not invalidate the general picture if we make the simplifying assumptions that G_2 and A are at the same dc potential and that this is large compared with the radio-frequency voltage on A. The transit times from G_1 to G_2 and from G_2 to the plane of A will be neglected. A parallel-plane geometry is assumed with a linear potential distribution between A and R, where d is the distance between the latter two electrodes.

Figure 13 shows the potential variation between anode and reflector for some (negative) voltage V on the reflector. Electrons will be reflected at the distance z from G_2 where the potential is zero with respect to the cathode.

$$z = d \cdot V_a/(V_a - V).$$

The transit time τ is $2z/v_{av}$ where v_{av}, the average speed, is ½ the speed corresponding to V.

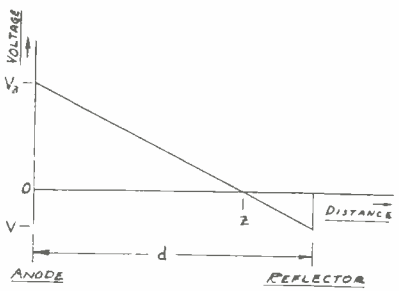

Fig. 13—Variation of potential between anode and reflector.

$$\tau = 4d \frac{V_a}{V_a - V} \sqrt{m/2e\, V_a} = \sqrt{8\, m/e}\quad d\sqrt{V_a}/(V_a - V)$$

$$\frac{d\tau}{dV} = \sqrt{8\, m/e}\quad d\sqrt{V_a}/(V_a - V)^2 = \tau/(V_a - V).$$

Substituting this value of $d\tau/dV$ in Equation (A-4) gives

$$s = -\frac{k\, Y_m\, \theta \cos\theta}{4\pi C\,[1 + (k/2\omega C)\, Y_m\, \theta \cos\theta]\,(V_a - V)}. \qquad \text{(A-5)}$$

The bracketed term in the denominator arises from the term in $d\omega/dV$ in Equation (A-3) and so its deviation from unity is a measure of how large the fractional change in frequency is compared to the fractional change in transit time for a given change in reflector voltage. For transit angles of the order of 1 radian, $\theta \cos\theta$ will have a maximum of about ½. Other typical values at 100 megacycles are $\omega = 6.3 \times 10^8$ sec^{-1}, $C = 10^{-11}$ farads, $Y_m = 2 \times 10^{-3}$ mhos, $k = 0.2$. Using these values gives $\frac{k}{2\omega C} Y_m\, \theta \cos\theta = 1.6 \times 10^{-3}$, and so we will neglect this term in Equation (A-5) as compared to unity for the present. Reasonable changes in some of the factors, however, might easily make it signifi-

cant. An approximate expression for the oscillator control sensitivity is thus given by

$$s = -\frac{k\, Y_m\, \theta \cos \theta}{4\pi C\, (V_a - V)}.$$

Appendix III

Reflector vs. Anode Control

In Appendix II it was found that $\tau = \sqrt{8m/e}\, d \cdot V_a^{1/2}/(V_a - V)$ where τ is the transit time, d is the spacing between G_2 and the reflector, V_a is the potential of G_2 (or the anode), V is the reflector potential (which is negative). For constant d, the anode voltage control sensitivity will be proportional to

$$\partial \tau / \partial V_a = -\tfrac{1}{2} \sqrt{8m/e}\, d \frac{V_a + V}{V_a^{1/2}\, (V_a - V)^2};$$

the reflector control sensitivity, to

$$\partial \tau / \partial V = -\sqrt{8m/e}\, d \cdot V_a^{1/2}/(V_a - V)^2.$$

The ratio of the sensitivities is $R \equiv \dfrac{\partial \tau / \partial V}{\partial \tau / \partial V_a} = 2\, V_a/(V_a + V)$.

Since $\qquad |R| > 1 \quad \text{for } 0 \leq -V < 3\, V_a,$

reflector control has the advantage for reasonable operating potentials.

MULTI-CHANNEL RADIO-TELEGRAPH SYSTEM FOR HIGH-FREQUENCY CIRCUITS*

By

THOMAS E. JACOBI

Engineering Products Department, RCA Victor Division,
Camden, N. J.

Summary—*In field tests of a number of frequency-division multi-channel radio telegraph systems for use in the high-frequency range (3 to 30 megacycles) it was found that frequency-modulated sub-carrier channels in conjunction with single sideband and space diversity provided the best method of transmission of those tried. Error rates of 0.02 per cent to 0.14 per cent were obtained on a transcontinental circuit. Furthermore, frequency spectrum and transmitter power are utilized most efficiently. Conventional double-sideband circuits proved unsatisfactory because of high error rates during periods of selective fading. If exalted-carrier receivers are used in the double-sideband circuit, the error rate can be reduced to the same magnitude as that for a single-sideband circuit; however, the other two advantages of single-sideband previously referred to are still lost. Because of the steadily increasing congestion in the high frequency range, methods of reducing spectrum usage and increasing message capacity are considered of paramount importance.*

INTRODUCTION

MAJOR radio-telegraph trunk circuits, such as those in the Tape Relay Network operated by RCA Communications, Incorporated,[1] require transmission systems of large traffic capacity and great reliability. With the object of meeting these exacting requirements more fully, a system† of multi-channel operation, transmitting in the high-frequency range (3 to 30 megacycles), has been developed for use in such long-distance, point-to-point services.

The most interesting features of this system from an operating viewpoint are its exceptionally large traffic capacity and its wide flexibility. The maximum traffic capacity of the experimental equipment, for example, is 72 automatic printer channels, each operating at 60

* Decimal Classification: R423.2.

[1] S. Sparks and R. G. Kreer, "Tape Relay System for Radiotelegraph Operation", *RCA REVIEW*, Volume VIII, No. 3, pp. 393-426, September, 1947. (In particular see Figure 26, p. 425.)

† Subsequent to the writing of this paper, it was learned that during the war the British had employed a system having similar features. See: J. A. Smale, "Some Developments in Point-to-Point Radiotelegraphy", *Jour. I.E.E.*, Volume 94, Part III A, No. 12, pp. 345-367, 1947. In particular see page 364.

words per minute, in only 6 kilocycles of radio frequency spectrum. In contrast, the only other comparable frequency-division multi-channel system known to the author[2] provides but 6 printer channels (operating at the same speed and occupying the same space as mentioned before).

The wide flexibility of the system results from its being fundamentally a frequency division channeling system. Because of this, the number and kind (i.e., narrow-band, wide-band, etc.) of channels may be readily changed. This flexibility applies both to the planning of new systems and the adjustment of existing systems to meet changing traffic demands.

The high order of reliability obtainable with the system has resulted largely from a judicious combination of several of the most outstanding technical developments of the radio and telegraph arts. These are: frequency modulation; single-sideband high-frequency radio transmission; directive antennas; space diversity reception; and synchronous time-division telegraph multiplexing.

In order to verify the workability of this system with quantitative experimental data, suitable equipment was assembled and two extensive series of field tests were made. Not all of the comparisons which were desired were completed however, and additional tests are being conducted. It is the purpose of this paper to present some of the more important details of the system and the results, to date, of the field tests.

DESCRIPTION

The system consists essentially of a number of audio-frequency subcarrier channels each of which is frequency modulated* in accordance with one of the telegraph signals being transmitted[3-5], and which are then used to amplitude modulate signal-sideband equipment[6].

---

[2] L. C. Roberts, "Multi-Channel Two-Tone Radio Telegraphy," *Bell Labs. Record*, Volume 24, No. 12, pp. 461-465, December, 1946.

* The term "frequency shift keying" is also used when speaking of frequency modulation applied to telegraphy.

[3] Earlier RCA work relating to this subject is described by W. H. Bliss, "Use of Frequency Modulation in Communication Systems", *Proc. I.R.E.*, Vol. 31, No. 8, pp. 419 to 423, August, 1943.

[4] The results of a comprehensive study of the merits of frequency modulation for radio telegraphy have been given by J. R. Davey and A. L. Matte, "Frequency Shift Telegraphy — Radio and Wire Applications", *B.S.T.J.*, Vol. XXVII, No. 2, pp. 265-304, April, 1948.

[5] Another important paper is that by T. W. Jones and K. W. Pfleger, "Performance Characteristics of Various Carrier Telegraph Methods", *B.S.T.J.*, Vol. XXV, No. 3, pp. 483-531, July 1946.

[6] The merits of single-sideband operation in the high-frequency range have been reported by F. A. Polkinghorn and N. F. Schlaack, "A Single-Sideband Short-Wave System for Transatlantic Telephony," *Proc. I.R.E.*, Volume 23, No. 7, pp. 701-718, July, 1935.

According to the method of classifying multiplex systems recently described by Landon[7], this system would be called PCM-FM-SS. It is of interest to note that the usual type of multiplex or start-stop printing telegraph apparatus, in which only the center fraction of the signalling pulse is actually utilized, corresponds to employing a gate narrower than the pulse width. Landon points out that this theoretically results in a perfect signal-to-noise ratio above threshold.

In addition to the use of PCM-FM-SS as the basic modulating method, there are several other features of the system which contribute materially to its successful performance. One of these is the use of space diversity reception[8,9]. Another is the use of directive, high-gain transmitting and receiving antennas[8,10,11]. A third is the use of time-division telegraph multiplexing apparatus[12]. Some or all of these latter features can be omitted, if desired, from those installations in which the performance requirements are not the most severe.

The principal advantages of this system are:

1. Frequency modulation of the sub-carrier channels makes them less susceptible to level variations and interference and also improves the signal-noise ratio.
2. The use of multiple sub-carrier channels provides a very flexible system since the number of channels employed may be readily changed to meet varying requirements both in system design and during regular operation. In addition, for a given total message handling capacity, lower keying speeds are possible in each sub-carrier channel than would be required in a single-channel system. This is of importance since multipath delay distortion frequently limits the maximum keying speed that can be used on a circuit.

---

[7] V. D. Landon, "Theoretical Analysis of Various Systems of Multiplex Transmission", *RCA REVIEW*, Vol. IX, No. 2, pp. 287 to 351, June 1948 and No. 3, pp. 433 to 482, September, 1948.

[8] H. H. Beverage and H. O. Peterson, "Diversity Receiving System of RCA Communications, Inc. for Radiotelegraphy", *Proc. I.R.E.*, Vol. 19, No. 4, pp. 531-561, April, 1931.

[9] H. O. Peterson, H. H. Beverage and J. B. Moore, "Diversity Telephone Receiving System of RCA Communications, Inc.", *Proc. I.R.E.*, Vol. 19, No. 4, pp. 562-584, April, 1931.

[10] P. S. Carter, C. W. Hansell, and N. E. Lindenblad, "Development of Directive Transmitting Antennas by RCA Communications, Inc.", *Proc. I.R.E.*, Vol. 19, No. 10, pp. 1773 to 1852, October, 1931.

[11] E. Bruce, A. C. Beck, and L. R. Lowry, "Horizontal Rhombic Antennas", *Proc. I.R.E.*, Vol. 23, No. 1, pp. 24-46, January, 1935.

[12] R. E. Mathes, J. L. Callahan and A. Kahn, "Time Division Multiplex in Radiotelegraphic Practice," *Proc. I.R.E.*, Volume 26, No. 1, pp. 55-75, January, 1938.

3. Single-sideband radio transmission requires a band only half as wide as for double-sideband. This is of considerable importance, inasmuch as the high-frequency range is becoming quite crowded. It also utilizes the transmitter power more efficiently. These two result theoretically in a 9-decibel improvement in signal-to-noise ratio over double-sideband.
4. The process of resupplying the carrier generally employed with single-sideband equipment results in a mitigation of the harmonic and inter-modulation distortion which occurs during selective fading of the carrier in conventional double-sideband operation.
5. Space diversity reception requires less than half as much bandwidth as frequency diversity.# Also past indications have been that its diversity action is superior to that of either frequency diversity or polarization diversity.
6. The use of time-division telegraph multiplex results in the saving of the time of the start and stop pulses of single-channel start-stop printing apparatus. This is true both when "multiplex"-type printers are used and when conventional single-channel start-stop printers, with auxiliary code storage apparatus, are used. A typical value for the amount of time saved is 32 per cent, and this is equivalent to a 47 per cent increase in words per minute. Another advantage of continuously synchronized multiplexes of the familiar types is that they are believed to be less susceptible to printing errors due to noise and interference. This follows from consideration of the fact that in the start-stop system noise peaks can affect a start pulse and a signal pulse in the additive manner, whereas this effect does not take place with the multiplex equipment. The experimental results tend to bear this out as will be shown later. Non-printing equipment, either automatic or manual, can be used when available, however, the desirability of automatic printer operation, especially for large systems, has been well established.[13]
7. Directive, high-gain antennas reduce the required transmitter power, reduce interference with and from other radio stations, and frequently improve the signal-to-noise ratio.

A typical system layout is shown in simplified diagram form in

The term frequency diversity as used throughout this paper applies to that type in which the two diversity channels are relatively close together in frequency (not more than 5 or 10 kilocycles apart at most).

[13] See Reference 1.

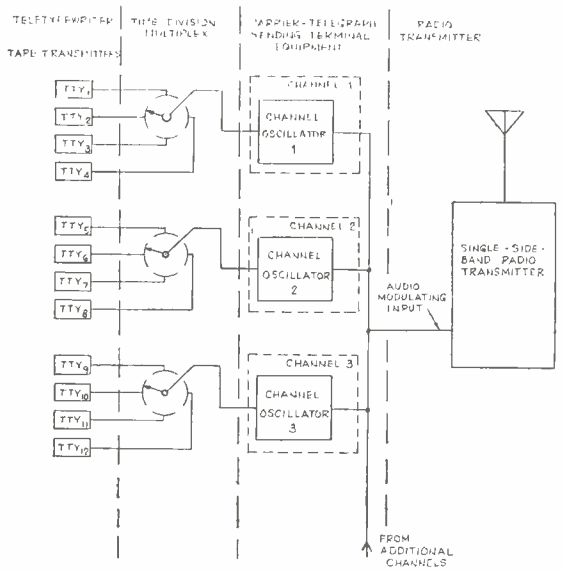

Fig. 1—Simplified block diagram of transmitting equipment.

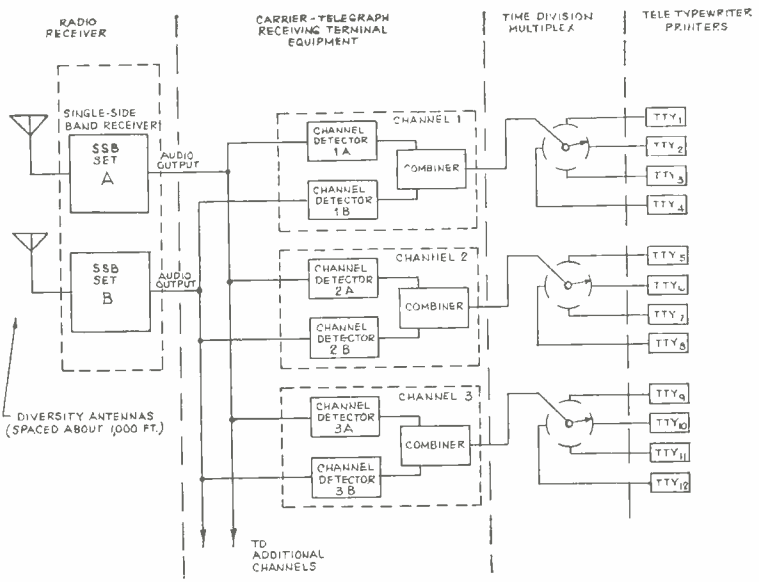

Fig. 2—Simplified block diagram of receiving equipment.

Figures 1 and 2. The dc telegraph outputs of the tape transmitters in Figure 1 are combined in time-division telegraph multiplexing equipment (shown in four-channel form) and then used to key the channel oscillators of the sending tone channels. Here the dc telegraph signals are converted into a series of frequency-modulated audio tones. The tones in turn amplitude modulate the single-sideband radio transmitter. When the single-sideband transmitter is of the multi-channel type, similar sets of tones from additional channeling equipments (or other signals) can be used to modulate these other channels of the transmitter.

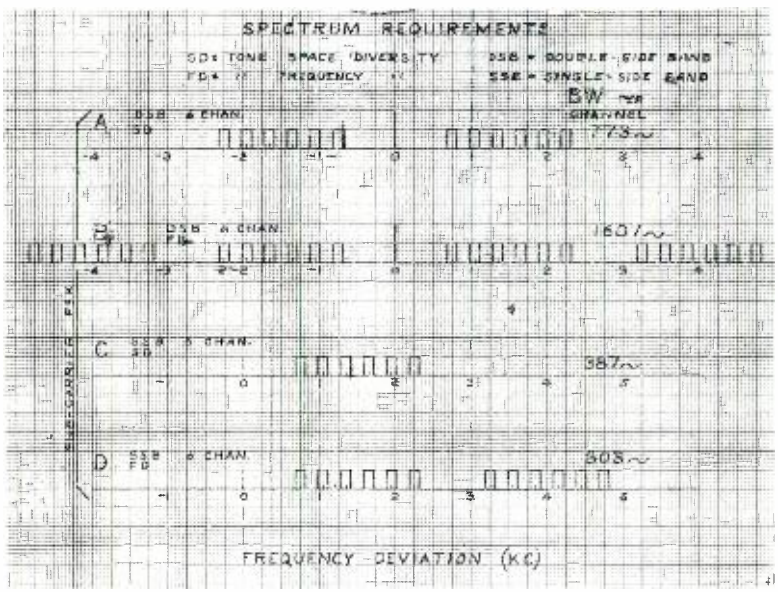

Fig. 3—Frequency spectrum requirement.

The radio signal is picked up on two antennas arranged for space-diversity reception as shown in Figure 2. The two antennas are connected to two single-sideband receivers (identified as A and B). Their audio outputs connect to the channel detectors of the receiving tone channels wherein they are selected, amplified, limited and converted back into dc telegraph signals. Each channel of the terminal has two channel detector units, one connected to receiver A and the other to receiver B. The output of the channel detector having the stronger signal input is selected in the combiner unit, amplified and shaped, and then fed to the time-division telegraph multiplexes and the printers.

An indication of the frequency spectrum requirements of a typical system can be obtained from Figure 3. A six-channel system with

300 cycle channel spacing has been selected as being representative. For comparison, single-sideband with frequency diversity and double-sideband with space diversity and with frequency diversity have also been shown. Single-sideband with space diversity is seen to have a two to one advantage over single-sideband with frequency diversity and also over double-sideband with space diversity, and a four to one advantage over double-sideband with frequency diversity.

The crucial portion of all diversity systems is the method of combining signals. Examination of data on the available methods indicated that positive selection of the stronger signal, as embodied in the Type V-1160 Frequency Shift Receiver Converter[14], was the best method available. The fact that it is considerably more complex was not felt to be an important disadvantage in fixed station equipment such as this where best performance is the prime criterion.

Tests

In order to study adequately the performance of the system it was planned to conduct tests on both single-sideband and double-sideband circuits inasmuch as double-sideband is in such extensive use compared with single-sideband. Furthermore, the tests were to include a comparison of frequency diversity with space diversity, since the former has found use in previous equipment of this general class.[15] In order to provide frequency diversity, a Channel Shifter and a Channel Restorer were provided at the sending and receiving ends respectively in the experimental channeling equipment. The experimental equipment will be described in detail in connection with the first series of tests which follows.

Double-Sideband Tests

Equipment

Frequency-modulated carrier-telegraph equipment has undergone extensive development and received considerable use for wire line applications[16, 17]. The channeling equipment designed for these tests was patterned after it and is shown in Figures 4 and 5. Three sub-

---

[14] This unit is described in: H. O. Peterson, J. B. Atwood, H. E. Goldstine, G. E. Hansell, and R. E. Schock, "Observations and Comparisons on Radio Telegraph Signaling by Frequency Shift and On-Off Keying," *RCA REVIEW*, Volume VII, No. 1, pp. 11-31, March, 1946.

[15] See Reference 2.

[16] F. B. Bramhall and J. E. Boughtwood, "Frequency Modulated Carrier Telegraph System", Trans. A.I.E.E., Vol. 61, No. 1, pp. 36-39, January 1942.

[17] F. B. Bramhall, "High-Speed Voice-Frequency Carrier Telegraph", A.I.E.E. Technical Paper No. 40-51, 1940.

carrier channels were considered to be sufficient to verify proper multi-channel operation.

The arrangement of all of the equipment for the first series of tests is shown in Figures 6 and 7 in functional diagram form. The transmitting apparatus consists of a five unit start-stop tape transmitter (operating at 60 speed, which is 368 operations per minute) repeating a recurring series of test words through a polar relay into the channel oscillator. The channel oscillator is keyed by the telegraph signal between 70 cycles below the channel frequency for mark and 70 cycles above for space. The channel frequencies were spaced approximately 300 cycles apart and were 650, 950, and 1330 cycles. After passing through a bandpass filter

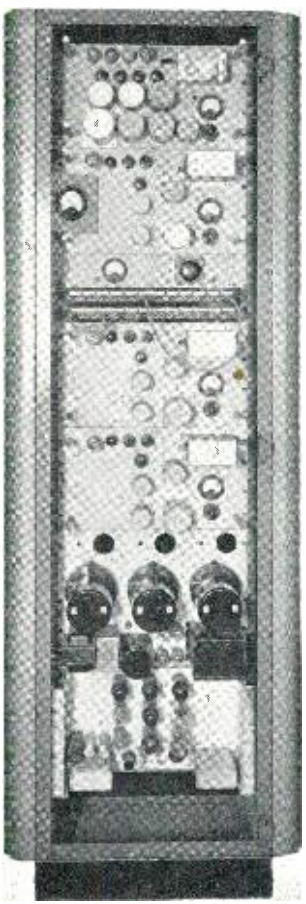

Fig. 4—Transmitting equipment for the tests.

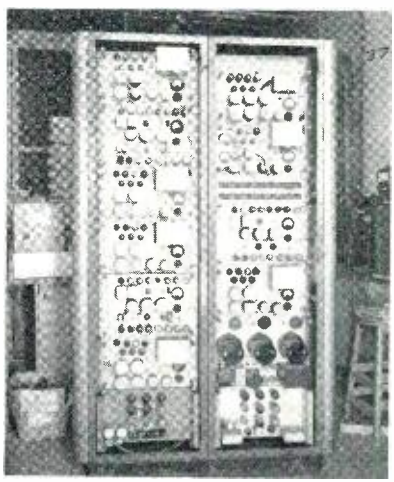

Fig. 5—Receiving equipment for the tests.

the keyed oscillator tone is paralleled with those from the other channels. For space diversity, this is the signal used to amplitude modulate the transmitter; for frequency diversity, this signal is passed through an amplifier and channel shifter in parallel before going to the transmitter. The channel shifter has the effect of adding 2500 cycles to each

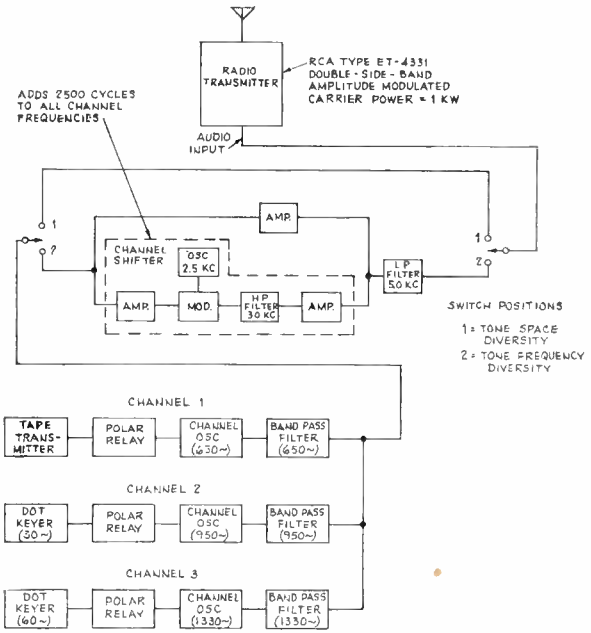

Fig. 6—Block diagram of transmitting equipment for tests.

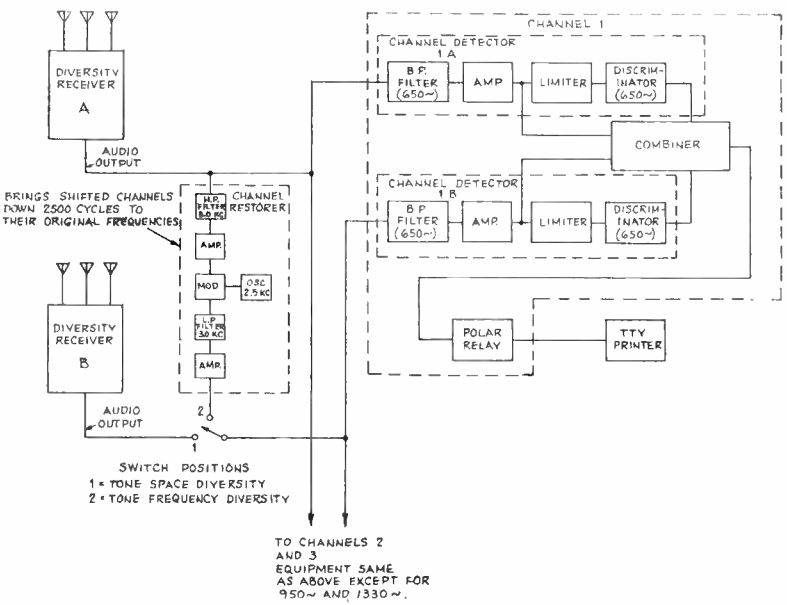

Fig. 7—Block diagram of receiving equipment for tests.

original channel frequency. Dummy traffic, consisting of unsynchronized 30 and 60 cycle reversals, was used on the second and third channels.

For space diversity reception, the audio outputs of the two receivers feed the two groups of receiving units. After selecting the desired channel by means of bandpass filters the signal is passed through a limiting amplifier having a range of over 40 decibels and then into a discriminator-type detector. In the combiner unit*, the detector output from the channel amplifier having the stronger input signal is selected and used to energize the polar relay which in turn drives a five-unit start-stop printer. For frequency diversity, only one radio receiver is used. One group of channel amplifiers takes the unshifted signals directly from its output. The shifted signals pass through a channel restorer which returns them to the original frequencies before passing them to the second group of channel amplifiers. The process of selecting and using the stronger signal is the same as that already described.

This first group of tests were made using double-sideband transmission. The transmitter was a Type ET-4331 communications transmitter of one kilowatt carrier power output, operated in the 4797.5 kilocycle experimental channel. It was amplitude-modulated by the tone channels. The peak modulation factor was kept at 100 per cent at all times. The output fed a horizontal half-wavelength folded dipole antenna oriented broadside to the receiving station.

Two kinds of receivers were used: The regular Triple Diversity Receiver[18] and the Exalted-Carrier Triple Diversity Receiver[19]. Both fishbone and rhombic antennas, directed toward the transmitter, were employed with the receivers. Field strength was measured and recorded continuously throughout the tests on separate equipment for this purpose.

The use of space diversity is so well known that it is felt that no description is necessary. However the exalted-carrier receiver is sufficiently new to merit a short description. It provides, in addition to the benefits of space diversity, a means of greatly reducing the distortion due to carrier fading. This is done by separating the carrier from its sidebands, passing it through a limiting amplifier which removes the variations due to fading, and then recombining it with the sidebands at low effective percentage modulation. This is substantially the same

---

* This unit is essentially similar to the V-1160 Frequency Shift Receiver Converter (see Reference 13) with suitable modifications for use at audio frequencies.

[18] J. B. Moore, "Recent Developments in Diversity Receiving Equipment", *RCA REVIEW*, Vol. II, No. 1, pp. 94-116, July, 1937.

[19] M. G. Crosby, "Exalted-Carrier Amplitude and Phase Modulation Reception", *Proc. I.R.E.*, Vol. 33, No. 9, pp. 581-591, September, 1945.

procedure as followed in a single-sideband receiver when using a filtered and re-introduced carrier.

Since one of the purposes in using single-sideband transmission is to avoid the effects of selective carrier fading, the same result can be accomplished on double-sideband by using the exalted-carrier receiver. However, as mentioned previously, single-sideband has very important additional advantages, such as requiring half as much frequency spectrum and providing better utilization of power output, which make it preferable.

Results

After a three day preliminary try-out of one channel in February 1946, full scale testing was begun in April and continued through May. This was on the 145-mile circuit from Camden, N. J. to Riverhead, L. I., N. Y. during daylight hours. The received signal strength was relatively high, averaging about 20 microvolts per meter or more and ranging from 1 to 100 microvolts per meter. The minimum occurred about midday which also seemed to be the time of greatest selective fading. To a greater or lesser degree, selective fading was present throughout virtually all of the testing. Thus, on this circuit the results are believed to be primarily a measure of errors due to selective fading and multipath distortion rather than due to noise. Rough checking of baud timing variations showed variations in the timing of leading and trailing edges of up to several milliseconds.

Single-Channel Results

Tests made with a single tone channel and regular diversity receivers yielded the following results:

	Errors	*Total Letters*	*Error Rate in %*
Frequency Diversity	2670	375,000	0.713
Space Diversity	720	375.000	0.192

$$\text{Error Ratio} = \frac{\text{Frequency Diversity}}{\text{Space Diversity}} = \frac{0.713\%}{0.192\%} = 3.7$$

A brief test made with no diversity in the channeling equipment gave 1.39 per cent.

In order to provide some comparison with an existing system of reception, a test was made using 850-cycle carrier-frequency shift keying over this same radio circuit, with a result of 0.019 per cent. Using 140-cycles shift a result of 0.062 per cent was obtained. These results are summarized in Figure 8. Dual diversity and the previously mentioned Type V-1160 Receiver Converter were used.

In making such tests as these, it it necessary to interleave the various types of operation at intervals of about 10 minutes because of the rapidly changing radio conditions and since it is not convenient to alternate more than two or three at one time, the tests have to be made in sections. The results from the several sections then are combined using one type of operation as the norm.

Multi-Channel Results

The first multi-channel tests, using regular diversity receivers, resulted in many errors. Space diversity produced 7.5 per cent errors and frequency diversity gave 9.2 per cent.

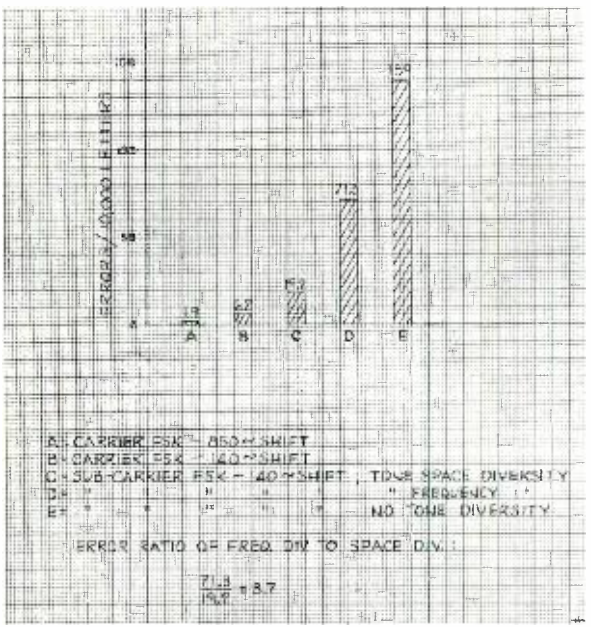

Fig. 8—Summary of double-sideband test results for one tone channel. (Improvement due to space diversity and a comparison with carrier frequency-shift-keying is shown.)

Investigation of the cause of the large number of errors obtained in multi-channel operation showed it to be harmonic and inter-modulation distortion of the tones in the final detector of the receiver when selective fading of the carrier took place. The exalted-carrier diversity receiver was then tried. Since only one receiver of this type was available, only frequency diversity could be tested. An error ratio of only 0.087 per cent resulted, which was better than a hundred to one improvement. It seems reasonable to assume, in the absence of any additional data, that the improvement from using space diversity would

be approximately the same as in single-channel operation, which was 3.7 to 1. Then multi-channel operation with exalted-carrier receivers and space diversity should result in an error rate of about 0.023 per cent. These results are shown graphically in Figure 9.

Single-Sideband Tests

Equipment

A single-sideband circuit transmitting from San Francisco, California to Washington, D. C. was used for the next tests.* This circuit is approximately 2500 miles long. The transmitting and receiving antennas were all of the rhombic type. The radio transmitter and

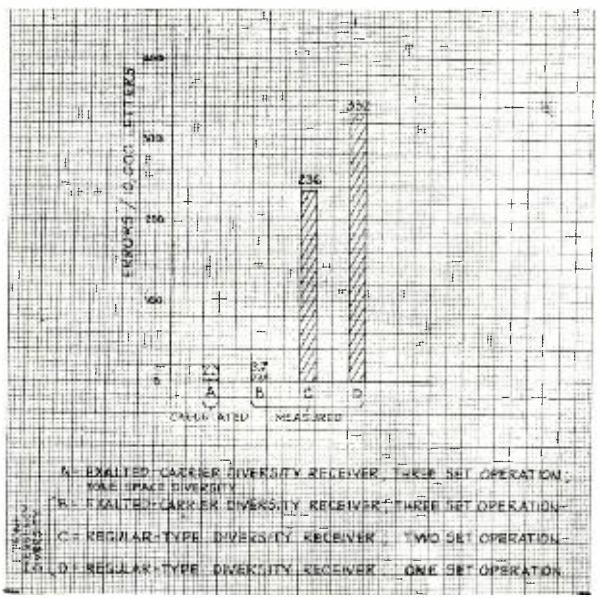

Fig. 9—Summary of double-sideband test results for three tone channels. (Improvement due to exalted-carrier receiver is shown.)

receivers were similar to those which have been described by A. A. Oswald.[20] The B channel, normally used for voice, was employed for these tests. The A channel carried its normal traffic. No impairment of the copy of the A channel printers was evident due to the presence of the experimental tone channels in the B channel.

* This circuit was made available through the courtesy of the U. S. Navy.

[20] A. A. Oswald, "A Short Wave Single-Sideband Radio Telephone System", *Proc. I.R.E.*, Vol. 26, No. 12, pp. 1431-1454, December, 1938.

The time-division multiplex equipment employed was similar to that used on wire telegraph circuits with the addition of a system of telegraph signal regeneration which squared up the telegraph dots and also enabled operation of start-stop printers from the multiplex signal.[21] Four-channel multiplex was used, with a repeating test message in the test channel and with the other three channels sending the letter R. The other two subcarrier channels carried dummy telegraph signals consisting of 30 and 60 cycle dots (not synchronized). The printer was operated at 368 operations per minute (about 60 words per minute).

When testing with a five-unit start-stop printer, it was operated directly from the output circuit of the channeling equipment at a speed of 368 operations per minute.

The tests were conducted during January and February 1947. Transmission was on approximately 13 megacycles. The modulating input level to the radio transmitter was such as to provide a power output of about 80 watts per subcarrier channel (for the three experimental channels in the B channel). Only space diversity was tested.

Results

Excellent printer copy was obtained throughout the entire tests. The equipment operated smoothly and without any breakdown. Multiplex range was checked several times. A range of seven points or more (10 is perfect) was obtained. These ranges were made with the control switch on the multiplex in the AC position (60 cycle reversals). Due to the signal regeneration in the multiplex, the range measured on the printer was the same on the radio circuit as on the local test circuit.

Start-stop printer range usually measured about 65, which was some ten points below the local printer range.

Following is a typical result of a day's operation using multiplex. The printer was operated without interruption for nearly six hours from early afternoon until evening. During this time hits‡ occurred 27 times and resulted in 54 errors. The total number of letters transmitted was 129,000 so that the average error rate was 0.042 per cent. The daily error rates during the multiplex tests ranged from 0.02 per cent to 0.14 per cent.

Start-stop printer tests were made for two days. The results are tabulated below. It will be seen that the average error rate was 0.032 per cent.

---

[21] R. Hoover, "The Application of Western Union Multiplex to Navy Radio", *Western Union Tech. Rev.*, Vol. 2, No. 1, pp. 29-35, January, 1948.

‡ The term hits is used here to denote a single error or a group of errors occurring consecutively.

	Hits	*Errors*	*Letters*	*Error rate in %*
1st day	10	23	113,600	0.0202
2nd day	16	34	65,030	0.0523
Total	26	57	178,630	0.0319

Although the multiplex operated at a keying speed of 60 cycles compared with only 23 cycles for the single start-stop printer, it is to be noted that their error rates are of the same magnitude. This may be attributable, at least in part, to the lesser susceptibility of the synchronous system to noise as was mentioned earlier.

During the course of these second tests some observations were made of fading-depth versus frequency-of-fade which appear to be of value since so little quantitative data on fading is available. The level of a tone channel was monitored at a point immediately following the receiving bandpass filter with the following typical result for a time interval of five minutes:

Number of fades to		
−10 to −19 decibels	−20 to −29 decibels	−30 decibels or less
14	5	0

It was noted further that the duration of the fade bore an inverse relationship to its depth. A fade of 15 decibels might last several seconds, whereas the occasional 30-decibel fade lasts only a fraction of a second. Fading over the range of plus 5 decibels to minus 10 decibels was noted almost continuously during both series of tests and on only a few occasions were the signals steady within about plus or minus one decibel over extended periods of time.

Some difficulty was encountered in tuning the single-sideband receiver during the tests since tones were present on both Channel A and B of the single-sideband transmitter. The problem was that of singling out the carrier from among the many channel tones. Quite likely some tuning device can be designed which will eliminate this problem.

Conclusion

These operational tests have shown that reliable service and low error rates can be obtained from a frequency-division multi-channel printing telegraph system operating on high-frequency (3 to 30 megacycles) radio circuits by employing frequency-modulated sub-carrier channels, single-sideband radio transmission and space diversity recep-

tion. Such a system presents further outstanding advantages from the standpoint of efficient utilization of the radio-frequency spectrum and transmitting power. The former is of great importance in this relatively crowded range, and the latter is of importance at all times in reducing the initial and operating cost of systems. Error rates of from 0.02 per cent to 0.14 per cent were obtained during the field test.

The tests verified that the use of a double-sideband instead of a single-sideband high-frequency radio circuit is not very practical for frequency-division multi-channel systems because of the large number of errors produced by harmonic and intermodulation distortion during selective fading of the carrier. Since the distortion occurs in the receiver, it could be overcome by using either a single-sideband receiver to receive the double-sideband wave, or a special double-sideband receiver known as the exalted-carrier receiver which has been designed by RCA Laboratories Division at Riverhead, L. I., N. Y. The errors obtained with the latter would be about the same as those obtained with single-sideband. However, the other two important advantages of single-sideband, namely, efficiency of spectrum and transmitter power utilization, are lost. Hence the principal use of double-sideband and the exalted-carrier receiver probably would be in temporary or emergency installations where it would be possible to save time or cost by using existing double-sideband radio circuits with modified receivers.

An interesting possibility, suggested by recent experiments conducted on the exalted-carrier receiver, is to design a unit which would convert a standard Diversity Receiver into an exalted-carrier receiver in such a manner as to make it usable both as a receiver of single-sideband and double-sideband. This would result in the standard Diversity Receiver becoming a universal receiver. Hence, existing double-sideband circuits could be used temporarily or part-time for multi-channel sub-carrier telegraphy merely by adding this unit to available standard Diversity Receivers. Interim error performance would approximately equal that of circuits using single-sideband equipment. Later the double-sideband transmitter could be replaced by a single-sideband transmitter with its several advantages, and with no further changes being required in the receiver.

The earlier operational test showed that a single sub-carrier channel could be operated on a double-sideband circuit having conventional receivers at a moderate increase in errors above those for single-sideband. The average error count when using a five-unit start-stop printer was about 0.2 per cent. This possibility may find some use on temporary or emergency circuits. It also has application where the disadvantage of the higher error rate is offset by the simple equipment, especially

when diversity is dispensed with also, and the ease of tuning, which is much greater, for instance, than that of carrier-frequency-shift equipment.

Another interesting possibility of the system which has not been mentioned previously is to use only half of the 6 kilocycle band, available in most present-day single-sideband apparatus, for automatic printer channels and to use the other half for a voice band. This plan has application to systems which are not used exclusively for telegraphy.

ACKNOWLEDGEMENT

As is usual on a project of this scope and duration, portions of the work have been done by many persons from various divisions. It is not possible to list them by name; however, their contributions are no less recognized. The system described herein was suggested by D. S. Bond and H. O. Peterson, both of RCA Laboratories Division. Their guidance and assistance throughout the project are gratefully acknowledged.

MICROWAVE OPTICS BETWEEN PARALLEL CONDUCTING SHEETS*

By

H. B. DeVore and Harley Iams

Research Department, RCA Laboratories Division,
Princeton, New Jersey

Summary—*For radar antenna applications in which rapid scanning is a requirement, it is frequently convenient to employ systems in which the microwave radiation is focused in one plane only, the radiation being guided from source to focusing element by means of a pair of parallel conducting sheets. Several unusual focusing systems of this type are described. These range from simple lens-like elements to more elaborate systems, in which advantage may be taken of arbitrarily variable refractive index and optical path length.*

These focusing systems produce a fan-shaped beam of radiation. When required, this may be converted to a pencil beam by using a cylindrical reflector or lens to effect focusing in the second direction. An extension of the parallel sheet techniques for guiding radiation permits the construction of metallic lenses for this purpose. A means for obtaining scanning in this direction is described.

A MICROWAVE radar problem of considerable interest is that of developing antennas capable of scanning a beam of the radiation across a comparatively large angular field, at a sufficiently rapid rate that the information received and presented on the cathode-ray indicator tube will form a substantially continuous map or picture of the field. This rapid scan is ordinarily required in one direction only—usually in the horizontal plane. When scanning in two dimensions is required, it can be done as in television by scanning rapidly along a line and displacing the scanned line relatively slowly in a direction perpendicular to its length.

By virtue of the reciprocity principle, any focusing system can be used in either direction, taking radiation from a point source and converting it into a parallel beam, as in transmitting, or accepting plane parallel radiation and focusing it to a point for receiving. Ordinarily, the same system is used for both purposes, first transmitting a pulse of radiation and then receiving the reflected signal.

A convenient attack on the problem may be made by dividing the focusing of the radiation beam into two, physically separate, parts, as shown in Figure 1. A vertical focusing element, which may be either a cylindrical lens or a section of cylindrical parabolic reflector, forms

* Decimal Classification: R310 × R537.11.

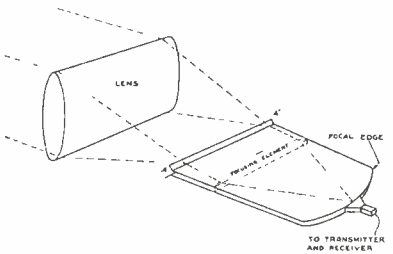

Fig. 1—General plan of scanning antenna using parallel plate optics.

a line focus of the incident beam at the aperture AA′ between two parallel conducting sheets. The radiation then travels between the sheets through a horizontal focusing element which produces a point focus at an edge of the parallel sheet system. The position of this focal point is determined by the azimuthal direction of the incident beam and, by moving a receiving element along the focal edge of the sheets, it is possible to scan across the field of the antenna. This element may have the form of the more or less modified end of a waveguide, carrying radiation between the antenna focus and the receiver or transmitter of the radar system.

It is the purpose of this paper to discuss some of the focusing elements we have employed for radiation guided between parallel conducting sheets, as well as some related lens-like structures.

The following requirements should be met by a satisfactory focusing element:

1) Aberrations should be small, in order that the radiation beam divergence may be kept near the limit set by wavelength and aperture.

2) The locus of the points representing best focus should lie as near as possible to a circle centered on the center of the focusing element. This permits comparatively simple mechanical arrangements for scanning and, at the same time, maintains good uniformity of illumination of the focusing element by radiation from the moving source.

3) The attenuation, or absorption of energy in passing through the focusing element should be as small as possible.

4) The element should reflect a minimum of energy back to the feed element in order to avoid detuning the transmitter.

5) The design should be such that production of the focusing element is feasible mechanically and, in the interest of reasonable cost, complexity should be held to a minimum.

6) Side lobes should be as small as possible. Side lobes are equivalent to a diffraction pattern, and are determined by the phase and the form of the illumination pattern produced at the focusing element by the source element.

In the following discussion, it will be assumed that the radiation is so polarized as to have its electrical vector vertical. In passing

through the parallel sheet system, the radiation will always maintain its electric vector perpendicular to the sheets, provided that the spacing between sheets is everywhere less than one-half wavelength.

Dielectric Lenses

An obvious approach to the focusing problem is to use lenses of dielectric material, exactly as one uses glass lenses in optical work. Such systems have been used and are frequently satisfactory. In this case, the lens has the form of a thin section of a cylindrical lens. To minimize deterioration of focus off-axis, the lens is usually chosen plano-convex, with the straight edge facing the focus. If the aperture of the system is large and the lens correspondingly thick, attenuation may present a serious problem. For the same reason, compound lenses have not, in general, been found very satisfactory. The choice of lens materials is rather limited, again for reasons of attenuation. Mycalex, with an index of refraction of the order of 2.6, and polystyrene, with an index 1.6, have been used.

It is possible to improve performance of a dielectric lens by reducing loss caused by reflection at the edges of the lens. This may be achieved by placing at the lens boundaries a layer, one-quarter wavelength thick, of a dielectric having an index of refraction which is the square root of that for the lens. Because of the fortunate relationship between the indices for mycalex and for polystyrene, a mycalex lens may be matched by attaching to its edges strips of polystyrene having a thickness equal to one-quarter of the wavelength of the radiation in polystyrene. For a polystyrene lens, the equivalent result may be obtained by machining in each edge a slot, one-quarter wavelength deep, and of sufficient height that the index of refraction of the compound polystyrene-air spacing between the metal plates is $\sqrt{1.6}$.

Long experience with optics has led us to think of focusing microwaves in terms of lenses or concave mirrors. Actually, it is neither the refraction nor the reflection which is of importance, but the fact that equal times are taken by all portions of the advancing wavefront in moving from a straight line (at the input of the focusing system) to a point (at the focus). When radiation is guided between two parallel conducting sheets spaced less than a half wavelength it is possible to shape or warp these sheets so as to achieve the focus without using reflection or changing the speed of propagation from its free-space value.[1]

[1] A general discussion of some focusing systems of this type has been given by S. B. Myers: "Parallel Plate Optics for Rapid Scanning," *Jour. App. Phys.*, Vol. 18, pp. 221-229, February, 1947.

THE R-$2R$ "LENS"

This method of configuration focusing has had no optical counterpart so far. It is particularly adapted to microwave radiation focusing systems. A particularly interesting example of this is represented in Figure 2. A pair of parallel circular sheets, spaced less than one-half wavelength apart, of radius R(I) are placed against a pair (II) bounded by a circular arc having radius $2R$.

With the aid of a little persuasion the metal sheets may be bent without stretching them in such fashion that the upper sheet of I may be fastened to the upper sheet of II all along the edge $Q_2 A P_2$. Likewise, the edges of the lower sheets may be joined. The process of joining the sheets forms a figure which is a section of a truncated cone. The assembly may then be completed by bending, without stretching, to bring the free edges of sheets II back to a straight line. The resulting configuration is as shown in the upper part of Figure 4. The microwave energy is then guided between the parallel sheets, and the path traversed is similar to that shown in the developed view of Figure 2. It can be seen that if the sheets are pulled together, points P_1 and P_2 will be brought together, since the arc lengths are $S_1 = R \cdot 2\theta$ for the circular sheets and $S_2 = 2R \cdot \theta$ for the other pair. The path length $A + B = 2R$, as shown, for any point on a plane wavefront entering the system, and hence a focus without aberration will be formed. If radiation enters at some angle α to the wavefront shown, all rays in the circular sheets will be deviated by the same angle α, and will be focused, still without aberration, at some new point on the edge of the circular sheets II.

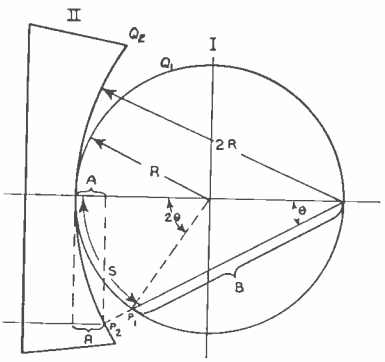

Fig. 2—Developed plan of "R—$2R$" lens. ($A = 2R(1 - \cos\theta)$; $B = 2R\cos\theta$; $A + B = 2R$ for all θ.)

It may be noted that a feed moving along the focal curve would not illuminate the lens aperture uniformly at any point off axis, as may be seen from Figure 3(a). In order to use this focusing element for scanning purposes, it is expedient to sacrifice perfection of focus by moving the feed along the arc of a circle centered at the center of the "lens" aperture, and having a radius R' chosen to give an approximation to the true focus. It is then convenient to insert between the sheets a diagonal reflector, transferring the focal curve

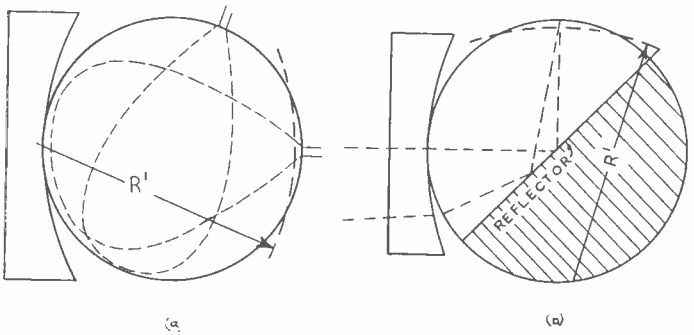

Fig. 3—Developed plan of "R-2R" lens, showing (a) preferred scanning region and (b) use of reflector between sheets.

to a region 90 degrees away as shown in Figure 3(b). The shaded parts of the sheets are removed, and the remaining assembly rolled into a section of a cone, having the focal curve as a base (Figure 4). This is now in a form adapted to rapid scanning, which may be achieved by rotating a waveguide feed around the base of the cone. This strange-looking all-metal assembly has been used for scanning a 1-degree beam through 40 degrees of azimuth at rates up to 60 sweeps per second.

Equality of Path Lenses

The R-2R "lens," just described, is one example of a variety of focusing elements designed by requiring that the radiation path length from some point, the focus, to some straight line, which is made the entrance slit for plane parallel radiation, shall be constant for all possible paths through the element.

Venetian Blind Lens

Another example of this is a variant of the R-2R principle which may be used as a "vertical lens" to focus an incident beam on the entrance slit for the horizontal focusing element. In this case, the lens is bounded by two cylindrical surfaces having radii R and 2R, respectively. Then a number of thin sheets of metal, all having the same width, are placed so as to connect points on the two surfaces having the same arcuate distances from the

Fig. 4—"R-2R" lens, constructed for use in a rapid scanner.

centers. The sheets are spaced so that the separation between them is always less than a half wavelength. This has the result that the path from the first to the second surface will be the same for all points and hence a focus will be obtained. Because of the rapidly increasing distance between the two surfaces, a point will be reached at which the straight line distance between corresponding points is less than the width chosen for the metal sheets. If at a previous point, a pair of sheets is used, with one sheet exactly one wavelength longer than the other, and with their edges joined, the new sheet width may be used in extending the lens, since radiation following the longer path will be in phase with that following the shorter one. This method may be used repeatedly for extending the height of the lens, but has the disadvantage that introduces a frequency sensitivity, which may be regarded as a form of chromatic aberration.

Multiple Waveguide Lens

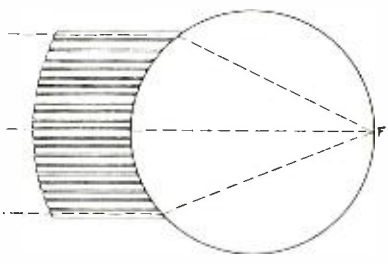

Fig. 5—Developed plan for multiple waveguide lens.

Another variant of the equal path lens, suitable for horizontal focusing, may be made in the manner shown in Figure 5. This "lens" is composed of an array of waveguides attached to a pair of parallel sheets represented by the circle. The lengths of the several guides are so chosen that the sum of the distance from the focus F to the point of attachment of the guide plus the phase length of the guide is a constant for all guides. (The phase length of a waveguide is the physical length of the guide multiplied by the ratio of the wavelength of the radiation in free space to its wavelength in the guide.) The guides may then be bent back on themselves in such a way that the free ends fall along a straight line which becomes the aperture of the "lens."

Wide Angle Waveguide Lenses

The use of waveguides to control path lengths, as exemplified in the two preceding structures, permits the introduction of two additional variables into lens design, neither of which has an obvious optical analogue. It is possible to design a system such that radiation entering at some given point A is constrained to leave the system at an arbitrarily selected point B. It is also possible to make the phase delay between A and B have any arbitrarily assigned value. The next

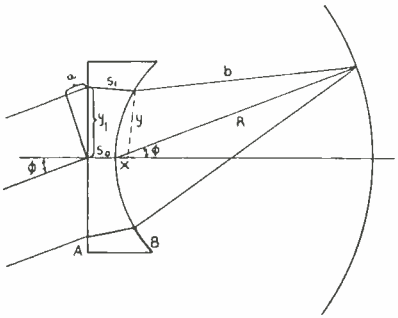

Fig. 6—Wide angle lens, with representative ray paths.

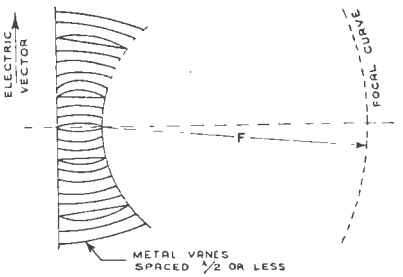

Fig. 7 — Sectional view of wide angle lens for vertical focusing.

lens design illustrates an application of this new freedom and shows two means for achieving it.

A lens is to be designed (Figure 6) having a straight face A and a curved face B, such that parallel incident radiation is focused at a distance R from the center of the curved surface, and such that the focal curve lies as closely as possible to the arc of a circle of radius R around this central point, with as wide angular coverage as possible.

By applying the requirement of equal radiation path for any possible path through the focusing system, it is possible to set up conditions on the lens which give a focus corresponding to constant path as the angle ϕ is increased, good to the second order of approximation in ϕ.

The appropriate conditions are:

$$\left(x - \frac{R}{2}\right)^2 + y^2 = \left(\frac{R}{2}\right)^2 ; \; y_1 = \sqrt{Rx} ; \; S_1 - S_0 = R\left[1 - \sqrt{1 - \frac{x}{R}}\right]$$

The first equation defines the curved surface of the lens as a circle passing through the principal focus. The other two equations specify the correlation between points on the first and second surfaces traversed by a given ray and the corresponding optical path through the lens.

Two forms of this lens are illustrated. The first, shown diagrammatically in Figure 7 and pictorially in Figure 8, is a vertical lens, similar to the Venetian Blind lens described above. Path lengths are controlled by the width of the metal sheets used. The second (Figure 9) is a horizontal lens and is, in effect, an array of slightly tapering

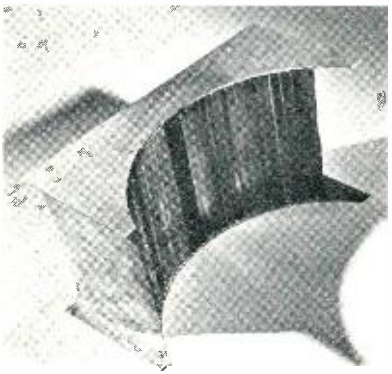

Fig. 8—Wide angle vertical lens.

Fig. 9—Wide angle horizontal lens.

waveguides. Optical path lengths are controlled by the width of the guides, since the phase velocity of radiation in such a waveguide is determined by the width of the guide and the wavelength of the radiation. Table I shows the measured beam widths, as the angle of incidence is varied, for the two lenses illustrated. The side lobe pattern showed little change over the range covered.

The technique of guiding microwave radiation between an assemblage of parallel metal sheets, spaced apart by a distance which is everywhere less than one-half wavelength, has been employed to make a high-speed vertical scanner. The method is illustrated in Figure 10. Radiation leaving the horizontal focusing element passes through some portion of a rotor which is so designed that as it rotates, the line of emergence of the radiation moves along the inside surface of a corresponding stator. The stator sheets terminate along the

Table I—Observed beam widths for lenses shown in Figures 8 and 9. ($\lambda = 1.25$ cm.)

Incident Angle (degrees)	3-decibel Beam Width	
	Vertical Lens (degrees)	Horizontal Lens (degrees)
0	4.7	2.2
10	4.8	2.2
20	4.8	2.2
30	5.1	
35	5.3	

focal surface of a suitable vertical lens. Hence, the radiation passing through the rotor and stator in succession, emerges at a position such that it is converted by the vertical lens into a parallel beam of radiation having a direction in the vertical plane determined by the particular region of the stator traversed. It may be seen that a uniform rotary motion of the rotor produces a beam scanned angularly in the vertical direction. The rate of scan is sawtooth in form and the field is swept twice for each revolution of the rotor.

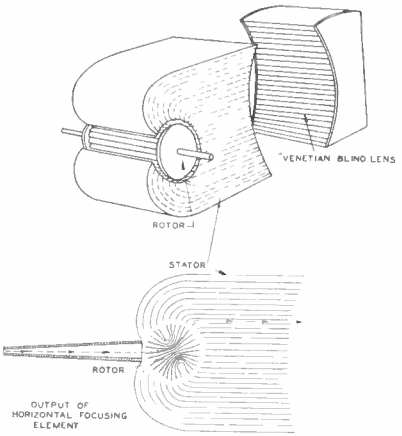

Fig. 10—Schematic representation of system for obtaining rapid scanning in vertical direction.

In order to prevent destructive interferences and hence severe reflections, as the radiation passes from one element of the rotor to the next, it is necessary that all paths through the rotor have the same length. Hence the rotor is made of an assemblage of thin sheets, all of which have the same dimensions. These are arranged so that their edges are uniformly spaced around the rotor, giving a sectional form similar to that shown in Figure 10. For the same reason, it is necessary that the path length for the radiation passing through the stator should be the same for all elements of the stator. Because of the form of the stator, this cannot be achieved by using a set of identical sheets, as in the case of the rotor. It was accomplished in our model by inserting short dielectric strips between the stator sheets; the lengths of the strips (in the direction of the radiation) being chosen so that the total radiation path length had the same value for all the elements of the stator.

Dielectric Disc Lens

It has been shown that aberration-free focus will be obtained on the surface of a sphere of radius R in which the index of refraction varies from 1 at the surface to $\sqrt{2}$ at the center, according to the law[2]

$$n_r = \sqrt{2 - \left(\frac{r}{R}\right)^2}$$

[2] R. K. Luneberg, MATHEMATICAL THEORY OF OPTICS, Brown University Press, Providence, R. I., 1944 (p. 213).

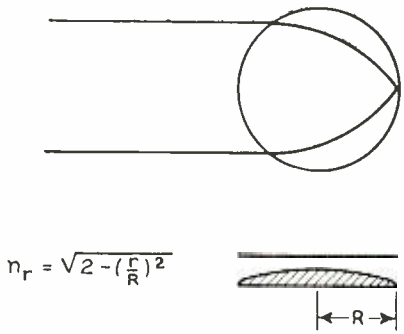

Fig. 11—Dielectric disc omnidirectional lens.

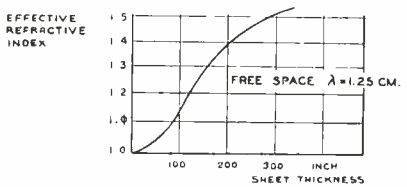

Fig. 12—Refractive index as function of thickness for polystyrene sheets.

A lens having this characteristic may be obtained by placing between parallel-metal sheets a disc of dielectric having a thickness varying in such a way as to give effectively this result. The general form of this lens is shown in Figure 11.

Further, it has been found that sheets of dielectric act as effective guides for radiation, even without metal covering sheets. In addition, the wavelength of the radiation guided by a dielectric sheet has been found to depend upon the ratio of the thickness of the sheet to λ_0 and thus the effective index of refraction is a function of sheet thickness. The variation in the case of polystyrene is shown in the curve of Figure 12.

It is then feasible to make a disc of polystyrene having thickness tapering from the center to the edge so as to give index of refraction following the above law, and this disc then serves as an omnidirectional lens. The performance of such a polystyrene omnidirectional lens (and others described herein) may be shown by the method previously described by Iams.[3]

*Circular "Reflector" with Correcting Element**

From the viewpoint of scanning, the use of a circular reflector as a focusing element has the merit of symmetry around the center of the reflector. This idea may be adapted to a parallel plate system by substituting for the reflector a toroidal bend, so that the radiation enters between the sheets in one plane, passes around the toroidal bend, and is brought to focus in another plane parallel to the first.

[3] The method for obtaining this phase front plot has been described by Harley Iams. "Phase-Front Plotter for Centimeter Waves," *RCA Review*, Vol. VIII, No. 2, pp. 270-275, June, 1947.

* This system was suggested by Dr. C. V. Robinson of Radiation Laboratory.

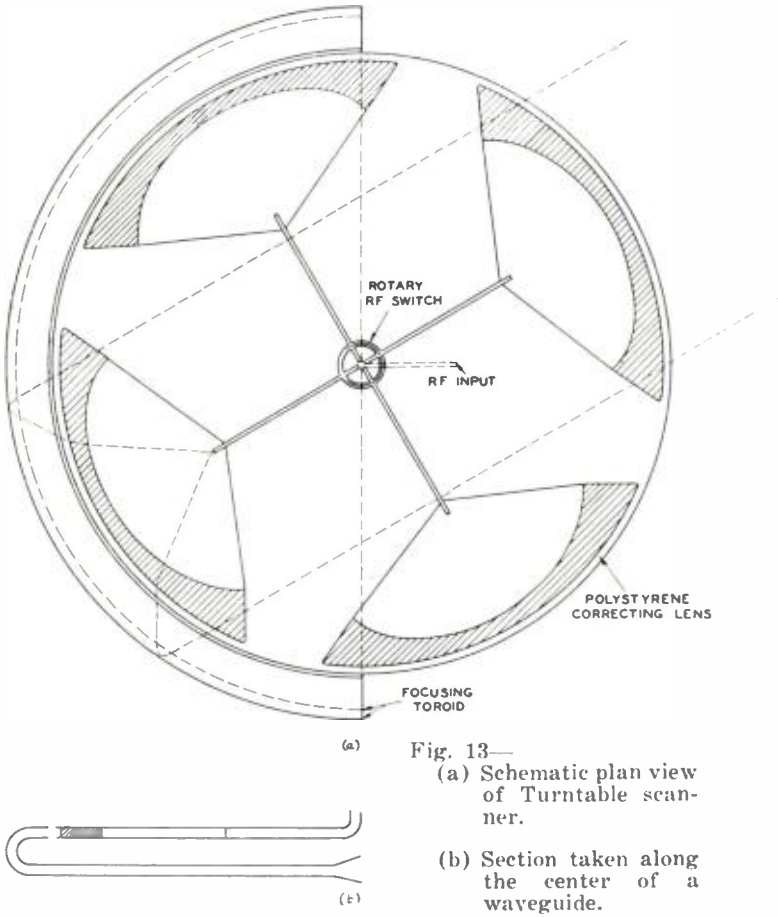

Fig. 13—
(a) Schematic plan view of Turntable scanner.

(b) Section taken along the center of a waveguide.

The image formed by this toroidal bend alone would suffer from spherical aberration, but this aberration may be removed by inserting in the path of the radiation a suitably designed lens. Figure 13(a) shows a plan view of a focusing element of this type and Figure 13(b) shows a sectional view taken horizontally through the center of Figure 13(a). The waveguide feed and the correcting lens may be fastened rigidly together and rotated around the center of the system to produce a scan which has a substantially constant pattern over very wide angles.

A scanner of this type was constructed, using four identical waveguide and correcting-lens units disposed 90 degrees apart around a rotor. As the rotors turns, the feed units are switched on in succession so that the field is scanned four consecutive times during each revolution of the rotor.

Figure 13 shows a schematic view of this scanner. The radiation, emerging from the space between the metal sheets, is focused in the vertical direction by a cylindrical reflector, not shown in this diagram. This scanner covered an 82-degree field 20 times per second with a beam which was 1.1 degrees wide up to ± 30 degrees, increasing to 2.3 degrees, at ± 41 degrees.

Conclusion

In this paper a number of microwave focusing systems have been described. These illustrate some of the ways in which well-known optical principles have been applied to the microwave field and show a number of ways in which the principle of guided radiation offers rather greater freedom to the designer than is available in optical work.

Acknowledgments

The authors wish to express appreciation for the information and assistance supplied by C. V. Robinson, L. J. Chu, and other members of the Radiation Laboratory. R. L. Burtner, formerly with RCA Laboratories Division, cooperated with the authors in many of the phases of this work.

RCA TECHNICAL PAPERS†

Third Quarter, 1948

Any requests for copies of papers listed herein should be addressed to the publication to which credited.

"Automatic Gain Controls for Television Receivers", K. R. Wendt and A. C. Schroeder, *RCA Review* (September) 1948

"The Brightness Intensifier", G. A. Morton, J. E. Ruedy and G. L. Krieger, *RCA Review* (September) 1948

"Chromatic Aberration and Resolving Power in Electron Microscopy", E. G. Ramberg and J. Hillier, *Jour. Appl. Phys.* (July) 1948

"Continuously Variable Band-Elimination Filter", Kurt Singer, *Jour. Soc. Mot. Pic. Eng.* (August) 1948

"D.C. Operated Servo Amplifier", Sidney Wald, *Radio News* (August) 1948

"Design Factors for Intercarrier Television Sound", S. W. Seeley, *Electronics* (July) 1948

"Details of the Simultaneous Equation Solver", E. A. Goldberg, *RCA Review* (September) 1948

"Developments in Large-Screen Television", R. V. Little, Jr., *Jour. Soc. Mot. Pic. Eng.* (July) 1948

"Electron Tube Phonograph Pickup", H. F. Olson, and J. Preston, *Audio Engineering* (August) 1948

"Electro-Optical Characteristics of Television Systems; Part III —Electro-Optical Characteristics of Camera Systems", O. H. Schade, *RCA Review* (September) 1948

"Engineering Responsibilities In Creating New Products", J. B. Davis & M. M. Brandt, *Product Engineering* (September).. 1948

"Flexible Low Friction Contact", Louis Pensak and Meier Sadowsky, *The Chemist Analyst* (September) 1948

"Maintenance of Preamp Equipment in Broadcast Transcription —Reproducing Systems", R. G. Peters, *Communications* (July) 1948

"New Test Equipment Speeds Video Servicing", Arthur Liebscher, *Radio News* (July) 1948
Radio Service Dealer (July) 1948

"An Optical Bench for Electron Optical Studies", J. H. Reisner & R. G. Picard, *Rev. Sci. Instr.* (September) 1948

"Optical Problems in Large-Screen Television", I. G. Maloff, *Jour. Soc. Mot. Pic. Eng.* (July) 1948

"The Pack Transmitter", J. L. Hathaway and W. Hotine, *RCA Review* (September) 1948

† Report all corrections or additions to RCA Review, Radio Corporation of America, RCA Laboratories Division, Princeton, N. J.

"A Peaked Audio Amplifier for Communication Receivers", G. D. Hanchett, Jr., *QST* (September) 1948

"Photometry in Television Engineering", D. W. Epstein, *Electronics* (July) 1948

"Some Applications of Frequency-Modulated Radar", I. Wolff and D. G. C. Luck, *RCA Review* (September) 1948

"Some Notes on Noise Theory and Its Application to Input Circuit Design", W. A. Harris, *RCA Review* (September) 1948

"Temperature Dependence of the Emission Bands of Zinc Oxide Phosphors", F. H. Nicoll, *Jour. Opt. Soc. Amer.* (September) 1948

"Theoretical Analysis of Various Systems of Multiplex Transmission (Concluding Part)", V. D. Landon, *RCA Review* (September) 1948

"What It Takes for a Good Standards Department", S. H. Watson, *Industrial Standardization* (July) 1948

"A 150-kw Transmitter for Standard Band Broadcasting", T. J. Boerner, *Elec. Eng.* (September) 1948

8-Bay Pylon Antenna, by O. O. Fiet, *FM and Television* (Sept.). 1948
Broadcast News (August) 1948

NOTE—Omissions or errors in these listings will be corrected in the yearly index.

Corrections:

On page 19 of the March 1948 issue, the parenthetical expression in the ninth line should read "($\bar{E}_r = 915$ Td)."

On the same page, the parenthetical expression in the tenth line should read "($\bar{E}_r = 26$ Td)."

On the same page, the twelfth line should read "ranges 260:1 for the test with white background and 9100:1 for the".

On the same page, in the fourth from the last line, the expression of equality should read "$\bar{B}/\bar{B} = 5$".

On the same page, in the last line the number "1000" should be changed to read "500".

On page 251 of the June 1948 issue, Equation (28) should read as follows: $rC_\delta = \%C_N = [1 - (1 - r\Delta\bar{\psi})/(1 + r\Delta\bar{\psi})]\ 100$

On page 265 of the same issue, Equation (32c) should read: $N_e = 2\sqrt{2}\, n_s$

On page 286 of the same issue, the ratio $N/N\delta_n$, for $r\Delta\bar{\psi} = 1$ is equal to zero (instead of unity) for the aperture numbers 1 to 4 for both round and square apertures.

AUTHORS

GEORGE H. BROWN—(See *RCA Review*, Volume IX, No. 2, June, 1948, page 367).

MURLAN S. CORRINGTON received the B.S. degree in electrical engineering in 1934, from the South Dakota School of Mines and Technology, and the M. Sc. degree in 1936, from Ohio State University. From 1935 to 1937 he was a graduate assistant in the physics department of Ohio State University. In 1937 he joined the Rochester Institute of Technology, and taught mathematics, mechanics, and related subjects. Since 1942 he has been engaged in mathematical engineering in the Advanced Development Section of the RCA Victor Division, Radio Corporation of America, at Camden, N. J.

HUGH B. DEVORE received the B.S. degree in physics in 1926 and the M.S. degree in 1927 from Pennsylvania State College and the Ph.D. degree in 1934 from the California Institute of Technology. From 1927 to 1931, he was employed at the DuPont Experimental Station. He joined the research division of RCA Manufacturing Co. at Harrison, N. J. in 1934, transferring to RCA Laboratories Division at Princeton, N. J., in 1942, where he worked on the development of television pick-up tubes and on microwave antenna problems. From 1945 to 1947, he was associated with Remington Rand, Inc. Since 1947, he has been at RCA Laboratories Division, Princeton, N. J., engaged in fundamental research on solids. Dr. DeVore is a Member of Sigma Xi and the American Physical Society and a Senior Member of the Institute of Radio Engineers.

HARLEY IAMS—(See *RCA Review*, Volume IX, No. 1, March, 1948, page 171).

THOMAS E. JACOBI received his B.S. degree in electrical engineering from Marquette University in 1942. Upon graduation, he joined the Engineering Products Department of the RCA Victor Division at Camden, N. J., as a Student Engineer. He has worked continuously since then on the design and development of commercial and government radio receiving equipment. Mr. Jacobi is a Member of Tau Beta Pi and Pi Mu Epsilon and a Member of the Institute of Radio Engineers.

JEROME KURSHAN received the B.A. degree with honors in mathematics and physics from Columbia University in 1939 and was an assistant in physics there during that year. From 1939 to 1943 he was an assistant in physics at Cornell University where he received the Ph.D. degree in 1943. Since then he has been with the RCA Laboratories Division at Princeton, working on FM magnetrons and special receiving tube problems. Dr. Kurshan is a Member of Phi Beta Kappa, Sigma Xi, the American Physical Society and the Institute of Radio Engineers.

RUSELL R. LAW received the B.S. degree and M.S. degree in electrical engineering from Iowa State College in 1929 and 1931, and the D.Sc. degree in communications engineering from Harvard University in 1933. From 1933 to 1934 he was a research associate at Harvard University. In 1934 he entered the Research Department of RCA Manufacturing Company at Harrison, New Jersey, and in 1942 transferred to RCA Laboratories Division at Princeton, N. J. Dr. Law is a member of Sigma Xi and a Senior Member of the Institute of Radio Engineers.

JOHN A. MITCHELL received the B.S. degree from the California Institute of Technology in 1944 and the M.S. degree from Stanford University in 1947. He is now studying for his doctor's degree at Stanford University. During the summer of 1947 he was employed as a summer research student at the East Pittsburgh plant of the Westinghouse Electric Corporation. He worked on the project described in the paper in this issue while temporarily employed at RCA Laboratories Division during the summer of 1948.

GEORGE A. MORTON—(See *RCA Review*, Volume IX, No. 3, September 1948, page 559).

T. MURAKAMI received B.S. degree in E.E. from Swarthmore College in 1944, and the M.S. degree from the Moore School of Electrical Engineering, University of Pennsylvania in 1947. From 1944 to 1946 he was an assistant and research associate in the department of electrical engineering at Swarthmore College. Since 1946 he has been with the Advanced Development Section of the Home Instrument Department, RCA Victor Division, Camden, N. J., working on radio frequency circuit development. Mr. Murakami is an Associate Member of the Institute of Radio Engineers and Sigma Xi.

LEON S. NERGAARD received the B.S. degree in Electrical Engineering from the University of Minnesota in 1927, the M.S. degree from Union College in 1930, and the Ph.D. degree from the University of Minnesota in 1935. From 1927 to 1930, he was in the research laboratory and vacuum-tube engineering department of the General Electric Company; from 1930 to 1933 a teaching assistant in the department of physics at the University of Minnesota; from 1933 to 1942 in the research and development laboratory of the RCA Manufacturing Company; and since 1942 at the RCA Laboratories Division in Princeton, N. J. He is a Member of Sigma Xi, the American Physical Society, the American Association for the Advancement of Science, and a Senior Member of the Institute of Radio Engineers.

OTTO H. SCHADE—(See *RCA Review*, Volume IX, No. 3, September 1948, page 560).

ROBERT P. STONE received the B.E.E. degree from the Ohio State University in 1940. In 1941 he received his M.S. degree from Purdue University. He joined Radio Corporation of America in that year and has been associated with RCA Laboratories Division since that time. Mr. Stone is a member of Sigma Xi and a Member of the Institute of Radio Engineers.

WILFRID B. WHALLEY received the degree of B.A.Sc., with honors from the University of Toronto in 1932, was on the staff of the Department of Electrical Engineering for the next four years and received the M.A.Sc. degree in 1935. In 1936, he was development engineer at the Radio Valve Company in Toronto. From 1937 to 1940 he was with RCA Manufacturing Company at Harrison, N. J., and in 1940 transferred to war work in Canada. In 1943, he returned to the Radio Corporation of America, RCA Laboratories Division. In 1947, he was appointed Assistant Professor of Engineering Physics at Cornell University. At present, Mr. Whalley is at the Research Laboratories of Sylvania Electric Products, Inc., New York. He is a member of Sigma Xi, American Association for the Advancement of Science, American Association of University Professors, and an Associate Member of the Institute of Radio Engineers.

RCA REVIEW

a technical journal

RADIO AND ELECTRONICS
RESEARCH · ENGINEERING

INDEX

VOLUME IX
1948

TABLE OF CONTENTS

March

June

INDEX, VOLUME IX

AUTHORS, VOLUME IX